

University of Louisville

ThinkIR: The University of Louisville's Institutional Repository

Electronic Theses and Dissertations

5-2023

Toward a comprehensive account of orientation selectivity in the retina.

Megan L. Zipperer
University of Louisville

Follow this and additional works at: <https://ir.library.louisville.edu/etd>



Part of the [Neurosciences Commons](#)

Recommended Citation

Zipperer, Megan L., "Toward a comprehensive account of orientation selectivity in the retina." (2023).
Electronic Theses and Dissertations. Paper 4078.
Retrieved from <https://ir.library.louisville.edu/etd/4078>

This Doctoral Dissertation is brought to you for free and open access by ThinkIR: The University of Louisville's Institutional Repository. It has been accepted for inclusion in Electronic Theses and Dissertations by an authorized administrator of ThinkIR: The University of Louisville's Institutional Repository. This title appears here courtesy of the author, who has retained all other copyrights. For more information, please contact thinkir@louisville.edu.

TOWARD A COMPREHENSIVE ACCOUNT OF ORIENTATION
SELECTIVITY IN THE RETINA

By

Megan L Zipperer
B.S., UNC Wilmington, 2016
M.S., University of Louisville 2020

Dissertation
Submitted to the Faculty of the
School of Medicine of the University of Louisville
in Partial Fulfillment of the Requirements for the Degree of

Doctor of Philosophy in Anatomical Sciences and Neurobiology

Department of Anatomical Sciences and Neurobiology
University of Louisville
Louisville, Kentucky

May 2023

©2023
Megan L Zipperer
All rights reserved

TOWARD A COMPREHENSIVE ACCOUNT OF
ORIENTATION SELECTIVITY IN THE RETINA

By
Megan L Zipperer
B.S., UNC Wilmington, 2016
M.S., University of Louisville, 2020

A Dissertation Approved on

4/19/2023

By the following Dissertation Committee:

Bart Borghuis, Ph.D.

Martha Bickford, Ph.D.

Ron Gregg, Ph.D.

Maureen McCall, Ph.D.

David Stirling, Ph.D.

DEDICATION

To Thomas, Lindsey, and Moira.

ACKNOWLEDGEMENTS

The work described in this manuscript would not be possible without the generous support and encouragement of my colleagues, friends, and family. More important than any knowledge, skills, or degree I gained during my time here is the immense personal growth I experienced as a direct result of excellent mentorship. With that, first and foremost, I want to start by thanking my mentor, Dr. Bart Borghuis, who provided the best possible environment for doing great science. Bart is a paradigm of scientific integrity, and has modeled all the attributes of a great scientist and mentor: enthusiasm, brilliance, patience, empathy, honesty, and so much more. Not only has Bart taught me what it means to be a great scientist, but, through great mentorship, has inspired confidence in myself. Bart has selflessly prioritized my career development, personal growth, and mental health over all else. The best decision of my career was choosing this lab to do my dissertation work.

I am grateful to the rest of my committee members for their guidance and insight, which has shaped this project: Dr. Ron Gregg, Dr. Maureen McCall, Dr. David Stirling, and Dr. Martha Bickford. Outside of the committee, I would like to thank Dr. Bill Guido for his career advice, opportunities, and support, and Dr. Chad Samuelsen for helping me realize the value of the work I have done here.

The friends I have made during my time in Louisville are the greatest friends I have ever had, and I know that these friendships will be lifelong. I want to especially thank Lisa for being not only a compassionate and genuine friend, but for her guidance as a peer mentor. At many points in my career, I leaned heavily on the comradery and advice of my other dear friends. It would take another 200 pages to fully describe every meaningful friendship I've had here, but I want to specifically thank a few: Cece A., Jess H., Kamille R., Easton F., Guela S., James W., and Justin R. I want to thank Lindsey — who has always been my sister but is now one of my closest friends; I am so happy to have grown together, here with you. I want to thank Moira, my sibling and dearest friend who, even from miles away, has always been at my side and has been such a champion of me. You and Lindsey are my world. I truly feel like I am the luckiest person on earth to have such amazing people in my life.

Lastly, I want to thank my partner, Thomas, for his unwavering dedication and support, both during my time as a graduate student and throughout life. Thomas encouraged me to push myself and see that I was more capable than I had ever thought possible. While asking for nothing in return, he has made my life infinitely better, and filled it with so much more happiness than I ever could have imagined. It will take a lifetime to give back all of the support and love that has been necessary to get me through my time here, and I fully intend to do that. I wish for every person to have somebody like you in their life, and I am so excited to start our next journey together.

ABSTRACT

TOWARD A COMPREHENSIVE ACCOUNT OF ORIENTATION SELECTIVITY IN THE RETINA

Megan Zipperer

4/19/2023

Retinal Ganglion Cells (RGCs) form functionally distinct signaling channels that selectively encode features of the visual input including direction of motion, contrast polarity, size, and color. A highly conserved visual channel amongst vertebrates conveys orientation selectivity, i.e., the selective firing of neuronal cells in response to elongated stimuli along a preferred orientation. Orientation selectivity is an apparent critical computation and several studies have reported aspects of it, including cell type identity in anatomical reconstructions, and functional characterization of at least four different identified RGC types. But how cell types in the different studies relate is not well resolved; the mechanisms that generate the orientation selective responses in mice remain incompletely understood; and the retinofugal projections of OS RGC types are unknown. The goal of this study was to comprehensively characterize Orientation Selective (OS) RGC types in the mouse retina, and to elucidate the mechanisms that contribute to their tuning properties.

We used population calcium imaging and hierarchical clustering to identify orientation selective RGCs in retinal explants. We then targeted these cells for detailed morphological and electrophysiological study. Our survey of RGC populations and subsequent morphological analysis distinguished 10 morphological types with apparent OS tuning. Electrophysiological analysis of 5 types identified specific tuning mechanisms, including a type with tuned excitation and inhibition, and a type with just tuned inhibition. Retrograde tracing from dLGN indicates that OS cells project to the shell region of the dorsal Lateral Geniculate Nucleus (dLGN), indicating that at least some OS RGC types contribute to dLGN OS tuning. We will present a comprehensive morphological complement of OS types in the retina and resolve their detailed circuit-level mechanisms, synaptic partners, molecular profiles, and retinofugal projections. This study will functionally define the function of RGC types that exhibit OS properties. Additional studies will be necessary to further solidify the full

TABLE OF CONTENTS

DEDICATION.....	iii
ACKNOWLEDGEMENTS.....	iv
ABSTRACT.....	v
LIST OF FIGURES.....	xii
LIST OF TABLES.....	xvii

CHAPTER I GENERAL INTRODUCTION AND LITERATURE REVIEW

1.1 INTRODUCTION.....	1
1.2 BACKGROUND AND LITERATURE REVIEW.....	3
1.2.1 Introduction.....	3
1.2.2 Organization of the Mouse Visual System.....	4
1.2.3 Retinal Ganglion Cells.....	8
1.2.3.1 RGC Typology.....	8
1.2.3.2 The Importance of Classifying Retinal Ganglion Cells....	14
1.2.4 Review of Orientation Selectivity.....	16
1.2.4.1 Early Observations of Orientation Tuning.....	16
1.2.4.2 Orientation Tuning is Highly Conserved Across Species...19	
1.2.4.3 Proposed Tuning Mechanisms for OS in Retina.....	20
1.2.4.4 Organization of OS Cells in Central and Cortical Regions..22	
1.2.5 Orientation Selectivity in the Mouse Visual Pathway.....	24
1.2.5.1 Orientation Selectivity in Mouse Primary Visual Cortex (V1).....	24

1.2.5.2 Orientation Selectivity in Mouse Superior Colliculus (SC).....	25
1.2.5.3 Orientation Selectivity in Mouse dLGN.....	26
1.2.5.4 Orientation Selectivity in Mouse Retina.....	27
1.2.6 The need for Innovative Methods to Investigate Orientation Selectivity in the Retina.....	30
1.4 SUMMARY OF CHAPTER I.....	31

**CHAPTER II- FUNCTIONAL IMAGING AND DEVELOPING AN
INTRAEXPERIMENTAL ANALYSIS METHOD**

2.1 INTRODUCTION.....	33
2.2 BACKGROUND.....	33
2.3 METHODS.....	38
2.3.1 Animals.....	38
2.3.2 Retinal Dissection.....	39
2.3.3 Two-Photon Calcium Imaging.....	40
2.3.4 Visual Stimulation.....	40
2.3.5 Harvesting Functional Responses.....	41
2.3.6 Cluster Analysis.....	41
2.4 RESULTS	
2.4.1 <i>Thy1</i> -GCaMP6f Mice Allow Imaging of Diverse RGC Types.....	42

2.4.2 RGC Survey Identifies OS Types.....	46
2.4.3 Developing an Intra-Experimental Analysis.....	48
2.5 SUMMARY AND DISCUSSION.....	48

CHAPTER III- TARGETED MORPHOLOGICAL ANALYSIS OF ORIENTATION SELECTIVE GANGLION CELLS

3.1 INTRODUCTION.....	50
3.2 BACKGROUND.....	50
3.3 METHODS.....	54
3.3.1 Intra-Experimental Analysis.....	54
3.3.2 Neurobiotin Fills.....	55
3.3.3 Immunostaining to Identify ChAT bands and Cell Morphology.....	56
3.3.4 Confocal Imaging.....	57
3.3.4 Imaris Analysis.....	57
3.3.4.1 Filament Reconstruction.....	57
3.3.4.2 Filament Dendrite Area.....	58
3.3.4.3 Filament Dendrite Length.....	58
3.3.4.4 Generating Sholl Intersections.....	58
3.3.4.5 Spine Reconstruction.....	58
3.3.5 Quantification of RGC Stratification Depth.....	59
3.3.6 Anatomical Quantification in Fiji.....	59
3.3.7 Determining Functional Responses for Each Cell.....	59
3.4 RESULTS.....	61

3.4.1 Using the Intraexperimental Analysis to Target OS Cell Types.....	61
3.4.2 Analysis of Stratification Depth Distinguishes 11 Morphological OS Groups.....	64
3.4.3 10 Target RGC Groups Demonstrate Apparent Orientation Selectivity.....	69
3.4.4 All Orientation Angles Represented in Survey.....	70
3.4.5 OS RGC Groups Show Consistent Contrast Polarity.....	71
3.4.4 Morphological Groups Demonstrate Heterogeneous Functional Responses.....	75
3.4.5 RGC Morphology Quantified with Imaris Analysis.....	80
3.4.6 Unique Morphological Features Observed Across Types.....	82
3.4.7 RGC Group Detailed Profiles.....	86
3.5 SUMMARY AND DISCUSSION.....	90

**CHAPTER IV- TARGETED PHYSIOLOGICAL ANALYSIS OF ORIENTATION
SELECTIVE GANGLION CELLS**

4.1 INTRODUCTION & BACKGROUND.....	96
4.2 METHODS.....	97
4.2.1 Retinal Dissection.....	97
4.2.2 Two-Photon Calcium Imaging.....	97
4.2.3 Intraexperimental Analysis.....	97
4.2.4 Targeted Electrophysiology.....	98

4.2.5 Determining OSI Value for Electrophysiological Recordings.....	98
4.3 RESULTS.....	99
4.3.1 ON hOS Type I Demonstrates Robustly Tuned Inhibition and Excitation.....	102
4.3.2 ON vOS Type I Demonstrates Tuned Inhibition Only.....	103
4.3.3 OFF vOS Type II Demonstrates Matching Tuned Excitation and Inhibition.....	104
4.3.4 OFF vOS Type III Demonstrates Modest Excitatory Tuning.....	105
4.3.5 OFF hOS Type II Demonstrates No Apparent OS Tuning Mechanism.....	106
4.3.6 Electrophysiological Tuning Corresponds with Fluorescent Responses.....	107
4.3.7 Inhibition, Not Excitation, Divides Cell Types.....	108
4.3.8 Fluorescent OSI Does Not Explain Difference in Tuning....	110
4.3.9 Cell Morphology Accurately Predicts Response Kinetics and Contrast Polarity	110
4.4 SUMMARY AND DISCUSSION.....	112

CHAPTER V- RETINORECIPIENT TARGETS OF ORIENTATION SELECTIVE TYPES

5.1 INTRODUCTION & BACKGROUND.....	118
5.2 METHODS	
5.2.1 Stereotaxic Virus Injections in SC and dLGN.....	121
5.2.2 Rabies Tracing Method to Identify Projections to Core and Shell of dLGN.....	122
5.2.3 Retinal Dissection.....	122
5.2.4 Histology.....	123
5.2.5 Two-Photon Fluorescence Calcium Imaging.....	123
5.2.6 Confocal Imaging.....	123
5.2.7 Determining the DSI Value for Each Cell.....	123
5.2.8 Determining the OSI Value for Each Cell.....	124
5.3 RESULTS	
5.3.1 Monosynaptic Circuit Tracing Method Reproduces Previous Study in WFV-Cre Mice.....	124
5.3.2 Retrograde Tracing from Shell Identifies OS and DS RGC Responses.....	127
5.3.3 Shell-Projecting OS RGCs Encompass hOS and vOS Types.....	132
5.3.4 ON and ON/OFF DS Types Project to dLGN Shell.....	134
5.3.5 Identifying RGC Projections to dLGN Core.....	134

5.5 SUMMARY & DISCUSSION.....	138
CHAPTER VI- SUMMARY, DISCUSSION, & FUTURE DIRECTIONS.....	141
REFERENCES.....	149
APPENDIX A: ABBREVIATIONS.....	165
APPENDIX B: TABLES.....	167
CURRICULUM VITAE.....	169

LIST OF FIGURES

Figure 1.1 Mouse Retina Illustration.....	5
Figure 1.2 Orientation Tuning in Cat V1.....	17
Figure 2.1 Retinal Dissection and Imaging Setup.....	44
Figure 2.2 Two-photon fluorescence image of GCaMP6f-expressing ganglion cells.....	45
Figure 2.3 Population calcium imaging resolves diverse RGC function.....	45
Figure 2.4 Visual Stimulus.....	46
Figure 2.5 Calcium Response Survey and Intra-Experimental Analysis.....	47
Figure 3.1 Experimental Paradigm Schematic.....	62
Figure 3.2 Gallery of Target RGCs.....	63
Figure 3.3 Gallery of RGC Stratification Depth.....	65
Figure 3.4 Immunostaining Against ChAT Used to Quantify Stratification Depth in IPL..	66
Figure 3.5 RGCs show distinct stratification profiles.....	67
Figure 3.6 Stratification Depths of Functionally Identified OS Types.....	68
Figure 3.7 Distribution of targeted OS RGC types identified in this study.....	69
Figure 3.8 Targeted RGCs show a broad range of OS tuning strengths.....	71
Figure 3.9 Orientation Angle Preferences of RGC Groups.....	72
Figure 3.10 Contrast Polarity of vOS Type OS RGCs. RGC contrast polarity (ON/OFF) is readily resolved from the calcium response.....	73
Figure 3.11 hOS Type Contrast Polarity. RGC contrast polarity (ON/OFF) is readily resolved from the calcium response.....	74
Figure 3.12 Distribution of RGC Type Contrast Polarity Preferences.....	75

Figure 3.13 Dendrogram of RGC Functional Responses.....	77
Figure 3.14 Size Tuning Functions of RGC Groups.....	78
Figure 3.15 Temporal Tuning Functions of Identified OS RGC Groups.....	79
Figure 3.16 Imaris Filament and Spine Reconstruction.....	81
Figure 3.17 Quantitative Morphological Analysis of OS RGCs Using Imaris Software.....	82
Figure 3.18 Quantifying OS RGC anatomical features using Imaris.....	84
Figure 3.19 RGC Spine Count.....	85
Figure 3.20 Ellipticity of RGC Arbors.....	85
Figure 3.21 Overview of morphologically identified OS RGC types.....	92
Figure 4.1 Potential Tuning Mechanisms of Orientation Selective Cells.....	97
Figure 4.2 ON hOS I Electrophysiology.....	100
Figure 4.3 ON vOS I Electrophysiology.....	100
Figure 4.4 OFF vOS II Electrophysiology.....	101
Figure 4.5 OFF vOS III Electrophysiology.....	101
Figure 4.6 OFF hOS II Electrophysiology.....	102
Figure 4.7 ON hOS Type I Demonstrates Robust Excitatory and Inhibitory Tuning....	103
Figure 4.8 ON vOS Type I Demonstrates Inhibitory Tuning and Minimal Excitatory Tuning.....	104
Figure 4.9 OFF vOS Type II Demonstrates Matching, Moderately Tuned Excitation and Inhibition.....	105
Figure 4.10 OFF vOS Type III Demonstrates No Distinct OS Tuning Mechanism.....	106

Figure 4.11 OFF hOS Type II Demonstrates No Apparent OS Tuning Mechanism.....	107
Figure 4.12 Comparing OS Tuning Across RGC Groups.....	109
Figure 4.13 Comparison of calcium imaging-based OSI values across RGC types.....	109
Figure 4.14 Orientation Angle Preference Distributions of Physiologically Recorded Cells.....	111
Figure 4.15 Cell Morphology Accurately Predicts Response Kinetics and Contrast Polarity.....	112
Figure 4.16 Dendrogram of identified OS RGC Types.....	115
Figure 5.1 Illustration of the G-deleted Rabies tracing method.....	120
Figure 5.2 Diagram of Monosynaptic Circuit Tracing Method to Identify RGC Projections to dLGN Shell.....	120
Figure 5.3 Diagram of Monosynaptic Circuit Tracing Method to Identify RGC Projections to dLGN Core.....	121
Figure 5.4 Retrograde Tracing in WFV-Cre Mice.....	126
Figure 5.5 USTIM-evoked calcium responses show diverse visual function of WFV- projecting RGCs in WFV-Cre Mice.....	127
Figure 5.6 Retrogradely Labeling Shell-Projecting RGCs.....	129
Figure 5.7 Survey of Shell-Projecting RGCs Identifies DS and OS Responses.....	131
Figure 5.8 USTIM-evoked calcium responses of shell-projecting OS RGCs.....	133
Figure 5.9 Shell-Projecting RGCs Include Diverse OS Types.....	134
Figure 5.10 Distribution of Shell-Projecting DS Cells.....	136
Figure 5.11 Monosynaptic Circuit Tracing to Retrogradely Label Core-Projecting	

RGCs.....	137
Figure 5.12 Core-Projecting RGC Morphologies.....	138

LIST OF TABLES

Table 1 Morphological and Functional Data for Target OS Cells.....	181
Table 2 Shell-Projecting RGC Data.....	182

CHAPTER I GENERAL INTRODUCTION AND LITERATURE REVIEW

1.1 Introduction

Vision is a sensory modality that is critical for most vertebrates to navigate the world around them. Therefore, the study of vision — and understanding the circuitry responsible for translating natural scenes around us in an electrical signal that can be perceived by the cortex — is critical. After a long history of study in cat, rabbit, and salamander, visual studies aiming to understand retinal circuitry shifted to mouse, a genetically amenable animal model. In mice, like in most other vertebrates, light is transduced into an electrical signal at the level of the photoreceptors. The signal is transmitted through retinal circuitry to the output neurons of the retina, Retinal Ganglion Cells (RGCs), and is shaped by inputs from interneurons, amacrine cells and horizontal cells (Demb & Singer, 2018).

Retinal ganglion cells (RGCs) comprise multiple types that form functionally distinct signaling channels that selectively encode visual features. A conserved channel among vertebrates conveys orientation selectivity, i.e., the increased response to elongated stimuli of a preferred orientation. Orientation selectivity is well-studied in central visual areas such as dorsolateral geniculate nucleus (dLGN), Superior Colliculus (SC), and primary visual cortex (V1), but is present already at the level of the retina (Wang et al., 2010; Ahmadlou and Heimel, 2015; Zhao et al., 2013; Piscopo et al., 2013; Suresh et al.,

2016). A calcium imaging survey and cluster analysis of RGCs in mouse identified four clusters with a high proportion of Orientation Selective Ganglion Cells (OSGCs) with multiple orientation preferences, but information on tuning mechanisms and morphology were lacking (Baden et al., 2016). Subsequent studies identified four OS types representing horizontal and vertical orientations (Nath & Schwartz, 2016; Nath & Schwartz, 2017). Cells were investigated for their electrophysiological and morphological properties, but shortcomings in OS cell targeting — such as identifying cells by their light-step response profile — and results of previous surveys suggest that this account of OSGCs is incomplete. Where these cells project is also an open question. While OS cells have been identified in dLGN, no studies have directly tested projections of OSGCs to shell versus core regions of dLGN, and the extent to which OSGCs contribute to orientation tuning in dLGN and other downstream visual areas is unknown. While Orientation Selectivity is a fundamental computation in the visual system, a comprehensive characterization of OSGC types is lacking, the cellular and circuit mechanisms that generate the OS response are incompletely understood, and contributions of OSGCs to subsequent stages of visual processing remain unknown.

In my thesis work, I have aimed to address three gaps in knowledge with regards to retinal OS. The first is the issue of efficiently targeting specific OS RGC cell types for study without molecular markers. The second problem is identifying the underlying mechanisms contributing to the OS response in the mouse model. While in-depth physiology and anatomical analysis have been performed for many cell types, distinct OS types were discovered more recently and few quantitative studies have been done. And the

third issue addressed by this study is that the retinorecipient targets of these cell types are unknown whether known OS and we do not know whether OS is computed locally in central visual nuclei or inherited from retina.

This study uses two-photon fluorescence calcium imaging to survey ganglion cell populations with genetically encoded calcium indicators in *Thy1-GCaMP6f* mice, followed by cluster analysis to identify functional types. With the help of my advisor, I developed an innovative intra-experimental analysis of visually-evoked responses to target OSGCs for detailed study using electrophysiology, and morphological reconstruction. Retrograde trans-synaptic circuit tracing was used to determine retinorecipient targets of OS types.

1.2 Background and Literature Review

1.2.1 Introduction

Retinal Ganglion Cells (RGCs) are the final output neurons of the retina that encode distinct visual features such as direction of motion, contrast, and size. Visual scenes are processed in the coordinated firing of RGCs and transmitted through parallel channels to subsequent visual centers. Our study focuses on the channel that conveys orientation selectivity, i.e., the firing of neuronal cells in response to an elongated stimulus along a preferred orientation. Orientation Selective (OS) cells were first described in cat V1 (Hubel & Wiesel, 1962) and have since been described in multiple vertebrate systems, including rabbit, cat, and mouse (Maturana & Frenk, 1963; Levick, 1967; Hubel & Wiesel, 1968; Niell & Stryker, 2008). OS cells have also been found in thalamic nuclei and retinae of mouse (Piscopo et al., 2013; Baden et al., 2016; Nath & Schwartz, 2016; Nath & Schwartz, 2017). They have been identified in mouse dLGN shell, and projections from orientation

selective ganglion cells (OSGCs) have been linked to dLGN as a possible mechanism of OSGC input to OS tuning in dLGN (Martersteck et al., 2017; Roson et al., 2019). However, while some RGC types have been mapped to specific regions of dLGN, no studies have directly implicated OSGCs as projecting to shell or core regions of dLGN.

Because orientation selectivity is a critical computation in downstream visual centers of mouse and other vertebrates, it is important to understand these cell types and how their orientation tuning is generated. Therefore, it is also important to understand, in the context of this study: the organization of the mouse visual pathway, the importance of RGC classification, the techniques related to RGCs typology, and the significance of a multimodal classification scheme. It is also necessary to understand Orientation Selectivity as a whole, with a focus on the mouse visual pathway. I will review this in the following sections.

1.2.2 Organization of the Mouse Visual System

The retina is a thin (~200 μm) sheet of light-responsive neural tissue in the back of the eye (Figure 1.1). The retina is anatomically layered, comprising three cellular layers separated by two plexiform layers (Sanes & Masland, 2015). The detection of light signals by photoreceptors and the subsequent sampling and filtering of those signals by horizontal, bipolar, and amacrine cells, results in diverse visual encoding at the level of the output neurons, the Retinal Ganglion Cells

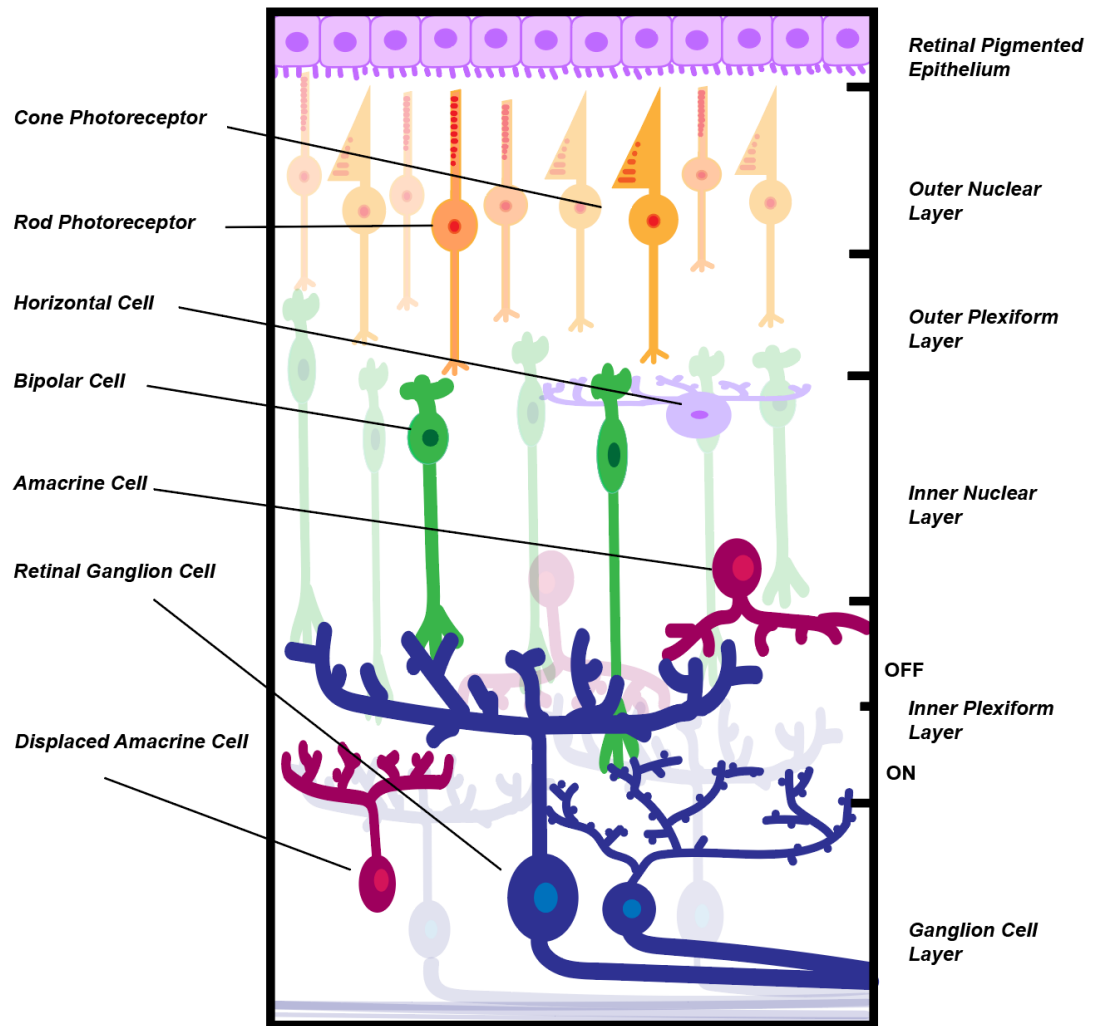


Figure 1.1 Mouse Retina Illustration

(RGCs). The ganglion cell output is then relayed in parallel axonal pathways in the optic nerve to subsequent visual processing regions in central and cortical regions of the brain. The intrinsic and circuit-level computations in the retina are sufficient to result in the selective encoding of complex visual features.

Light passes through the inner layers and is transduced into an electrical signal

when it hits the outermost layer, the photoreceptor layer where the rod and cone photoreceptors reside. Rods and cones differ in their response to light. Rods mediate visual responses in low light — scotopic and mesopic conditions. Cone photoreceptors detect color and function in brighter light, or photopic light conditions (Baylor, 1996). Both photoreceptor types utilize specialized *opsin* proteins called *rhodopsin* to transduce light into an electrical signal. After the opsin absorbs a photon, it initiates a rapid cascade that results in the closing of cation channels in the outer segment, hyperpolarizing the cell and reducing synaptic release at the axon terminals (Purves, 2017). The result is a decrease in glutamate release from the photoreceptor terminals. Photoreceptors tonically release glutamate, but hyperpolarize in response to light.

Photoreceptor signals are sampled by two major cell categories: horizontal cells and bipolar cells. Horizontal cells are GABAergic interneurons that provide inhibitory feedback at the photoreceptor-bipolar cell synapse, suppressing glutamate release from photoreceptors, and generating spatial surround inhibition (Thoreson & Mangel, 2012). The bipolar cells are feed-forward excitatory neurons that sample responses from the photoreceptor layer and relay light signals to the RGCs. 12-15 bipolar cell types split visual information into distinct channels by encoding information such as contrast polarity and response kinetics (Euler et al., 2014; Tsukamoto & Omi, 2017). The assignment of polarity to bipolar cell types stems from their glutamate receptors. OFF bipolar cells have AMPA and kainate receptors — which are opened by glutamate; these bipolar cells hyperpolarize in response to light since photoreceptor cells hyperpolarize in response to light. Conversely, ON bipolar cells are “sign inverting” and have mGluR6 metabotropic receptors. When glutamate binds to these receptors, it leads to the TRPM1 (cation channel)

closing (Morgans et al., 2009). So, the cell depolarizes in response to light. Bipolar cells also convey sustained or transient characteristics; this may arise from the response kinetics of inactivating glutamate receptors and for temporal interactions with inhibitory amacrine cell (AC) circuits.

Bipolar cells synapse in different sublayers of the inner plexiform layer (IPL). The IPL is a synaptic layer that is divided into an inner (ON) layer and outer (OFF) layer, with ON and OFF type responses, respectively. Where the bipolar cells synapse in relation to these layers determines which RGCs and Amacrine Cells they will synapse with (review, Demb & Singer, 2018). RGCs sample bipolar cell inputs through glutamate release in the inner plexiform layer. The RGC response is shaped, in part, by the characteristics of the bipolar cells that they co-stratify with in the IPL, such as polarity and sustained/transient responses. If a ganglion cell stratifies in more than one layer, it can acquire the features of more than one type. For example, a ganglion cell that activates in response to both light increments and decrements would likely be bistratified and sample from bipolar cells in the OFF and ON layers of the IPL. Amacrine cells further shape the RGC response through type-specific connections.

The ability of RGCs to detect complex features arises from the interplay of this excitatory input from bipolar cells and mostly inhibitory input from interneurons. Amacrine cells are broadly split into either glycinergic narrow-field types or GABAergic wide-field types (Zhang & McCall, 2012), with one recently discovered exception — a vGluT3-expressing amacrine cell (Lee et al., 2014). These cells generate context-specific responses such as center surround antagonism and motion detection (review, Gollish and Meister, 2010). They can shape RGC responses through direct inhibition onto RGC neurites,

disinhibition of other amacrine cells, or inhibition onto the terminals of bipolar cells, thus shaping context-dependent excitatory glutamate release onto RGCs. RGC axons carry the feature detecting signals of these output neurons and converge to form the optic nerve which projects to approximately 40 retinorecipient regions (Morin & Studholme, 2014), making up both image forming pathways and non image forming pathways. There have been many studies dedicated to the typology of RGCs, and it is important to have an understanding of RGC typology to give this study context.

1.2.3 Retinal Ganglion Cells

1.2.3.1 RGC Typology

An early finding, and a critical one, in the field of RGC typology was that physiological responses to “ON” and “OFF” light stimuli — light increments and decrements, respectively — could be related to RGC dendritic arbor stratification (or arborization) in the retinal IPL. Initial comparisons of known ganglion cell properties compared against Golgi preparations in cat retina indicated that ganglion cells could be anatomically subdivided by their level of stratification in the sublamina of the IPL (Famiglietti & Kolb, 1976). Subsequent studies of cat RGC light responses using light stimulation followed by intracellular dye injection demonstrated that cells discharging in response to an OFF stimulus stratified in the outer half of the IPL termed “sublamina a” and cells responding to an ON stimulus stratified in inner half of the IPL, “sublamina b” (Nelson et al., 1978). Thus, arborization of ganglion cell dendrites in the IPL could inform whether their receptive field had an On or OFF center response.

Another major milestone in RGC classification was the discovery of an

organization scheme called the “tiling principle” was. This term was coined by Boycott & Wässle (1981) and variations of the tiling principle to validate cell types are still widely used today. Boycott and Wässle theorized that ganglion cells must cover the retina with their dendritic fields sufficiently so that any given point in the visual field was accounted for. Boycott and Wässle stained for the “alpha” ganglion cell and observed cell bodies arranged in a regularly spaced mosaic. Gaussian analysis of their “nearest-neighbor distribution” demonstrated that this tiling effect was nonrandom (Boycott & Wässle, 1981). Essentially, the tiling principle states that true cell types’ dendritic fields will have a fixed amount of overlap in the ganglion cell layer (Borghuis et al., 2008). As a classification technique, this is a useful way to verify that a categorized cell is a true type. For example, Nath & Schwartz (2017) discovered somas of two orientation selective ganglion cells in close proximity, which defied the tiling principle. This instigated further investigation into the physiological and morphological properties of the cells, which demonstrated that, indeed, they were not of the same type and, in fact, exhibited unique functional characteristics.

Uniform physiological properties are a major indication of an RGC type. Early work with recording electrodes in cat retina distinguished RGCs that respond preferentially to either an increment or decrement in light stimuli, respectively known as “ON-center” and “OFF-center” types. They found that ON, OFF, or ON-OFF discharges could be obtained from one ganglion cell if specific areas within its receptive field were stimulated with small spots of light (Kuffler, 1953). This was a first step at classifying RGCs into functional types in the mammalian retina. In 1966 a survey of ganglion cells via electrophysiological recordings in rabbit yielded cell types with more complex receptive

fields such as “orientation-selective” cells, “local-edge-detectors”, and “uniformity detectors” (Levick, 1967). Because functional information on ganglion cells provides such valuable insights for the encoding of visual features, studies classifying functional RGC types are important for understanding the full complement of visual encoding that is available to the CNS. Unfortunately, older studies on physiology yielded small datasets due to the laborious process of auditory evaluation of responses and manually manipulated stimuli. Compared to studies classifying morphology, RGC physiology studies have been a fairly low-throughput enterprise and, therefore, progress on that front has been slow by comparison.

Optical imaging methods using genetically encoded bulk electroporation of calcium indicators offer a powerful, high-throughput alternative to the study of RGC receptive fields. A study by Baden et al. (2016) used bulk electroporation of a calcium indicator Oregon-Green BAPTA-1 to nearly completely stain the ganglion cell layer and resolve functional responses of the labeled population with two photon calcium imaging. They recorded light-evoked responses in over 11,000 cells and split the cells into types using an unsupervised clustering method. The results of the study yielded two to three times the anticipated number of functional types in the retina, each with a distinct combination of characteristics representing a range of preferred stimuli such as: response polarity, receptive field size, frequency tuning, and contrast sensitivity. Thus, optical imaging has been paramount in uncovering new functional types. The vast library of responses produced in the Baden study provided a reference for future work on ganglion cells. High-throughput studies help researchers circumvent issues in classification that arise due to bias and under-sampling. Subsequent large scale studies on physiological, morphological, and genetic classification have further accelerated the study of RGC types (Bae et al., 2017;

Rheume et al., 2018).

Another milestone in RGC classification is the completion of a digital “museum” of RGCs using 3D electron microscopy (EM) to determine RGC morphology after determining functionality with calcium imaging (Bae et al., 2018). The combination of these two methods produced a dense sample of ganglion cells with groundbreaking coverage of anatomy with information on functionality. Previous large-scale morphological surveys had been performed, but did not include information on visual functionality (Sümbül et al., 2014; Völgyi et al., 2012). The survey by Baden et al. produced 47 clusters of RGC types based on morphological criteria. They also revealed new ways to organize the retina based on the anatomical information they gathered; they determined that the optimal way to divide the IPL is to separate the IPL by two marginal sublamina flanking a central sublamina. The study also proposed an alternative to the tiling principle that Boycott & Wässle conceived. Based on their large dataset of morphological types, they proposed a “density conservation” principle. The new conservation principle suggested that dendritic arbors of a true type should be approximately uniform across the retina, and allowed for a certain degree of overlap. Using the density conservation principle — and comparing clusters to “securely known types” from previous studies — they reported a total of 35 cell types, which is consistent with the findings of Baden et al. (2016).

For a more complete classification of ganglion cells, knowledge of projections to downstream visual centers can provide hints at ganglion cell classification. Knowledge of central projections is also necessary for understanding how each ganglion cell type contributes to visual processing in the midbrain and cortex. Axons of RGCs carry information about specific visual features in “parallel” pathways and project to laminar-

specific areas in downstream vision processing centers (Seabrook et al., 2017). Retinorecipient targets include the dorsal lateral geniculate nucleus (dLGN), which relays information directly to primary visual cortex (V1), and the superior colliculus (SC), which drives non-image forming functions but also signals to the cortex through the lateral posterior nucleus (LP) or dorsal lateral geniculate nucleus (dLGN) (Seabrook et al., 2017). Specific computations occur in different sections of circuitry to produce tuning for specific visual features. Martersteck et al. (2017) aimed to create a comprehensive map of retinal projections using Cre driver mice — with selective gene recombination to express fluorescent proteins in neuronal subpopulations. They were able to map RGC connections to dLGN and SC in Cre-defined RGCs. Results of the study confirmed specific termination patterns of alpha RGCs and ON/OFF directionally selective RGCs (ON/OFF DSGCs or ooDSGCs) in the dLGN and SC. The connectomics map is available for other researchers to access in the Allen Mouse Brain Connectivity Atlas. This study was significant because it provided insight into how information is distributed by the retina and provided a resource by which other researchers could investigate central signaling. A subsequent study sought to characterize the population of dLGN projecting RGCs and compare them against neurons in the dLGN. After measuring calcium signals in response to full-field stimuli they determined that the majority of previously identified RGC types project to dLGN. They also observed a wide diversity of dLGN responses, similar to that of the diversity of retinal ganglion cells (Román Rosó et al., 2019).

The advent of genetic labeling strategies has been critical in RGC research. They allow for targeted recording and selective manipulation of specific types by live imaging, silencing, optogenetic stimulation or ablation. They also provide valuable insights for refining classifications of previously documented types. A great accomplishment in terms

of genetic classification was the single cell transcriptome profiling of over 6000 RGCs by Rheume et al. (2018). Cells were sorted into 40 subtypes with the use of a clustering algorithm, matching the number of categories based on functional classifications (Baden et al., 2016). The study produced a hierarchy of RGC types that could then be further split into subtypes, some reflecting known specializations, for example, the link between molecular marker ISP 1 and ooDSGCs. The study demonstrated the extent of gene expression necessary for subtype separation. They also created a website for analyzing and comparing gene expression profiles in RGC subtypes (Rheume et al., 2018). Further investigation into how the genetic markers discovered in this study link with known RGC types will be crucial in establishing true and objective RGC classifications.

Combining genetic classification with other modes of classification has proven to be another successful method for RGC classification. Smbl et al. (2013) approached the categorization of RGCs with a combination of genetic and structural parameters. They clustered cells based on their dendritic arbor geometry and validated them by molecularly defined cell types. This sorting method was demonstrated to be both precise and reproducible, with ramifications for typology based on multiple parameters.

Innovations in studies of RGC classification have propelled the field of RGC typology. Effective strategies for unambiguous classification of RGCs will likely require a multimodal approach to unify independent classifications based on morphology, function, or gene expression. While there is not yet a complete consensus on what defines a cell type, continued innovation of techniques and investigation of RGCs will be necessary for a complete inventory of cell types and how they contribute to visual processing.

My project has been innovative because it combines cluster analysis of large scale functional GC surveys with targeted physiological and morphological investigation. I used intra-experimental analysis of light-evoked responses from two-photon calcium imaging and compared those with my library of imaged cells to selectively investigate functionally identified types while the tissue is alive and available for further investigation. This method of targeting cells resulted in a robust analysis of physiological and morphological properties for cell types of interest. The approach offers a major advantage over ‘blind patching’ (recording unaided by fluorescent markers) and circumvents the issue of not having a transgenic line. It prioritized visual function as a determining criterion of a type. The results that my project has generated demonstrate the effectiveness of this approach in targeting cells.

1.2.3.2 The Importance of Classifying Retinal Ganglion Cells

There are several reasons why a complete typology of retinal ganglion cells is important. First, systematic classification of ganglion cells into identified cell *types* is necessary for reproducibility; we cannot study a cell type repeatedly without a working definition of what that type is. Continuity of categorization allows researchers in different labs to know that they are investigating the same cell type. Proper identification of cell types for repeated study is also requisite when determining circuitry, because to understand a circuit we must be able to specify the “parts list” that composes it. Certain modes of classification can also advance techniques for future research. For example, molecular classification of RGCs has provided access to genetic strategies that can be used to mark and manipulate a specific cell type for study (Sanes & Masland, 2015).

RGC typology is clinically relevant as well. There is increasing evidence that RGCs are differentially susceptible to optic diseases (Santina et al., 2013, 2017; Ou et al., 2016). A 2016 study on the effects of transient ocular hypertension in mouse retina revealed selective vulnerability of specific RGC types to cell death (Ou et al., 2016). This study contributed to the emerging consensus that “OFF” RGC types seem to be more susceptible to intraocular pressure elevation than “ON” RGC types. Another study using a glaucoma mouse model described that different RGC types had varying structural, functional, and temporal responses to IOP elevation (Santina et al., 2013). A better understanding of the mechanisms contributing to this selective vulnerability in RGC types could lead to improved strategies for neuroprotection in retinal diseases. Furthermore, identification of protective factors could be expedited by knowledge of RGC typology based on molecular criteria. Thus, a comprehensive understanding of the types of RGCs that exist is a necessary and pressing first step in approaching these clinical issues.

Understanding the complete inventory of RGC types also has implications for the study of visual processing in downstream nuclei. Until orientation selective cells were discovered in the retina and dorsal lateral geniculate nucleus (dLGN), this computation was thought to arise within the cortex. Thus, the discovery of novel RGC types altered the working model for tuning in other visual centers. Furthermore, categorization schemes developed for the retina can be used to classify other cell types in the brain. The effectiveness of hierarchical clustering methods in the retina can be vetted by adding more parameters to the classification. Fine-tuning these classification methods in the relatively accessible retina with clearly defined input and output stages will be useful tools for neuron classification in the brain. A systematic characterization of retinal ganglion cell types is necessary for understanding the mechanisms of their encoding, understanding their

embryonic and postnatal development, and understanding evolution and conservation of cell types within and across species.

1.2.4 Review of Orientation Selectivity

There are many visual features that are ubiquitous across species, such as direction selectivity, contrast polarity, and orientation selectivity. Orientation Selectivity appears to be a highly conserved computation that has been documented across invertebrate and vertebrate models. OS has also been observed at multiple stages of the visual processing pathway in many vertebrates. To best understand and study this computation, it is important to understand orientation tuning at the earliest stages of orientation tuning — the retina. It is also important to understand what the central targets of the specialized cells that generate this response project to, and start making inferences about the degree of tuning that is either directly inherited from retina or computed *de novo* in subsequent visual processing centers, e.g., the dorsolateral geniculate nucleus (dLGN), Superior Colliculus (SC), and Primary Visual Cortex (V1). In the following sections, I will give the most up-to-date account of what is known about orientation selectivity, with a heavy focus on orientation selectivity in mouse.

1.2.4.1 Early Observations of Orientation Tuning

The earliest observation of orientation selectivity was described by Hubel and Wiesel in 1962. In this study, they used microelectrode penetration of cat primary visual cortex to investigate functional activity. They discovered that there was a subset of cortical cell types that responded preferentially to a “slit” of light, with the orientation of the slit

being critical for cell firing. They noted an increase in firing when the slit of light was moved steadily across the visual field. They also noted significant *reduction* in the response when the orientation angle was moved by just 5-10° in either direction (Figure 1.2). These cortical cell types demonstrated preference for either vertical, horizontal, or obliquely oriented stimuli, with a similar percent incidence for all preferred orientations. This description of a cell with both a preferred and non-preferred stimulus orientation was the first observation of what we now know to be Orientation Selectivity (OS).

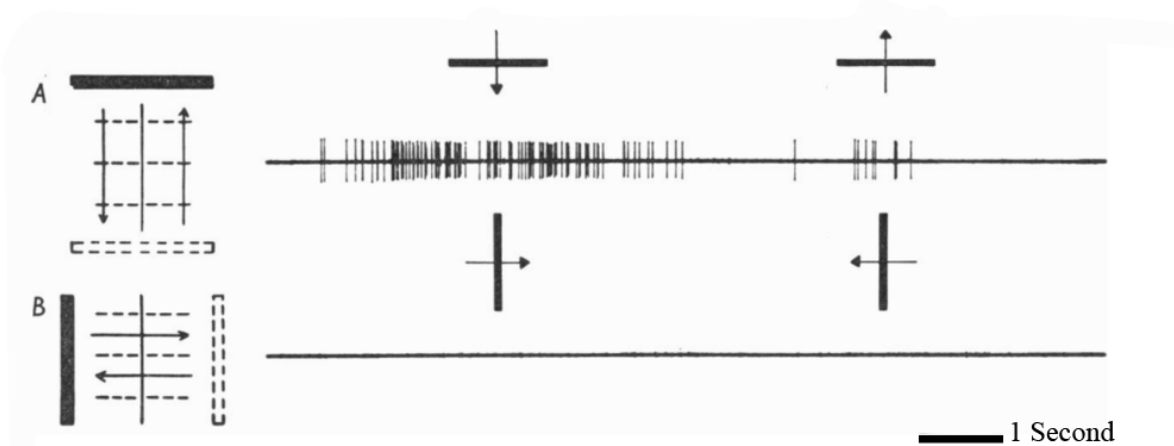


Figure 1.2 | Orientation Tuning in Cat V1. Adapted from Hubel & Wiesel (1962). Movement of a black rectangle $1/3 \times 6^\circ$ back and forth across the receptive field, (A) horizontally oriented (parallel to receptive-field axis) and (B) vertically oriented.

Shortly after the discovery of orientation selectivity in cat V1, OS was reported in pigeon retina. Maturana and Frenk (1963) recorded from individual retinal ganglion cell

axons in pigeons using micropipettes. They noted a maximum response in cells they called “horizontal edge detectors” — accounting for approximately 5% of recorded cells — when a horizontally-oriented bar was moved “vertically up or down across the receptive field”. The response was significantly reduced when the angle of the bar was changed by 20-45%.

Early studies implicated OS in the retina of other animal models as well. Levick et al., (1967) recorded ganglion cell function in rabbit retina. When they presented an elongated, rectangular stimulus, they observed cell types that responded preferentially to a bar that was oriented horizontally, moving upward or downward along a vertical axis of motion. They observed no response when the bar was oriented vertically and moved in a nasal or rostral direction. Like the study by Maturana and Frenk, they also observed that there was firing in response to the horizontal bar moving horizontally across the visual field. This indicated that, in both studies, the preference was indeed for the orientation of the bar, not the axis of directional movement. Levick observed cell types with a preference for either horizontal or vertical orientations, which is consistent with previous and subsequent reports of cardinal orientations being represented in studies of orientation selectivity. This study was the first to classify these cell types as “Orientation-Selective”. Already, these early studies led researchers in the field to speculate that there may be a mechanism for an inhibitory effect from an antagonistic, asymmetric surround.

OS has also been identified in the retinas of predatory mammals. Levick and Thibos (1980) reported cells in cat retina with a bias toward horizontal or vertical orientations. They noted an ideal spatial frequency which yielded a maximum response when presented at the preferred angle of the drifting grating stimulus. They also noted that there appeared to be “patches” of orientation-selective cells with a bias towards a particular orientation in

a given patch of tissue. This indicated some level of retinotopic organization that occurred with regard to OS cells in the cat retina.

1.2.4.2 Orientation Tuning is Highly Conserved Across Species

The apparent conservation of the OS computation across the aforementioned vertebrate species is highlighted by the incidence of orientation selectivity observed even at the level of insects (Fisher et al., 2015). In drosophila, visual information is passed from the photoreceptors to interneurons in the lamina, where information about direction of moving stimuli is already processed. Neurons link laminar cells with T4 and T5 neurons, which go on to innervate specific regions of drosophila called the medulla and lobula. To investigate the occurrence of OS, the group performed two-photon calcium imaging of T4 and T5 neurons to evaluate motion and orientation computations in the drosophila visual system. To investigate the responses of these neurons, they expressed a calcium indicator in T4 and T5 cell types and used two-photon calcium imaging to record from cells in response to moving stimuli. They used drifting gratings to test whether there was orientation tuning present at the output of these cells. They observed a layer-specific organization of cells with preference for vertical or horizontal orientations. To test the underlying mechanisms responsible for orientation tuning, they applied picrotoxin to block inhibitory chloride channels. They noted a marked reduction in the amplitude of orientation tuning under these conditions, indicating that inhibition was critical in generating the antagonistic surround necessary to create an orientation-selective response in T4 and T5 cells.

In the previous section, I described orientation tuning in higher order vertebrates, such as mouse, cat, and rabbit. There is evidence to suggest that RGCs in the retina of primates, too, selectively encode oriented stimuli. In 2002, orientation selectivity was reported at the level of the retina in the macaque model (Passaglia et al., 2002). Ganglion cell responses were recorded extracellularly from anesthetized animals. In the study, they noted elongated receptive field centers with preference for oriented bars moving along a particular axis of motion. They noted that the degree of orientation tuning was higher in cortical neurons than retinal neurons when compared with available studies.

The incidence of orientation tuning across species indicates that orientation tuning is a widespread computation amongst species. Because the computation appears to be a critical and conserved visual feature, it is important to investigate the mechanisms contributing to the tuning of these cell types.

1.2.4.3 Proposed Tuning Mechanisms for OS in Retina

Early studies lead researchers in the field to hypothesize that there was a mechanism for OS that included an asymmetric, inhibitory surround. Predictions about the tuning mechanisms for orientation selective ganglion cells were tested in rabbit by Venkataramani & Taylor (2010). They identified ganglion cells selective for horizontal and vertical orientations and targeted them for analysis of their inhibitory and excitatory inputs. They reported that a combination of tuned inhibition and excitation was responsible for shaping the orientation selective response. Through pharmacological perturbation, they identified GABAergic inhibition onto OS ganglion cells as the mechanism for tuned inhibition. For tuned excitation, they reported that inhibition of glutamatergic bipolar cells

via presynaptic GABAergic inhibition, and serial inhibition by glycinergic ACs was responsible.

There is evidence to suggest that OS tuning is not just generated at the level of RGCs, but even earlier in the visual pathway. If this were true, the tuning of OSGCs might not only be generated from integration of synaptic contacts generating OS, but may also be inherited from orientation-tuned amacrine cells. Bloomfield (1991) identified amacrine cell types in rabbit that displayed highly elongated, oriented dendritic arbors that corresponded with their preferred angle of stimulus orientation. Antinucci et al., (2016) identified elongated amacrine cells in zebrafish with a preference for oriented stimuli, and Nath & Schwartz identified OSGCs in mouse that were electrically coupled to highly elongated amacrine cells (Nath & Schwartz, 2017).

Nath & Schwartz (2016) were the first to describe orientation selective RGCs (OS RGCs) as a discrete type in mouse. They identified unique physiological properties and reported on cell morphologies. They discovered both ON and OFF OS RGCs representing vertical and horizontal orientations. Like in prior OS studies, these cells are described as firing action potentials in response to their “preferred” orientation, and show inhibition when presented with the non-preferred or “orthogonal” orientation. OS tuning could arise through 1) an asymmetric sampling of bipolar cell contacts with an elongated arbor. 2) Tuned excitatory glutamate release from bipolar cell terminals. 3) Tuned inhibition as a result of synaptic contacts with amacrine cells. In an OS cell, we would expect some combination of these features to be at play.

To determine the cause of tuning, whole-cell voltage clamp recordings were used to isolate excitatory and inhibitory currents. They noted that the reported OS RGC types

had excitatory currents tuned to the cell's preferred orientation. However, whereas ON OS horizontal RGCs (hOS) in mouse have inhibitory currents tuned to the orthogonal direction, all other OS RGCs — ON vertical OS RGCs (vOS) and OFF vOS and hOS RGCs — receive inhibitory inputs that are not tuned to orientation. Nath and Schwartz suggested that there is a level of redundancy among the synaptic mechanisms that shape the orientation tuned response. Blocking either GABA or glycine receptors did not change the orientation tuning but blocking both types completely abolished inhibitory currents and did not affect excitatory currents. The group also demonstrated that OFF OS RGCs acquire some level of tuning from electrical coupling to orientation-selective amacrine cells through a series of pharmacological and anatomical experiments (Nath & Schwartz, 2017). Nath & Schwartz (2017) also reported highly asymmetric amacrine cells coupled to OFF vOS RGCs. AC's elongated dendritic arbors indicate that their morphology may play a role in their orientation tuning, as they could derive their orientation selectivity from the asymmetric sampling of the bipolar cell mosaic.

While the previous OS studies carried out in mouse were detailed in their analysis, it is possible that potential OS types were left out due to the sampling method of blindly patching and targeting cells via their light-step profile. A targeted approach using broad labeling optical methods and unsupervised clustering to determine the functional responses before reconstructing morphologies should yield substantial sample sizes while limiting bias that may occur when patching at random.

1.2.4.4 Organization of Orientation Selective Cells in Central and Cortical Regions

Hubel and Wiesel (1967) recorded from the striate cortex in macaque and spider monkeys. They described columns of cells with similar preference for orientation of a stimulus, like the ones they observed in cat primary visual cortex. They described cells that responded maximally to the specific orientation of a slit, and decreased firing in response to the opposing angle. They made an interesting observation that, in spider-monkey, there was a very specific organization of the orientation-selective cells in columns. At incremental depth of recording, there were regular shifts in the orientation preference, demonstrating what appeared to be a “counter-clockwise” motion of change occurring over about 10-15 cells-worth of depth before completing a total rotation. This study highlights a particular cortical organization for orientation selective cells in the striate cortex of primate. In several species, and across central processing areas and cortex, there have been incidences of topographical organization of orientation selective cells.

Two types of orientation-selective inputs were observed in zebrafish in a study by Nikolaou et al. (2015). In this study, they recorded the visually evoked activity of RGC axons at the level of the tectum. They used a genetically encoded calcium sensor (SyGCaMP3) to measure activity at the level of presynaptic boutons; they performed population level imaging to determine the preference of the cell inputs to tectum and their distribution across this central visual processing region. When they presented drifting bars, they found cells selective for either the horizontal or vertical orientation. They also noted that there was a specific distribution of these orientation selective inputs across the zebrafish tectum. Inputs from cells with a preference for the vertical orientation were predominant in the posterior region of the tectum, and horizontal responses were concentrated in the anterior region. Recent studies in mouse have also highlighted an

apparent organization of OS in a central visual processing region (Piscopo et al., 2013). They have identified a bias in OS cells towards the “shell” region of the dLGN. Those studies, along with studies describing the organization of mouse SC, will be described in greater detail in a later section of this chapter.

1.2.5 Orientation Selectivity in the Mouse Visual Pathway

OS in mouse has been observed in multiple processing areas along the visual pathway, including V1, SC, dLGN, and retina (Neill & Stryker, 2008; Ahmadlou and Heimel 2015; Zhao et al., 2013; Nath & Schwartz, 2016). The following sections will summarize what is known about OS tuning in mouse. There is still debate as to how much orientation tuning is inherited from retina versus what is computed *de novo* at each visual processing region after the retina. Although the degree of tuning inherited from retina is not known, some studies have already begun pointing to a synaptic organization that involves the sharpening of OS tuning along the visual pathway. The review will start with the earliest observation of OS tuning — in the primary visual cortex — and work towards the most recent observation of OS tuning at the beginning stage of the mouse visual pathway — the retina.

1.2.5.1 Orientation Selectivity in Mouse Primary Visual Cortex (V1)

Due to their smaller brain volume, mice have less cortical ‘real estate’ for visual processing, and concomitant decreased visual acuity compared with primates. However, presented with bars of varying orientations, cortical cells that were highly selective for particular stimulus orientations have been found during extracellular recordings of mouse

V1 (Neill & Stryker, 2008). Organization specific to OS cells was reported as well, including a reported change in preference of orientation across layers of the visual cortex, with more incidences of finer tuning and a higher OSI value in the more superficial layers (Neill & Stryker, 2008).

1.2.5.2 Orientation Selectivity in Mouse Superior Colliculus (SC)

Orientation Selectivity was reported in mouse Superior Colliculus by Wang et al., (2010). The author presented drifting gratings and recorded from cells in the superior colliculus. They found neurons with a high degree of orientation selectivity. They continued to report orientation selectivity with cortical lesion, indicating that this computation is not due to feedback from the primary visual cortex. Ahmadi and Heimel also (2015) recorded responses of neurons in the Superior Colliculus. They noted that, with a single penetration at different depths, neurons preferred the same orientation. This is juxtaposed to findings in cat and primate visual cortex, where the orientation preference incrementally changed to eventually complete a full rotation with increased depth in SC. They noted that different orientations were nearly equally represented across the SC in these columns. Pharmacological silencing of V1 did not result in reduction of orientation tuning in the SC. They also observed no change in orientation tuning when they presented a static grating compared to a moving one, indicating that these cells are in fact orientation selective, not axial motion-selective.

These findings were corroborated by another study that found orientation columns in mouse SC (Feinberg & Meister, 2015). To study the organization of the mouse SC, Feinberg & Meister used calcium indicator GCaMP6s and recorded cellular responses with

two-photon fluorescence microscopy. Imaging across the superior colliculus at varying depths, they reported that patches of cells across the SC were similar in orientation preference, and that in the same area at different depths cells were more likely to share similar orientation preference than they would by chance. Different “columns” were found to have significantly different preferences for orientation. This study, and the one described previously, are interesting observations of OS cell organization, because they are similar to those described as OS in the cortex of larger mammals such as cat.

1.2.5.3 Orientation Selectivity in Mouse dLGN

Orientation-selective responses have also been found in the mouse thalamus, specifically the dLGN. To identify visual features present at the level of dLGN, electrophysiological recordings were performed in mouse dLGN which demonstrated the incidence of orientation-selective responses in this region (Zhao et al., 2013). Zhao et al., used Muscimol to selectively silence the visual cortex, thus removing potential for feedback and isolating the responses to those computed within the dLGN or inherited from retina. They noted a range of orientations from vertical to horizontal, with a preference for vertical orientations. They also noted that, when compared to V1, the degree of orientation tuning is sharper in V1 than in dLGN. They noted that 60% of the cells recorded from dLGN had an OSI value over .33 (Zhao et al., 2013). Marshel et al., (2013) observed that orientation selective cells in dLGN were biased to the “shell” region. They used two-photon calcium imaging in the superficial layers of mouse dLGN and electroporated OGB, a small molecule calcium indicator, before presenting drifting gratings. With this

population level imaging they could correlate response type with anatomical location in the dLGN. They reported cells selective for axial motion at a single orientation of the grating.

Piscopo et al., (2013) used multisite extracellular recordings to probe for direction and orientation selectivity in the dLGN. Their study indicated that there was a functional separation of cell responses in the dLGN. Direction and Orientation selective responses were biased to the posterior and dorsolateral dLGN.

There is evidence already to suggest that some level of orientation tuning is inherited from retina in the rodent model. A study by Suresh et al., (2016) looked at tuning of retinogeniculate inputs and thalamic neurons in response to drifting grating stimuli. They identified receptive fields of cells that were elongated and corresponded with their preferred axis of orientation. They reported that Excitatory Postsynaptic Currents (EPSCs) had similar characteristics to previously described retinal inputs. They determined that tuning was sharpened by suppression at the level of the dLGN. It is reasonable to suspect that some degree of tuning is inherited from retina, considering there have been multiple OS ganglion cell types reported in the mouse model.

The synaptic organization of the mouse dLGN and how it relates to the retina will be described in greater detail in Chapter V.

1.2.5.4 Orientation Selectivity in Mouse Retina

Orientation selectivity was originally thought to be computed at the level of V1, with the thalamus serving simply as a relay between the retina and the cortex. The previous section described instances of OS tuning in dLGN, indicating that it is not merely a relay, but a region of visual processing that performs its own computations to further filter the

visual input received from retina. There was speculation as to whether or not the dLGN was where OS was first computed in rodent, but several studies have documented the occurrence of OS in mouse retina, identifying discrete types with specific mechanisms of tuning to create the OS response.

One of the earliest reports of OS in retina came out of a large-scale microelectrode array by Pearson and Kerschensteiner (2015). They surveyed ganglion cells in the mouse model and described functional responses to different light levels. They observed orientation selective responses of RGCs and noted that orientation selectivity was maintained across different light levels. However, this study did not describe individual OS types.

A major study contributing to the typology of ganglion cells in mouse, including orientation selective cells, was the large-scale calcium imaging survey performed by the Euler group (Baden et al., 2016). They obtained dense recordings of retinal ganglion cells by electroporation of a small molecule calcium indicator — Oregon-Green BAPTA-1 (OGB-1). They used a moving bar to probe for direction and orientation selective cells. The group used an unsupervised clustering approach to group a net of 11,210 recorded cells into functional types. Four types which they named $G_{1, 14, 17, 30}$ contained a higher proportion of Orientation Selective cells than other types. Within each type, the OS cells could be further subdivided by their angle of preferred orientation. For example, the G_{14} type included cells with preferences for vertical and horizontal orientations, and the G_{17} type included “many” preferred angles of orientation. They reported that the OS types could be further split when presented with additional stimuli.

Orientation Selective ganglion cells were recently described as a discrete type with a dedicated OS circuit in mouse retina (Nath & Schwartz, 2016). They screened the ganglion cell layer for light response properties, then targeted cells for further study based on their light response profile. They used flashed bars of different orientations and reported a high proportion of cell responses (over 93%) with an orientation selectivity index (OSI) value over 0.2. They were able to divide the ON orientation selective cells into vertical and horizontal-preferring types. Both types demonstrated bistratified dendritic fields. The ON hOS type demonstrated an elongated dendritic field, while the vOS type was more symmetrical. They used whole-cell voltage clamp to assess the inhibitory and excitatory contributions to the OS tuning. They reported both tuned inhibition and excitation in the ON hOS RGC. The ON vOS type exhibited tuned excitation but inhibition was not tuned to the orthogonal orientation.

Nath and Schwartz identified OFF OS cells in a separate study (Nath & Schwartz, 2017). Here, too, cells were surveyed in cell-attached mode and targeted based on their light response profile. The authors used drifting gratings to measure cell responses to orientation and direction. They identified a subset of OFF cell types with a specific light response profile that were selective for orientation, with over 95% of those cells having an Orientation Selectivity Index (OSI) value over .2 — with OSI being the value assigned a cell based on the relationship between the summed responses of the preferred orientation and the summed responses of the null orientation. They determined that this group could be further subdivided into an OFF horizontal preferring OS type (OFF hOS) and OFF vertical preferring type (OFF vOS). They noted that the morphology of the OFF vOS cell matched that of previously reported JAM-B RGCs, with characteristic, highly asymmetric dendrites.

The OFF hOS cells had more symmetric dendritic fields. However, there were discrepancies within these types, with some vOS cells having symmetric dendrites. They noted amacrine cell coupling to the OFF vOS cells. They reported tuned excitation in both types, while inhibition was not tuned. The electrophysiological properties of known OS types and potential OS types will be described in greater detail in Chapter 3.

In mouse, OS has been reported as early as the level of retina, with OS additionally being described in dLGN, SC, and V1. While some studies have investigated underlying mechanisms for OS types in retina, there is still much room for improvement on what we know about how this visual feature is computed. Because there are no molecular markers for OS types, and thus limited opportunity to use Cre reporter lines to identify projections, we also do not know the location of downstream targets of OS RGCs. Filling this gap would help move the field forward and ultimately contribute to what we know about the complete circuitry of visual OS. Advanced knowledge of OS in mouse would also allow for greater comparison amongst species and provide insight into how this computation emerged.

1.2.6 The Need for Innovative Methods to Investigate Orientation Selectivity in the Retina

The study by Baden et al., (2016) identified four clusters with a high proportion of orientation selective cells and, within two of those clusters, could further divide the cells into types based on their preference for vertical or horizontal orientations. If this were true, this indicates then that the study performed by Nath and Schwartz cannot be the complete

account of the orientation selective cell types in the mouse retina. The method used by Nath & Schwartz to probe for orientation selective cells in the retina was limited based on the method of identifying cells by light response profile. Therefore, it is likely that the light response profile for *all* OS types is not yet known, meaning OS types could be left out of their more detailed study. We developed a method of identifying OS cells based on a combination of their light step profile, oriented drifting grating response, flicker response, and white noise response. We used this to perform a calcium imaging survey of ganglion cells. We anticipated a robust typing of OS cells, with little potential for any to be left out. Thus providing a comprehensive way of targeting OS cells for study.

It is necessary to employ a multimodal method for investigation of ganglion cell types, since there appears to be functional and morphological diversity within many well-described “types”. So, our paradigm targeted OS cells for morphological investigation as well as electrophysiology. Since the downstream targets of OS cell types in mouse are unknown, we also investigated the projections of these cell types to dLGN, a region of the mouse visual system that has been reported to have orientation selective responses.

1.4 Summary of Chapter I

A multimodal classification of OSGCs is a step toward complete categorization of cell types in the retina, which is a central goal in retinal neuroscience research and a requirement to resolve retinal circuitry and function. Since RGC types are differentially susceptible to disease, a comprehensive account on retinal typology is also translationally relevant.

This project utilized a combination of advanced techniques for a comprehensive characterization of OSGCs to provide insight into the tuning mechanisms of these cells and how they contribute to visual processing in downstream visual areas. It is our hope that information on how retinal OS relates to OS in the rest of the visual system will be a valuable resource to the field of visual neuroscience.

CHAPTER II FUNCTIONAL IMAGING AND DEVELOPING AN INTRAEXPERIMENTAL ANALYSIS METHOD

2.1 Introduction

There has been a long-standing debate as to what combination of parameters are sufficient to define an RGC type. Cells within a given type may be homogeneous in one property but unique in another, does that mean they must be divided into subsets? Discrepancies between the number of different types reported across studies has driven innovation in research to resolve them. To achieve the first goal of this study, it is important to have an in-depth understanding of RGC typology and why there is a need for updated and innovative classification methods.

2.2 Background

When Farrow and Masland (2011) performed a physiological survey of RGCs in mouse retina with microelectrode array recordings, they sorted the RGCs into 12 functional types. However, morphological classification studies around the time Farrow & Masland conducted their physiological survey varied between approximately 10 types and 22 types (Kong et al., 2005; Völgyi et al., 2012). Connectomic studies demonstrated that projections from mouse retina are received by more than 40 retinorecipient brain regions (Morin & Studholme, 2014) — suggesting that there could be as many as 40 RGC types.

Historically, there have been attempts to correlate functional, anatomical, and genetic types, but there have been inconsistencies in classification. These discrepancies have catalyzed further investigation to bridge the gaps. For example, a physiological survey may only produce 12 types because the visual stimuli was not sufficiently diverse to resolve every possible response, potentially obscuring functional differences. Using other modes of classification could inform the separation of those cells into more faithful types.

The Baden group cited these discrepancies in classification and the high number of retinorecipient targets as a reason for seeking a high-throughput, comprehensive classification of functional RGC types. They used bulk electroporation of a fluorescent calcium indicator (OGB-1) to record light-evoked activity in a nearly completely stained ganglion cell layer in mouse (Baden et al., 2016). This study produced over 30 functional types, including novel cell types that had not been previously described. This study was groundbreaking because up to this point it was assumed that there were approximately 15-20 functional channels carrying information about distinct features to the brain; this study revealed that there were more than 30. This contributed to a deeper understanding of RGC classification and provided a wealth of information for other retinal neuroscientists to utilize in their studies.

A second issue in RGC typology is that even when there are thoroughly described cell types, the use of different methods of classification, and inconsistencies and gradients within a defined “type” can cause even more confusion. Bipolar cells have been nicely divided into clear, reproducible types by converging sets of morphological, physiological, and molecular data (Masland, 2013). In an ideal world, molecular, morphological, and physiological parameters would produce the same types in RGCs, but varying modes of

classification have been consistently misaligned. Indeed, even under ideal circumstances where thorough studies produced large datasets and reproducible types within each parameter, eventual harmony between the types is not guaranteed.

A well-studied RGC type that provides an excellent example of heterogeneity within a type is the directionally selective ganglion cell (DSGCs). ON-OFF DSGCs are ganglion cells that fire in response to light increments or decrements and respond preferentially to directional motion. Based on purely morphological criteria, these bistratified cells have homogenous dendritic geometries and would be classified as a single type if additional parameters were not examined. Each of these cells also express the same neuropeptide, CART, which distinguishes them from non ON-OFF DSGC types. If they were to be classified by molecular and morphological criteria, they alone may compose a single type. However, their physiological response to directional motion divides them into four distinct functional types. Then, Rivlin-Etzion et al. (2011) discovered ON-OFF DSGCs with preference for posterior direction in two different transgenic mouse lines expressing protein (GFP) under the control of the thyrotropin-releasing hormone receptor (TRHR-GFP), and dopamine receptor 4 mice (DRD4)-GFP. ON-OFF DSGCs expressing TRHR and DRD4 had different projection patterns and they demonstrated different degrees of direction tuning. So, even within the posterior-direction-preferring ON-OFF DSGCs there is an argument for further divisions in classification based on distinct differences in projection pattern. These issues of typology have prompted the development of classification schemes that circumvent these issues and define a type.

One possible solution to the question of what defines a cell type is establishing a specific mode of classification as the priority. A review by Vlasits et al. (2019) argues that

function should be prioritized when classifying retinal ganglion cells. One argument for “function first” classification is the JAM-B (junctional adhesion molecule B) RGC. JAM-B cells are characterized by their strikingly asymmetric dendritic arbors aligned in a dorsal-to-ventral direction. Their receptive fields correspond closely with their structure, as the cells preferentially respond to upward motion across the retina (Kim et al., 2008). However, in some contexts, cells meeting the morphological and molecular criteria of a JAM-B cell demonstrate selectivity for orientation tuned stimuli (Nath & Schwartz, 2017). The physiological properties of these cells reportedly vary depending on their location in the retina. While molecular criteria would sort them into a single type, they should represent more than one type if classified primarily by their functional properties (Vlasits et al., 2019).

Another argument presented in the case of “function first” typology is that one of the major goals of studying retinal circuitry is understanding the array of signals projecting to the brain for vision encoding. With a goal of determining how the retina works, it may be prudent to simply use characteristics of morphology and connectomics to better understand the functionality of the cell — which would be the ultimate decider of a type.

While the issue of deciding how to classify RGCs has not yet been resolved, ideas like this are a step in the right direction to having standard classifications of cells. Likely, there will have to be some consensus on what a type is. If we divide cell types by every possible difference, the amount of types could be inordinate and unmanageable. Conversely, if our definitions of a type are too broad they may no longer be useful for experimental purposes. We need a parts list of cells if we are going to effectively study neural circuitry. We need working definitions of types that lies somewhere in a “sweet

spot” between the two extremes. This study addresses that issue by utilizing an intraexperimental analysis of responses and multimodal approach to characterizing RGC types. For the purposes of this project, we focus on a subset of functionally defined types, Orientation Selective RGCs.

Until recently, orientation selective cells were not known to represent a discrete type. Despite being reported in a large-scale physiological survey (Baden et al., 2016) it was not until 2016 that orientation selective cells were labeled as a unambiguous type by the Schwartz group, and analyzed by their physiological properties (Nath & Schwartz, 2017). They identified an On and Off vertical-preferring OS (vOS) cell and On and Off horizontal-preferring OS (hOS) type. The large-scale imaging study by the Baden group, however, identified 4 clusters with a high proportion of OS types, with several types representing more than one preference of orientation. This indicates that the Schwartz studies undersampled the OSGC population and provides an incomplete account of OS types in mouse.

In sum, thorough descriptions of RGC types are crucial both for the study of neurons across labs, and for reliably identifying cells to study their circuitry. Unambiguous categorization of a type should involve multiple levels of description, including functionality, morphology, circuitry, and type-specific gene expression. While some types have been ‘completely categorized’ in this sense, such as several Directionally Selective Ganglion Cell types and Alpha Type RGCs (Sanes & Masland, 2015), most others have not. This includes the Orientation Selective Ganglion Cells (OSGCs). Functional surveys of RGC populations have identified four clusters with a high proportion of OSGCs representing multiple orientation preferences per cluster in high throughput calcium

imaging surveys (Baden et al., 2016). But Orientation Selective cells in mouse were not described as a discrete type until a more recent study by the Schwartz group in 2016 (Nath and Schwartz, 2016), who targeted cells based on their light-step response profiles during blind cell-attached recording. This strategy is inefficient and has the potential to leave out functional OS types. However, there is not yet a transgenic line to identify OS cells. The incidence of orientation selectivity across both vertebrate and invertebrate species and across multiple stages of the visual pathway suggest that orientation selectivity is a fundamental computation (Hubel & Wiesel, 1962; Maturana and Frenk, 1963; Levick, 1963; Piscopo et al., 2013; Fisher et al., 2015, Baden, 2016).

To address the gap in knowledge requires an innovative solution so that the study of OSGCs can be streamlined. We developed a novel method for targeting OSGCs for study with a function-first approach, so that we could efficiently investigate their various features. *Our first goal was to create an intra-experimental analysis method to target OSGCs based on their functional light responses.*

2.3 Methods

2.3.1 Animals

All animal procedures were approved by the Institutional Animal Care and Use Committee at the University of Louisville and were in compliance with National Institutes of Health Guidelines. Calcium imaging surveys were performed using *Thy1* GCaMP6f transgenic mice (<https://www.jax.org/strain/024276>) that express the green fluorescent calcium sensor protein GCaMP6f in Retinal Ganglion Cells. GCaMP6f reports neuronal action potentials with an increase in fluorescence. Jax labs reports that, “The mouse *Thy1*

promoter drives expression of the transgene Tg(*Thy1*-GCaMP6f)GP5.5Dkim that includes green fluorescent calcium indicator (GCaMP6f), woodchuck hepatitis virus posttranscriptional regulatory element (WPRE), and a bovine growth hormone (bGH) polyadenylation sequence. GCaMP consists of a circularly permuted green fluorescent protein (cpGFP), calcium-binding protein calmodulin (CaM), and CaM-interacting M13 peptide. The strain was created and maintained on a C57BL/6J genetic background.” Adult mice (p30-p90) of either sex were dark adapted for over 30 minutes.

2.3.2 Retinal Dissection

Mice were anesthetized under dim red light using isoflurane and euthanized using cervical dislocation. The eyes were enucleated one at a time with curved scissors. The eyes were dissected in oxygenated Ames medium (95% O₂ and 5% CO₂; Sigma-Aldrich) under infrared illumination (OWL Night Vision Scopes, third generation; B.E. Meyers). The eye was hemisected by inserting a scalpel near the anterior eyecup, and then cutting around the eye completely with iris scissors. Once the anterior eyecup was removed, the second eye was excised from the animal using the same method. Using scleral landmarks, the eye was cut in such a way as to delineate the ventral from the dorsal portion of the eye. Three incisions were made along the dorsal aspect of the eyecup; a specific cut was made to separate the two halves of the ventral portion of the eyecup. A modified fluid knife was used to separate the retina from the eyecup. Once the retina was completely separated and was only held in place by the optic nerve, the optic nerve was cut with the iris scissors. The retina was mounted photoreceptor-side down on perforated nitrocellulose filter paper (Millipore) filter paper, centered on a square pattern of four, 1.3-mm-diameter apertures to

allow for the visual stimuli to pass through from below, and allow electrode access from above. A fifth aperture was offset ventrally to focus the stimulus at the level of the photoreceptors. The filter paper — with the retina sitting on top of it — was placed in a custom 3-D printed chamber and held in place with a custom-made harp.

2.3.3 Two-Photon Calcium Imaging

The retina and chamber apparatus were placed in a custom-built two-photon fluorescence microscope (Olympus BX-51) with IR and two-photon imaging capability. Tissues were perfused continuously with oxygenated Ames medium at physiological temperature (~6 ml/min; 34-36°C) for up to 6 hours.

2.3.4 Visual Stimulation

Visual stimuli were generated in MATLAB (Mathworks, Natick, MA) using the Psychophysics toolbox (Brainard, 1997) version 3.0.14 for Mac OSX. The USTIM stimulus consisted of five stimulus epochs. The first epoch started with a 150 μ m squarewave spot 1Hz at 100% contrast on a gray background, with a duration of 7.05s. We then present flashed spots to probe for light increment and decrement preference at 10, 20, 50, 100, 200 square pixels or a 33, 66, 165, 333, 666 μ m spot for a duration of 25.25s. For the third stimulus, a drifting grating was presented at 100% contrast at angles 0-315° in increments of 45°. The temporal frequency was set to 1Hz, spatial wavelength was 50 pixels, equal to 250 μ m, the total duration of each drifting grating direction was 4.2 seconds for a total of 33.87s. The fourth stimulus, at a diameter of 33 μ m, was presented as a contrast-modulated spot flashing at 0.5-15 Hz for 30.2s. The fifth stimulus was a 150 μ m

spot, contrast-modulated following a pseudorandom white noise sequence for 33.35s. Stimuli were focused and projected onto the photoreceptor layer using the DLP video projector (HP AX325AA; Hewlett-Packard).

2.3.5 Harvesting Functional Responses

Each recording generated two files, an imaging file and a .mat file that were combined in a custom MATLAB program — called Fluoanalyzer. Fluoanalyzer produced files that were then loaded into a second custom MATLAB program called ROIgui. In ROIgui, a region of interest was defined to cover each soma, and measure the change in fluorescence over time. Typically 10-15 cell responses were harvested from each imaged area. All cell responses from that acquisition were stored in a .mat file that contained an ID for each cell, the coordinates of the area relative to the optic nerve, and a vector with the numerical values for the measurement of fluorescent response for each cell.

2.3.6 Cluster Analysis

To create a template of reproducible cell types, we developed a partially supervised, custom hierarchical clustering algorithm in MATLAB. The response vector of individual RGCs — evoked using our spatiotemporally diverse USTIM stimulus — was split into 26 response segments and assigned weight to more strongly emphasize size, drifting grating response, and temporal tuning, while de-emphasizing the white noise response. The algorithm was adjusted by overlaying all cell responses assigned to each cluster and verifying that they match up. The algorithm was adjusted until it sorted clearly apparent different response types into different clusters, including vOS and hOS types.

2.4 Results

I used two-photon calcium imaging to initially collect approximately 3000 functional responses of RGCs from 10 *Thy1*-GCaMP6f mice of either sex. With the help of my advisor, I sorted the cells by signal-to-noise ratio of their responses and used the top 500 to generate a response type template through hierarchical clustering. All responses assigned to a cluster were averaged and those averages served as templates to compare new record responses to, in subsequent experiments. This approach presents a novel and innovative strategy for targeting cells for study.

2.4.1 *Thy1*-GCaMP6f Mice Allow Imaging of Diverse RGC Types

When a neuron generates an action potential, calcium rushes into the cell as a result of calcium-permeable ion channels opening (Purves, 2017). Calcium sensors present a method of measuring this neuronal activity directly. When there is neuronal activity, the calcium ions bind to the calcium sensor, which results in an increase in fluorescence — permitting the use of calcium imaging as an effective and high throughput method for quantifying neuronal activity (Chen et al., 2014; Baden et al., 2016). For the purposes of our study, I used genetically encoded GCaMP in *Thy1*-GCaMP6f mice. *Thy-1* is a retinal ganglion cell marker in mice (Barnstable & Drager, 1984). So, in this line, the *Thy1* promoter is used to express GCaMP in RGCs (Chen et al., 2012). GCaMP6 indicators have been shown to be more sensitive than earlier GCaMP variants, and GCaMP6f is the fastest genetically-encoded calcium indicator (Chen et al., 2014), which makes this transgenic line ideal for measuring light-evoked activity.

I isolated the retinas of dark-adapted *Thy1-GCaMP6f* mice aged P30-P90, of either sex (Figure 2.1, A; Figure 2.2) and mounted them in a chamber to be perfused with an oxygenated Ames's solution (Figure 2.1, B). Two-photon fluorescence measurements were made using an Olympus 60X, 1.0NA objective with the laser tuned to 910 nm. Using a video projector, I exposed RGC populations in whole-mount retina to spatiotemporally diverse stimuli (Figure 2.4), presented through the condenser lens of the microscope. The stimulus included flashing spots to probe polarity, drifting gratings to probe direction/orientation preference, a 'flicker' stimulus, and white noise sequence (Figure 2.4). I extracted the responses of these cells to visually evoked stimuli using a custom MATLAB program (Figure 2.3), placing a region of interest 'mask' over the somas to harvest their fluorescence responses. Those responses were added to our library of imaged cells. In each acquisition there were 10-15 responding cells. I collected approximately 20-40 acquisitions in an experiment day, averaging ~360 responses in an imaging day.

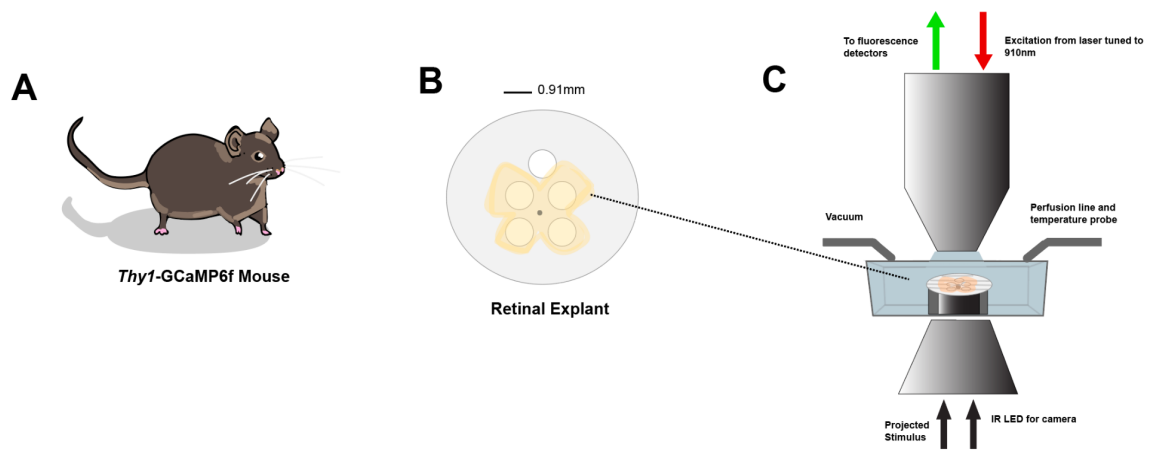


Figure 2.1 Retinal Dissection and Imaging Setup | (A) *Thy1-GCaMP6f* Mouse and excised retina (B) mounted ganglion cell layer-side up on a nitrocellulose filter paper with five apertures. The fifth aperture indicates the ventral side of the tissue and permits focusing the visual stimulus on the photoreceptors. (C) Retina and chamber apparatus placed in a custom-built two-photon fluorescence microscope (Olympus BX-51) with IR and two-photon imaging capability

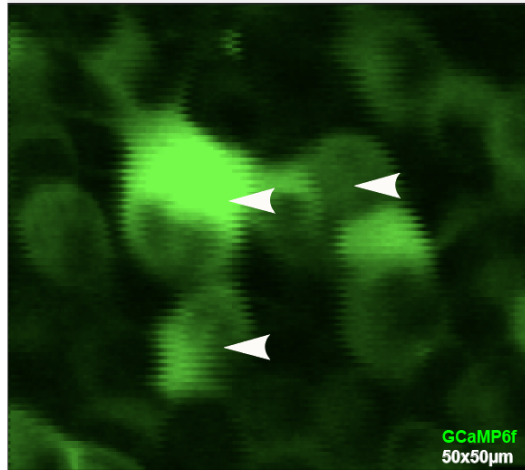


Figure 2.2 Two photon fluorescence image of GCaMP6f-expressing ganglion cells. 50x50µm Imaging window of the ganglion cell layer in a Thy1-GCaMP6f retinal explant, under 60x magnification. White arrows indicate example somas of Retinal Ganglion Cells that express GCaMP6f.

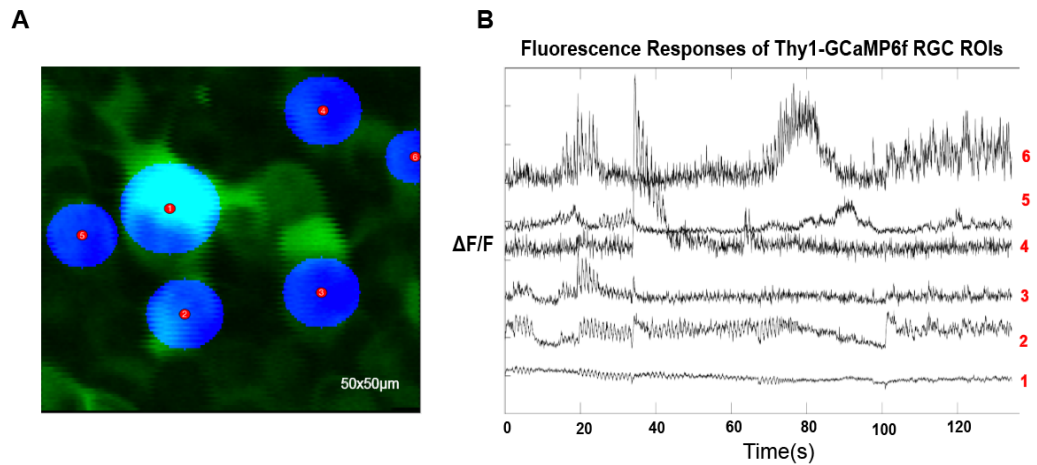


Figure 2.3 Population calcium imaging resolves diverse RGC function | (A) 50x50µm scan field image of the Retinal Ganglion Cell Layer in Thy1-GCaMP6s mouse explants, with RGC Region of Interest (ROI) masks. GCaMP-positive somas shown in green. Blue circles indicate ROI for response harvesting. (B) Corresponding fluorescent response vectors (in response to spatiotemporally diverse stimulus shown in figure 2.4) for cells in (B) identified by numbers on the right in red.

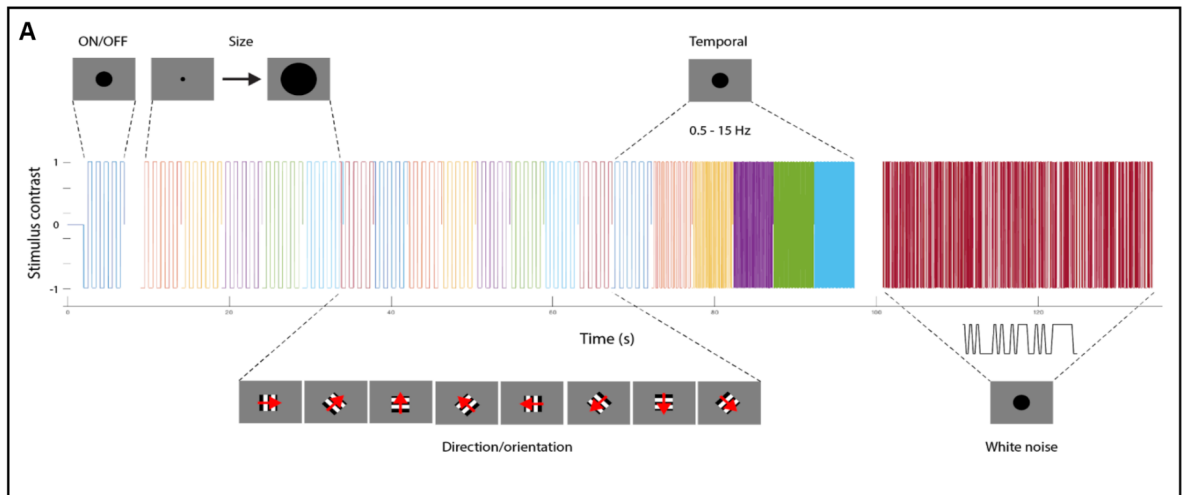


Figure 2.4 Visual Stimulus | The USTIM stimulus sequence consisted of a squarewave 150 μ m spot, 1Hz at 100% contrast on a gray background. Flashed spots to probe for light increment and decrement preference at 10, 20, 50, 100, 200 square pixels was presented as a second stimulus. For the third stimulus, a drifting grating was presented at 100% contrast at angles 0-315 $^{\circ}$ in increments of 45 $^{\circ}$. The temporal frequency was set to 1Hz. The spatial wavelength was 50 pixels, equal to 250 μ m. The total duration of each drifting grating direction was 4.2 seconds. The fourth stimulus that was presented was the temporal spot flashing at 0.5-15 Hz. The fifth stimulus was a 150 μ m spot, contrast-modulated following a pseudorandom white noise sequence.

2.4.2 RGC Survey Identifies OS Types

To identify the functional response types of the imaged population of RGCs, I — with the help of my advisor — utilized an unsupervised clustering approach to sort the cells from our collection into 30 functional types based on their light-evoked responses (Figure 2.5, A). This allowed for objective and quantitative analysis of RGC functional responses. Our data produced clear groupings of previously documented types from the body of literature on RGC classification, including ON, OFF, ON-OFF, large RF and small RF — indicating that this was an efficacious method for functional classification. If I cluster, I routinely find cells of similar types. By averaging responses from the cluster analysis my advisor and I created a ‘template’ with which to compare new responses (Figure 2.5, B).

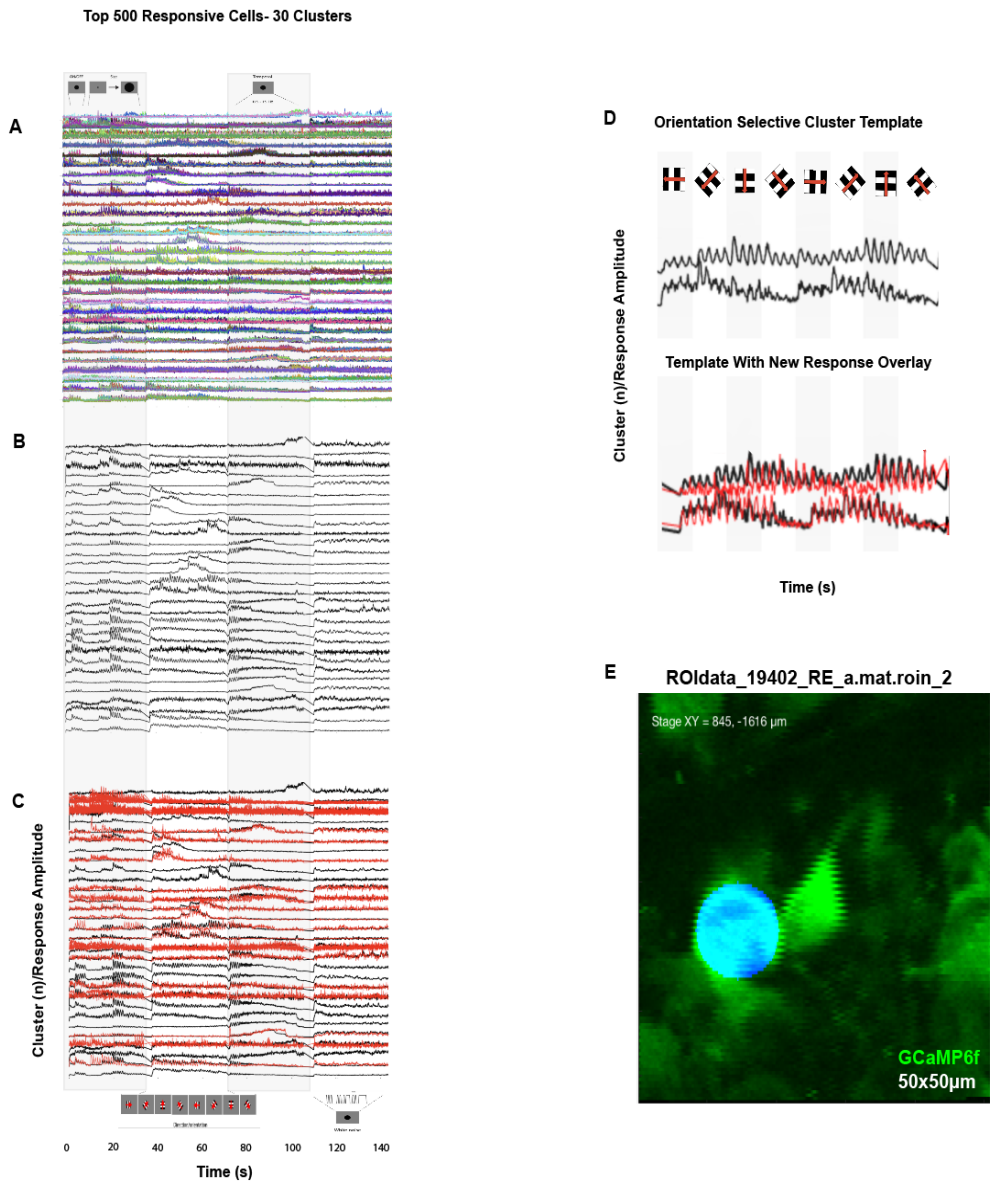


Figure 2.5 Calcium Response Survey and Intra-Experimental Analysis | (A) Retinal Ganglion Cells were clustered into 30 types using hierarchical clustering. 3000 individual RGC response vectors were collected; the 500 top signal-to-noise ratio responses were included in the cluster analysis. Each colored trace represents the calcium response recorded from an individual cell stimulated with the USTIM sequence (Figure 2.4). (B) Each line (black) represents the averaged responses from the individual clusters in (A). (C) Template of clusters (black) overlaid with new responses (red). The cluster analysis (A-C) revealed RGCs with preferences for both horizontal and vertical orientations. (D) Template of orientation selective types from cluster analysis (black, top) with overlaid responses (red, below). (E) Scan image with cell ID, stage coordinates, and ROI (blue) identifying cell of interest for target analysis.

Importantly, the cluster analysis data also revealed RGCs with preferences for both horizontal and vertical orientations.

2.4.3 Developing an Intra-Experimental Analysis

I took the cluster averages from our unsupervised cluster analysis (Figure 2.5, B) and used it as a template with which to compare new responses. My advisor developed a MATLAB program to sort new responses from a given experiment day into one of the thirty clusters from the template (Figure 2.5, C). This method was used to target cells with an apparent orientation selective response (Figure 2.5, D). Cells that get sorted into an orientation selective category could be selected to retrieve the “address” of the cell so it could then be targeted efficiently for study (Figure 2.5, E). The innovation of the approach is that cells could be analyzed and targeted for study while the tissue was still alive on the microscope stage. With this method, I can, in principle, target any functional cell type of interest.

2.5 Summary and Discussion

The first goal of this study was to develop an efficient method to identify orientation selective cells among a labeled RGC population — cell types for which there are currently no molecular markers. By using the *Thy1* GCaMP6f mouse model, I was able to collect responses from 3000 RGCs. When my advisor and I sorted those types into 30 clusters, we identified two clusters with an apparent preference for oriented stimuli, representing a group of cells that respond preferentially to a horizontal grating moving upwards or downwards across the visual field and a vertical grating moving rostrally or nasally across the visual field. Responses from subsequent experiments consistently aligned with low root-mean-square deviation (RMSD) with the clusters in the template. This represents a

novel method for targeting a cell for study, and has implications for targeting other cell types in the retina and studying neural activity in other areas.

CHAPTER III TARGETED MULTIMODAL ANALYSIS OF ORIENTATION SELECTIVE GANGLION CELLS

3.1 Introduction

The second goal of our study was to selectively target cells with orientation tuning, quantify their functional and morphological features, and group them into types. To understand the need for morphological classification — and, more accurately, the necessity of a multimodal classification scheme for RGCs — it is important to understand 1) The history of morphological RGC classification; 2) How morphology can influence feature selectivity in RGCs; 3) How dendritic structure relates to functional tuning.

3.2 Background

In the late 1800s, Spanish neuroscientist Santiago Ramón y Cajal, the “father of modern neuroscience,” classified different types of ganglion cells in the retina via Golgi staining. He labeled cells with silver chromate and observed them with a light microscope. Cajal’s detailed drawings of the retina revealed cell types divided into distinct classes with laminar-specific organization. Retinal ganglion cells (RGCs) were characterized by their dendritic morphology, dendritic tree size, soma, and dendritic arbor stratification within the inner plexiform layer (IPL) (Cajal, 1899). This work laid the foundation for RGC type classification based on morphology, and uniform morphology continues to be an important

mode of classification in the retina today.

Cajal theorized that dendritic branches played a role in transmission. Since these early morphological surveys, further investigation has implicated type-specific dendritic arborization as an indicator of function. The unique shape and size of the dendritic field of a neuron is determined by the need to cover the area that encompasses its sensory inputs (Boycott & Wässle, 1991). However, there is a metabolic cost associated with the expansion and elaboration of dendrites. Furthermore, arbor shape affects receptive field resolution — with increasing arbor size decreasing visual resolution. The optimal balance between this metabolic cost and the physiological requirements necessary for neural function determines dendritic arbor structure and thus the dendritic field (Wen & Shklovskii, 2008).

The relationship between dendritic fields and receptive fields has been thoroughly examined in many RGC types. RGC feature encoding is shaped by converging inputs from bipolar cells, filtered by the interneurons of the retina (Masland, 2013; Seabrook et al., 2017). The dendritic arbors of RGCs are distributed in the retinal inner plexiform layer (IPL) where the axon terminals of bipolar cells, relaying visual information from the photoreceptors, synapse with the dendrites of RGCs and amacrine cells (Masland, 2013). Receptive fields of RGCs are shaped by the (primarily) inhibitory input from amacrine cells integrated with excitatory input from bipolar cells. The depth of RGC stratification level limits the type of input that bipolar cells and amacrine cells can have on the RGCs. Thus, the stratification depth and arbor arrangement directly influences the nature of synaptic inputs to the RGC. While the correspondence between dendritic structure and receptive field properties are well known in some types, such as DS RGCs (Sanes &

Masland, 2015), others, such as OS RGCs, are less well known.

As reviewed, orientation selective (OS) cells have been identified in the retina, midbrain, and cortex of mouse (Baden et al., 2016; Scholl et al., 2013; Hubel & Wiesel, 1962). Typically characterized by their elongated receptive field, they respond preferentially to elongated visual stimuli oriented along a specific axis. The elongated dendritic fields of specific OS cell types of some animal models are aligned to match their preferred axis of orientation (Bloomfield, 1991; Antinucci et al., 2016), which makes them ideally shaped to produce the elongated receptive field, but that is not always the case. The correlation between the shape of the dendritic field and receptive field makes them interesting to evaluate when examining the effects of form on function. Receptive fields of course can be shaped by a combination of excitatory and inhibitory inputs, but an elongated dendritic field could explain the orientation selectivity without the need of this excitatory/inhibitory interplay. There is evidence to suggest that the structure of OS RGC dendritic arbors could provide the basis for these elongated receptive fields in several animal models (Bloomfield, 1991; Antinucci et al., 2016).

Tuning mechanisms for orientation selectivity have been described in amacrine cells. OS amacrine cells representing both horizontal and vertical orientations have been reported with dendritic arbors elongated along the axis of their preferred orientation (Antinucci et al., 2016; Nath & Schwartz, 2017; Bloomfield, 1991,1994). Bloomfield (1991, 1994) discovered three types of “orientation-tuned” amacrine cells in rabbit: two types were labeled as orientation-selective cells, meaning that inhibition of the non-preferred “orthogonal” orientation contributed to the orientation tuning of the cells. They described the third type of amacrine cell as having a highly elongated dendritic field. The

selective firing of which seemed to arise exclusively from excitatory inputs received along the axis of its dendritic arbor. This cell type was termed “orientation-biased”. The results of Bloomfield’s studies suggested that the oriented dendritic field alone could provide the structural basis for the observed elongated receptive fields in OS amacrine cells, thus assigning a preference for oriented stimuli. There is another OS amacrine cell type in rabbit whose firing selectivity could be attributed to morphological mechanisms. These cells are termed “polyaxonal wide-field amacrine cells”. The elongation of the dendritic arbor in conjunction with the arrangement of excitatory inputs has been proposed as the driver of the orientation-selective response (Murphy-Baum & Taylor, 2015).

The phenomena of elongated dendritic arbors in orientation-tuned amacrine cells has also been described in zebrafish and mouse models (Antinucci et al., 2016; Nath & Schwartz, 2017). The case for morphological influence in amacrine OS receptive fields is quite strong in larval zebrafish. Not only is the preference for orientation selective stimuli directly related to the orientation of the dendritic field, but the level of preference of the amacrine cells for stimulus orientation—measured by the orientation selectivity index (OSI)—is directly proportional to the magnitude of dendritic arbor elongation (Antinucci et al, 2016).

Nath and Schwartz (2016) established, through a series of pharmacological and electrophysiological experiments, that orientation selectivity in mouse OS RGCs is produced through the integration of bipolar cell inputs and asymmetric inhibition from amacrine cells. Their study also suggested that OS RGC dendritic structures could have a direct effect on their highly elongated receptive fields, as OS RGCs that preferred the horizontal orientation (hOS RGCs) possessed highly asymmetric, elongated dendritic arbors coinciding with their preferred stimulus orientation (Nath & Schwartz, 2016).

Pharmacologically blocking inhibitory inputs in the ON hOS RGCs in mouse did not affect the orientation tuning (Nath & Schwartz, 2016). This indicates that the morphology of the cell may be responsible for the asymmetric integration of excitatory inputs shaping the orientation response. It is not yet certain whether morphology is the primary cause of orientation selective responses in these cells, as there is not currently a way to selectively manipulate their morphology. Nevertheless, these are good indications that the dendritic fields of certain OS RGC types could give rise to their elongated receptive fields.

There is a wealth of literature correlating dendritic fields and receptive fields. I have elaborated on some studies directly implicating dendritic fields in the formation of receptive fields. To understand the complex circuitry of the retina, downstream visual centers, and even other sensory modalities, it is important to have an understanding of the relationship between dendritic structure and receptive fields. This includes designating clear definitions of morphological and physiological cell types. Further investigation into the nuances of dendritic structure and how it directly affects the physiological responses and thus the receptive fields of neurons will be an important task in understanding the tuning mechanisms of OSRGCs.

3.3 Methods

3.3.1 Intra-Experimental Analysis

The imaging and response harvesting methods described in Chapter I Methods were used to collect cell responses. While the tissue was still perfusing, new responses from each imaging day were aligned with the template of imaged cells using a custom MATLAB program. Each annotated cell corresponds with a response vector and is assigned a number.

Additionally, the coordinates relative to the optic nerve were stored, allowing us to later locate a specific population of RGCs. Cells could then be targeted for morphological analysis depending on the cluster that they aligned with.

3.3.2 Neurobiotin Fills

One aliquot of neurobiotin (~10 μ L) in 200mM KCl (Vector Laboratories) was added to 1 μ L Alexa Fluor 488 invitrogen (Thermo Fisher Scientific). Borosilicate glass capillaries from world precision instruments, Inc. were pulled using a Sutter Instrument Co. model P-97 Flaming/Brown micropipette puller. High-impedance, intracellular glass pipettes with filament were pulled at settings P=500, Heat=511, Pull =150, Vel = 80 Time =250. The pipette was backfilled with 200mM KCl after the combination neurobiotin and green alexa was drawn into the pipette via capillary action.

Using the micromanipulator, the pipette was positioned with the coordinates of the cell relative to the optic nerve and was lowered in the Z plane enough that it entered the oxygenated Ame's solution. Once it entered the solution, the objective was changed to 60x. The glass pipette was lowered until it was near the cell and was pushed towards the cell from the side until a "dimple" appeared in the soma. Once the dimple appeared and it was clear that the pipette was in contact with the cell, the stage was tapped lightly so that the pipette tip pierced the membrane. The "buzz" function was then used to push the solution into the cell. Penetration of the pipette was visualized using the two-photon laser. The current clamp settings were then set to +500pA for 15 minutes. Once 15 minutes passed, the pipette was removed and the neurobiotin was allowed to diffuse through the cell for an additional 15 minutes.

3.3.3 Immunostaining to Identify ChAT bands and Cell Morphology

To nuance OSGC stratification depth, I used a common depth marker of the IPL, the ChAT bands, i.e. the dendritic arbors of ON and OFF Starburst Amacrine Cells (SACs). To stain for ChAT bands, retinas were fixed for 1 hour in 4% PFA 4°C. To remove the fixative completely, retinas were washed 3x with 750 microliters of fresh PBS for 5 minutes on a shaker at room temperature. The retinas were then blocked in a solution of 30µl normal donkey serum, 10µl triton x-100, 500µl of PBS for one hour on a room temperature shaker. The tissues were then washed with PBS for 10 minutes, PBS was removed, and the tissue was washed for another 10 minutes on a room temperature shaker. The tissues were then incubated with primary antibody (AB144P Anti-Choline Acetyltransferase Antibody; Sigma-Aldrich) at a ratio of 1:250 in 10µl normal donkey serum, 1µl triton, 500µl PBS, 2.5µl antibody for 5-7 days on a shaker at 4°C . To visualize the injected RGC, tissues were also incubated with 1µl of streptavidin, Alexa Fluor 488. The tissues were removed from the 4°C shaker and washed twice with PBS at room temperature for 15 minutes. They were then incubated with a secondary antibody in a blocking solution of 10µl normal donkey serum, 1µl triton, 500µl PBS, 2.5µl antibody for 12-24 hours at a ratio of 1:250 in 4°C. The second antibody used was donkey anti-goat IgG, Alexa Fluor 647 conjugate AP180SA6 from EMD Millipore Corp. After 5-7 days the tissues were washed with PBS for 1-2 hours and then mounted on a glass slide, ganglion cell side up and preserved with VectaShield Antifade Mounting Medium with Dapi (Vector Laboratories, Inc).

3.3.4 Confocal Imaging

RGCs were analyzed using an Olympus Fluoview FV1000 confocal laser scanning microscope with a 60x objective. One channel was set to the Alexa Fluor 488 at 500-540 nm, 2.5% laser power, high voltage (HV)= 564 V. Gain and offset were adjusted as needed to reduce background noise. The second channel was set to Alexa Fluor 647 at 650-750 nm, 2.7% laser power, and HV = 616, gain and offset were adjusted as needed. Serial optical sections were obtained at a step size of .5 μm .

3.3.4 Imaris Analysis

3.3.4.1 Filaments Reconstruction

Imaris software version 6.4.2 (Bitplane) was used to reconstruct morphologies of filled ganglion cells. OIR files from the Olympus Fluoview Confocal Software were loaded into the program in Surpass View. For anatomical reconstruction, only the red channel was kept (the channel with the filled cell), ChAT staining in green was deleted for the sake of reconstruction. Background thresholding was performed to reduce noise from non-specific staining.

Cells were reconstructed using the Filament function. Within the filaments function, cells were reconstructed using the AutoPath function. The AutoPath function automatically computes all the paths from a user-defined starting point to the end of the structure. The starting point was set at the center of the filled soma using shift + right-click. The cursor was then placed at the end of a dendrite and the computed path was displayed. Using shift + click the displayed path was drawn in the program. This was done for all dendritic structures until the cell reconstruction was complete.

3.3.4.2 Filament Dendrite Area

The filament dendrite area was calculated as the sum of the area between all segment edges created during filament reconstruction.

3.3.4.3 Filament Dendrite Length

To determine the filament dendrite length, the sum of all edges between a branch point and a terminal point or two branch points was taken.

3.3.4.4 Generating Sholl Intersections

Once a filament has been created in the Imaris program, a sholl analysis can be generated. This is done by creating 1 μm step concentric circles around the beginning point of the filament (defined here as the RGC soma). The number of intersections is given as a sum of all dendritic intersections at each step.

3.3.4.5 Spine Reconstruction

To reconstruct spines, the “rebuild” function was used within the filaments function. Initially, the automated spine count function was utilized to create “seed points” where spines are located, but this function appeared largely inaccurate (selecting hundreds of spots where there were clearly no spines). So, spines were manually selected by raising the spine threshold until there were no seeds, then seed points were manually placed at each position where a spine was clearly observed.

3.3.5 Quantification of RGC Stratification Depth

I used a custom MATLAB program to identify the representative intensity values of OS RGCs. To confirm stratification depths of all cells, I also manually identified stratification depth using the Imaris slider function. I normalized the ON and OFF ChAT bands to 0 and 1 respectively, and computed for the dendritic stratification depth using the formula:

$$z_i = (x_i - \min(x)) / (\max(x) - \min(x))$$

Where z_i is normalized dendritic depth, x_i is actual dendritic depth in the IPL, $\min(x)$ is the location of the ON ChAT band, and $\max(x)$ is the location of the OFF ChAT band. I averaged three recorded normalized depths to obtain the normalized stratification value for each cell using the formula.

3.3.6 Anatomical Quantification in Fiji

Ellipticity of target cells was determined using ImageJ Version 2.0.0-rc-69/1.52. Confocal z-stack projections were loaded into Fiji (ImageJ) and RGCs were fitted with a polygon. Ellipticity was then determined by fitting an ellipse to the polygon. The major and minor ellipse axis was then produced as a measurement. The elliptical value was determined using the formula $1 - (\text{AxisMajor} / \text{AxisMinor})$ with a 0 denoting a perfect sphere and 1 denoting a line.

3.3.7 Determining Functional Responses for Each Cell

To determine the OSI value for each cell I utilized the commonly used OSI formula (Zhao et al., 2013; Mazurek et al., 2014):

$$OSI = (R_{pref_ori} - R_{orth}) / (R_{pref_ori} + R_{orth})$$

Where R is the cell's fluorescent response, and $pref_ori$ indicates the preferred orientation, and $orth$ indicates the non-preferred orientation. I determine the preferred orientation by first doing a fast fourier transform of the average $\Delta fluorescence / fluorescence$ response for each presentation of the stimulus. This transforms the signal from the time domain to the frequency domain as three features: magnitude, frequency, and phase. I then took the maximum combination of the response to two oppositely moving gratings with matching orientation. The orthogonal orientation is perpendicular to the preferred orientation.

To determine receptive field center size, I did a fast fourier transform of the average $\Delta fluorescence / fluorescence$ response to each of the five spot sizes (33 66 165 333 666 μm) in the light-step stimulus. To determine polarity, I took the average fast fourier transform response of the cell to the combined ON and OFF stimuli for the stimulus that evoked the strongest response.

To determine the temporal frequency preference, I also did a fast fourier transform of the average response to each presented temporal stimulus from 1 Hz, 2 Hz, 5 Hz, 7 Hz, 10 Hz, 15 Hz.

3.4 Results

The goal of these experiments was to identify OS RGCs and provide a multi-modal classification of OS RGC types. I provide a detailed quantification of anatomical and functional features and compare across, and within types. I also aimed to link types from our study with types from the literature, thus contributing to continuity between studies.

3.4.1 Using the Intraexperimental Analysis to Target OS Cell Types

Retinal Ganglion Cells were targeted using the methods and experimental paradigm described in detail in the previous chapter (illustrated by the schematic in Figure 3.1). The ganglion cell layer of *Thy1*-GCaMP6f mouse retinae was surveyed using two-photon calcium imaging. RGC responses were harvested using a custom MATLAB program and then compared against a template of RGC cluster averages from our library of imaged cells. All cells that fell into type 15 or 16 (OS clusters) were targeted for morphological reconstruction. Cell types that clustered into type 9 demonstrated mild OS properties and were also targeted for morphological reconstruction. Cell morphologies were reconstructed via electrophoresis of neurobiotin combined with a fluorophore to visualize penetration of the glass pipette. Tissues were then fixed and stained with streptavidin for high resolution imaging using a confocal microscope.

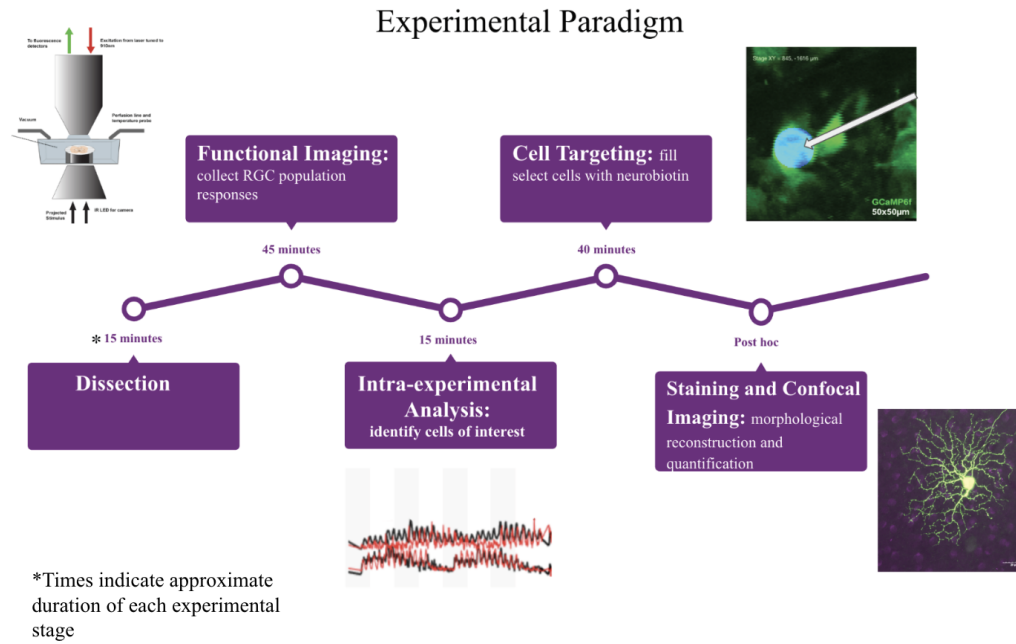


Figure 3.1 Schematic of Experimental Procedure

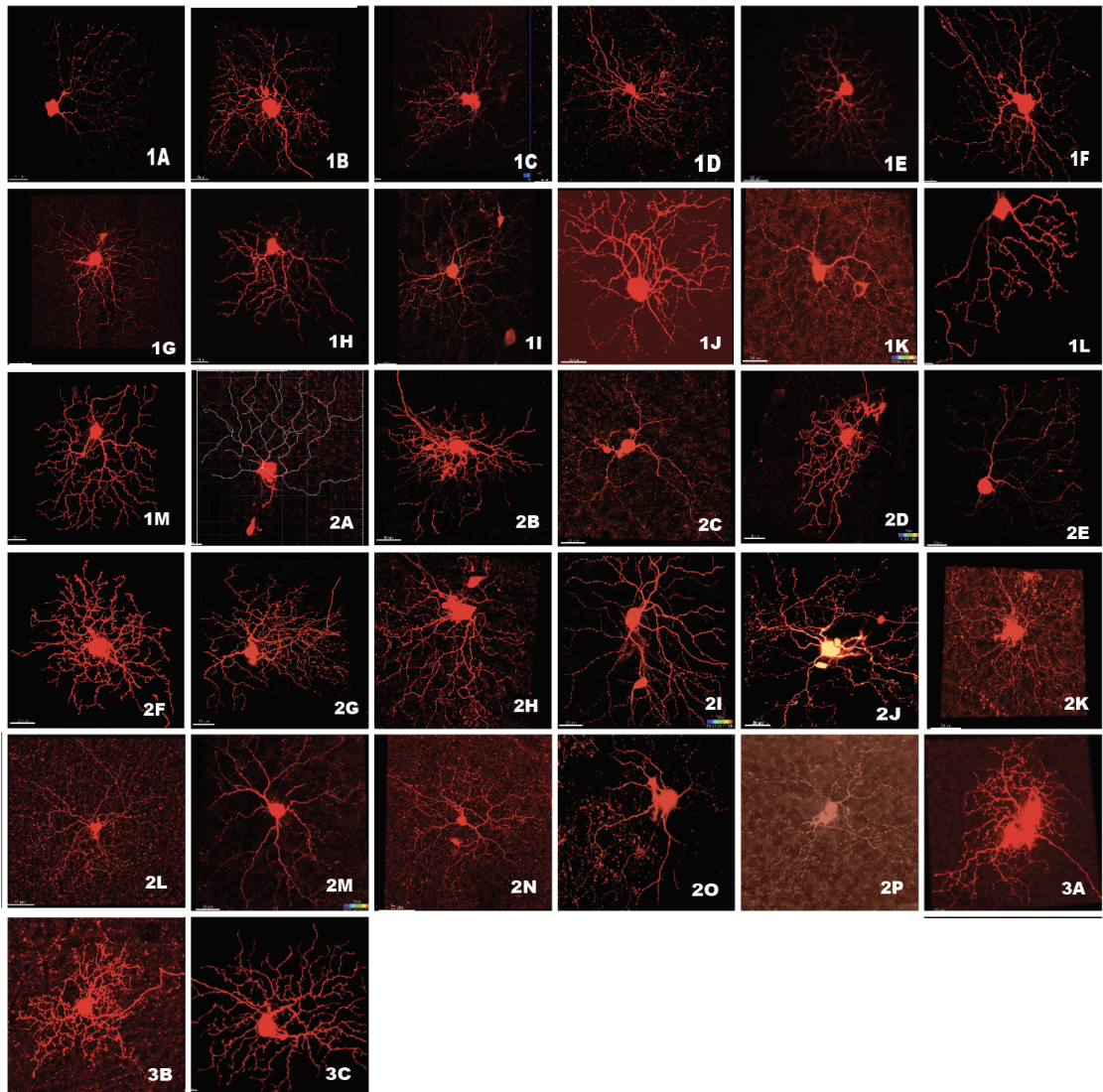


Figure 3.2 Gallery of Target RGCs | (1A-3C) indicates Confocal Z-projections of individual Retinal Ganglion Cells filled with neurobiotin and stained with streptavidin-Alexafluor conjugate. Red indicates neurobiotin. Cell IDs (in white) correspond with calcium responses (figure 3.13) and stratification profiles (figure 3.3).

I reconstructed morphologies for 40 RGCs from 28 mice of either sex (Figure 3.2). I collected light-evoked responses from each cell before reconstructing its morphology. This

allowed us to pair morphological types with their corresponding fluorescent response to the spatiotemporal

diverse stimuli from Chapter II — including a response to the drifting grating stimulus.

Using the formula for OSI/DSI I isolated RGCs that demonstrated DS behavior, or otherwise needed to be precluded (n=7).

3.4.2 Analysis of Stratification Depth Distinguishes 11 Morphological OS Groups

Stratification depth has been accepted as the most reliable form of anatomical identification (Sumbul et al., 2014; Bae et al., 2017). So, I used stratification depth as the basis for comparing groups and clustered cells according to their stratification profile. After targeted cells were filled, the retinas were fixed and stained against choline acetyltransferase so as to locate ChAT bands and subsequently quantify cell stratification depth in the IPL (Figure 3.3; Figure 3.4). Stratification depth was determined using a combination of manual stratification depth calculations, an automated MATLAB program, and visual confirmation of the dendritic architecture using the Imaris slider view. Prior work identified four discretely OS tuned RGC types, each specifically representing either a vertical or horizontal orientation (Nath & Schwartz, 2016; 2017). A large-scale calcium imaging survey identified four clusters of RGC types, with two groups representing *multiple* orientations (Baden et al., 2016). To account for this, I initially anticipated finding at least six different types. I, in fact, identified 11 morphologically distinct types of RGCs based on their stratification profile and the specific arrangement of their dendritic architecture (Figure 3.5; Figure 3.6; Figure 3.7). These cell types ranged from inner IPL

ON layer stratification — proximal to the ON ChAT band, to outer IPL OFF layer stratification — distal to the OFF ChAT band.

Most cell types were nicely clustered into distinct stratification profiles with no overlap, with few exceptions. The ON/OFF vOS I type and OFF vOS III type demonstrate some overlap with each other based on quantification of intensity peak (Figure 3.6). However, visual observation of dendritic stratification and visualization of fluorescent intensity profiles (Figure 3.5) differentiate the two, revealing multiple stratification peaks in the OFF layer as a tangle of highly overlapped and recursive dendrites for the ON/OFF vOS I type and more central and “neat” looking dendrites for the OFF vOS III type.

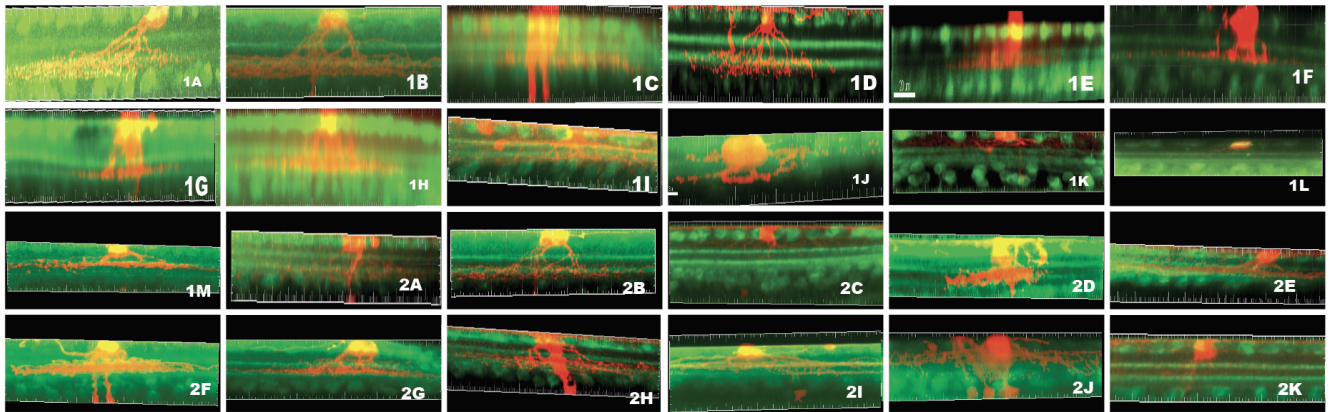


Figure 3.3 Gallery of RGC Stratification Depths | 1A-2K shows XZ projections of individual RGCs (red). For comparison of stratification depth in the IPL, ChAT staining is shown in green. Labels correspond with the Z-projections shown in Fig. 3.2 and calcium responses shown in Fig 3.14.

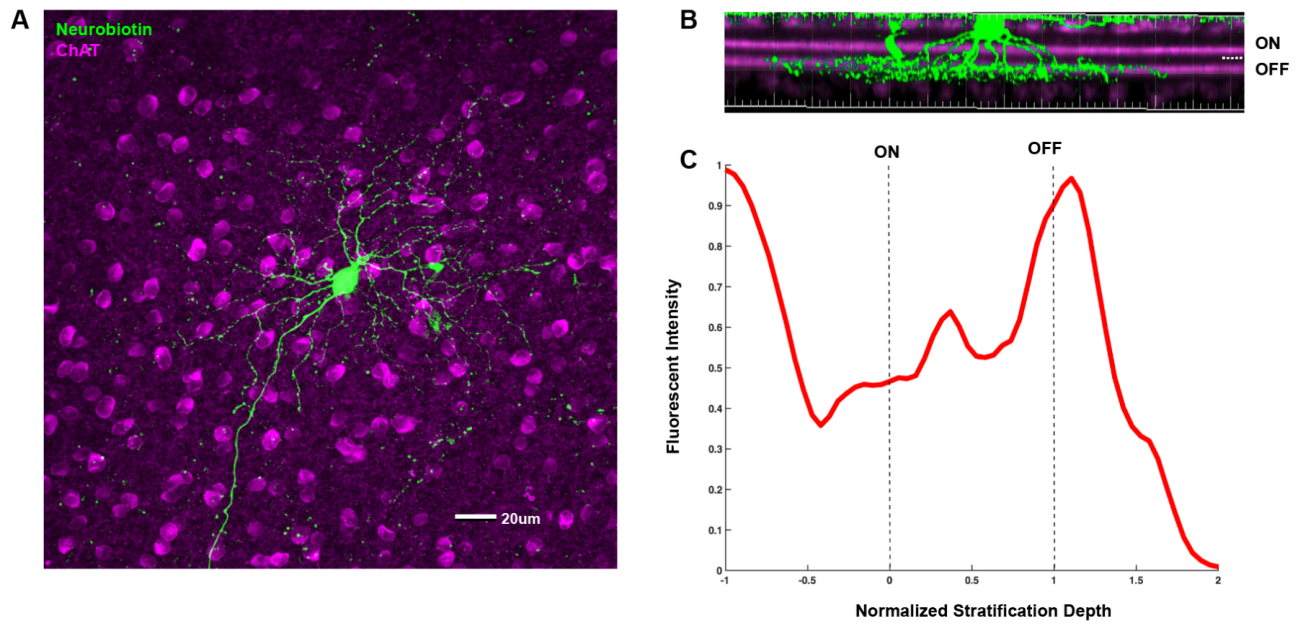


Figure 3.4 Immunostaining Against ChAT Used to Quantify Stratification Depth in IPL | (A) Z-projection of neurobiotin-filled OS RGC stained against streptavidin with Alexa Fluor 488 (green). Choline Acetyltransferase (ChAT) was stained with Alexa Fluor 647 (magenta). (B) Profile view of RGC from (A). (C) Intensity profile for cell in (A) and (B) with ChAT bands normalized to 0 and 1 (ON and OFF respectively).

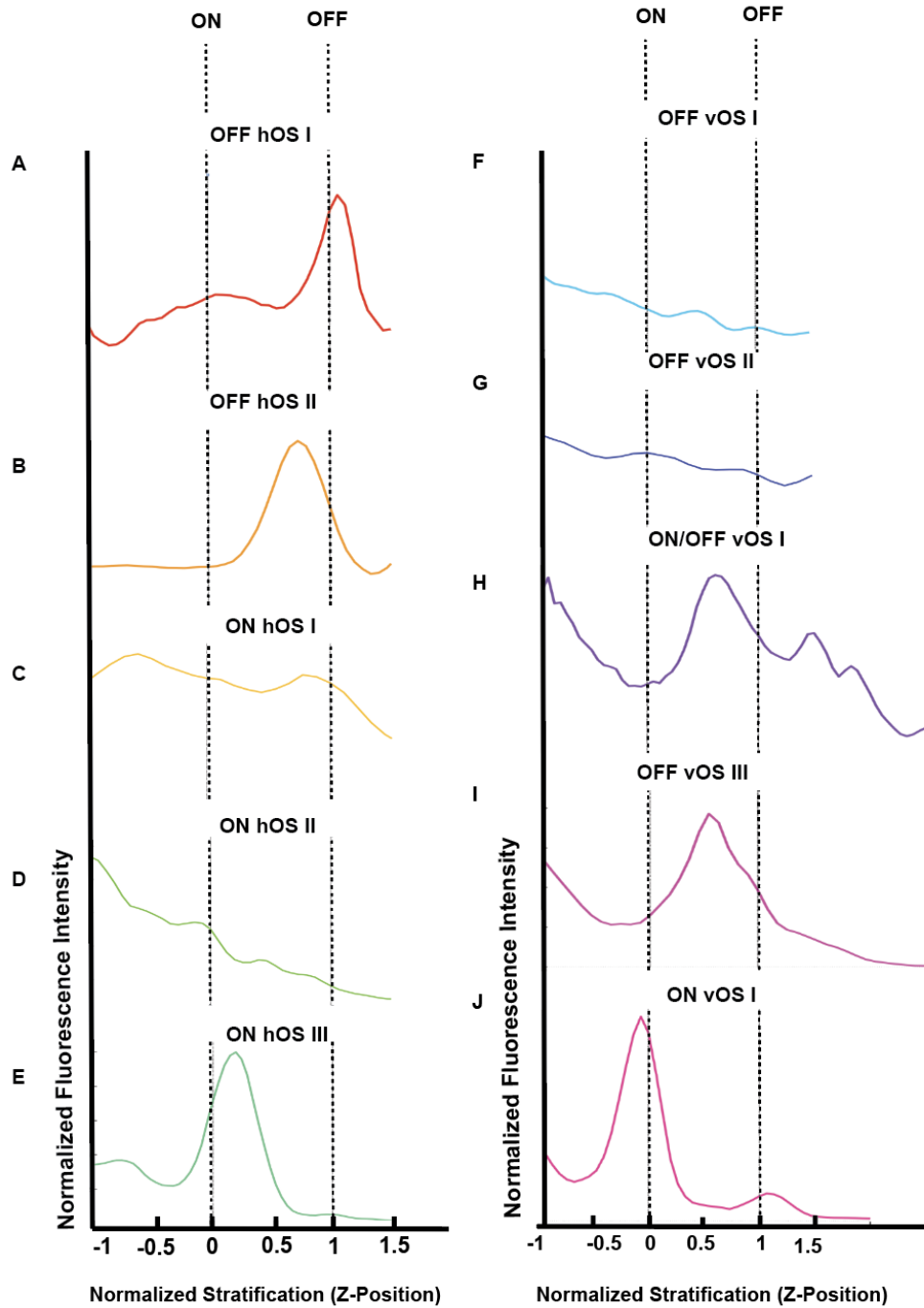


Figure 3.5 RGCs show distinct stratification profiles | (A-J) Representative examples of stratification profiles of tracer filled RGCs that were functionally identified as OS using the USTIM paradigm (see 2.4). Individual lines indicate representative cell values. Dotted lines indicate ON and OFF ChAT bands—0 indicates the ON ChAT band and 1 indicates the OFF ChAT band.

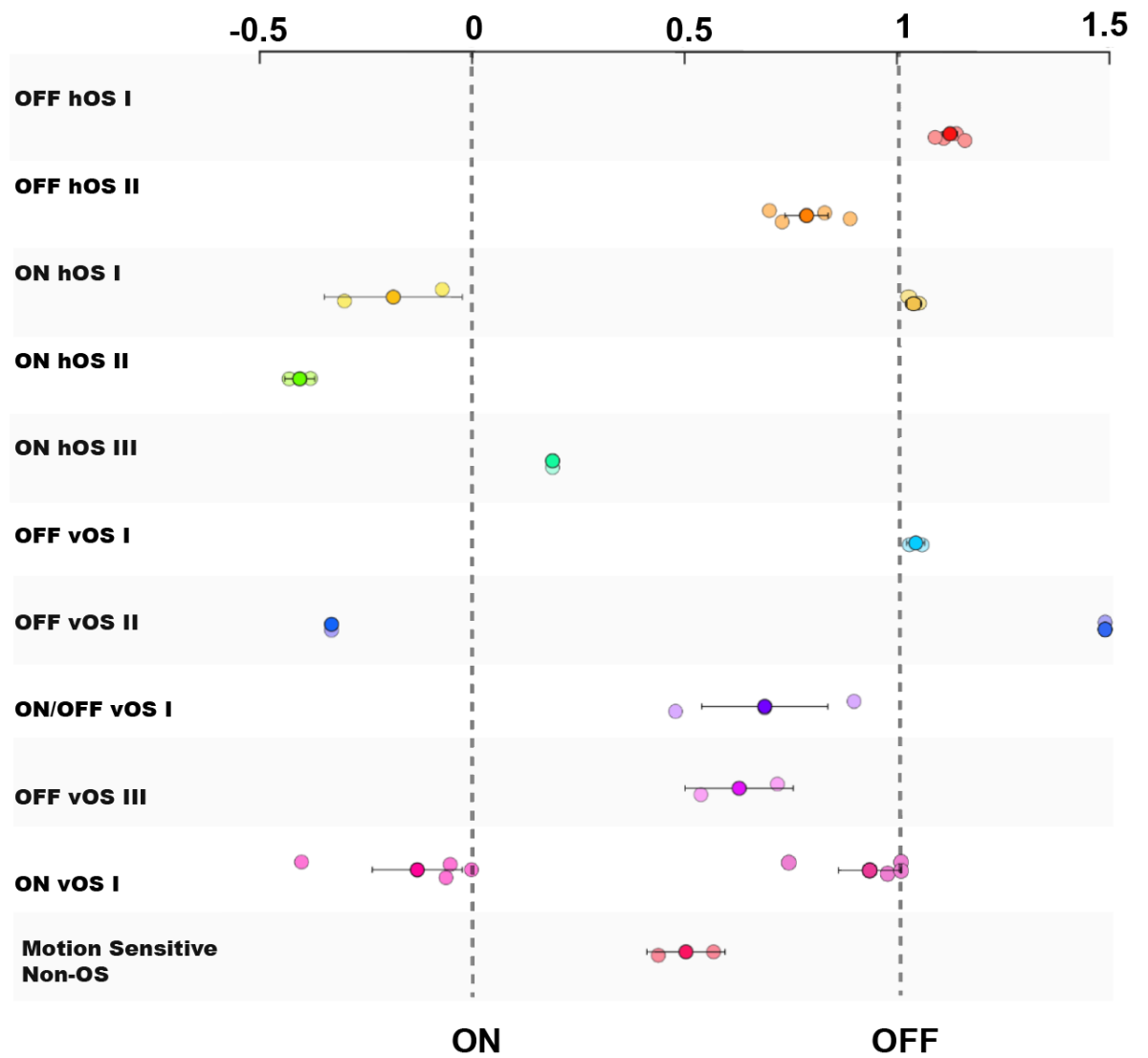


Figure 3.6 Stratification Depths of Functionally Identified OS Types | Quantified stratification depths of OS types (n=27 individual RGCs, n=22 mice). X axis indicates normalized depth. 0 indicates ON ChAT band and 1 indicates OFF ChAT band. Individual colored markers indicate individual cells. Mean indicated with darker shading and standard deviation is indicated with black bars.

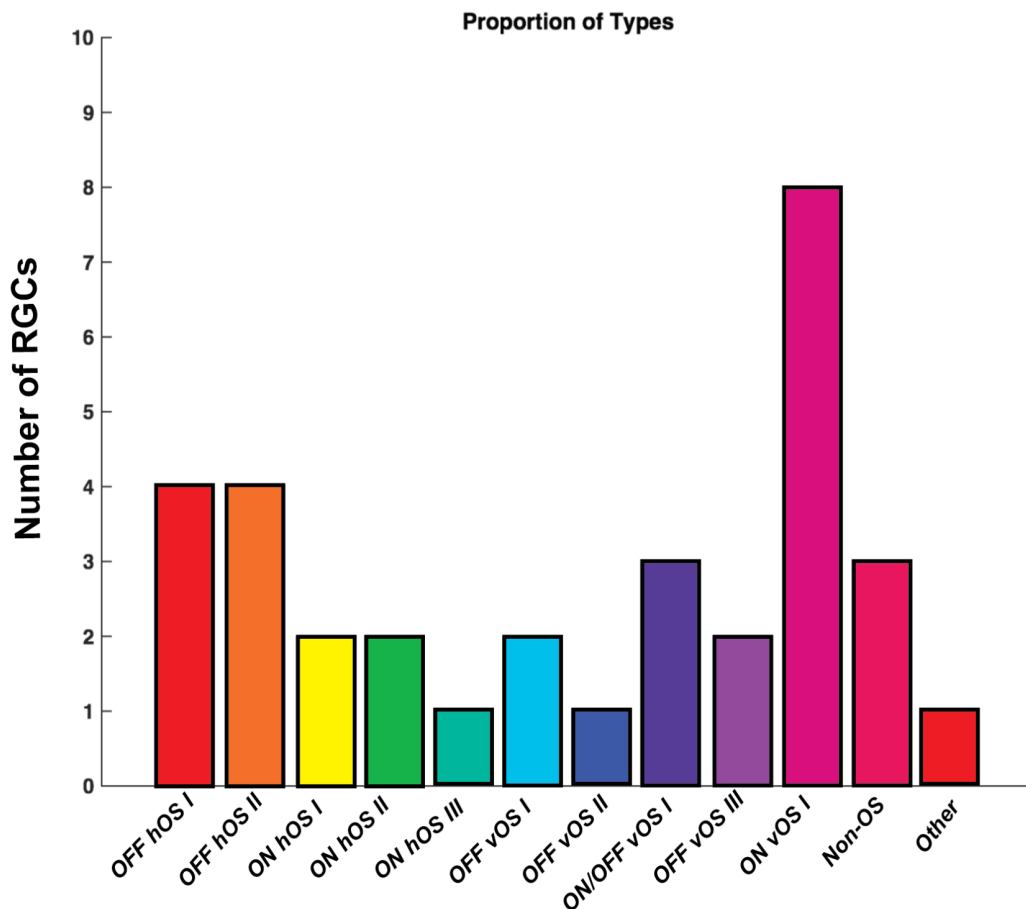


Figure 3.7 Distribution of targeted OS RGC types identified in this study | Individual Cell groups determined by stratification depth are indicated as separate colored bars with their names denoted in the x-axis (n=28 mice, n=34 individual RGCs).

3.4.3 10 Target RGC Groups Demonstrate Apparent Orientation Selectivity

Since I collected a functional response and cell morphology for each individual RGC, I was able to analyze and compare fluorescence responses among types. By analyzing the response to the drifting grating stimulus, I determined the Orientation Selectivity Index (OSI) Value for each individual RGC. I observed a range of OSI values from 0.01-0.91 with an average of OSI=0.41 (Figure 3.8, A). By comparing OSI values

amongst groups, I determined that 10 of the groups could be classified as orientation biased based due to an average OSI value of over 0.2, the common value for an OS or DS RGC, as it reflects a preferred stimulus response that is at least 33% more robust than it's response to the non-preferred or orthogonal stimulus orientation. Based on their average OSI value, ten of the RGC groups were classified as OS and one was classified as non-OS based on its below-threshold OSI average (Figure 3.8, B). There was no significant difference in OSI value across the determined OS groups ($p=0.165$; One-Way ANOVA). Groups comprised of just one cell were excluded from statistical tests (ON hOS III and OFF vOS II).

3.4.4 All Orientation Angles Represented in Survey

For every analysis of an RGC drifting grating response, I determined the peak orientation angle by summing the $\Delta f/f$ value for all oppositely moving gratings. The maximum summed response of axial grating motion was used to determine the preferred orientation angle (Figure 3.9, A). All orientation angles were represented in our survey (Figure 3.9, B) consistent with prior studies (Baden et al, 2016; Nath & Schwartz 2016, 2017) . Most groups were fairly consistent in their angle preference; if there was a preference for more than one angle there was at least a bias towards a cardinal orientation. The ON/OFF vOS I

group was an exception and demonstrated inconsistent orientation angles. Not surprisingly, the motion sensitive non-OS group also demonstrated inconsistent orientation angles.

3.4.5 OS RGC Groups Show Consistent Contrast Polarity

I determined contrast polarity (preference for light or dark stimuli) for each group by averaging the fluorescence response to light and dark stimuli for individual RGCs (Figure 3.10, 3.11, 3.12). I identified both ON and OFF vOS and hOS cell types (Figure 3.12, A) For each grouping, cells were consistent in their polarity (Figure 3.12; Figure 3.6)

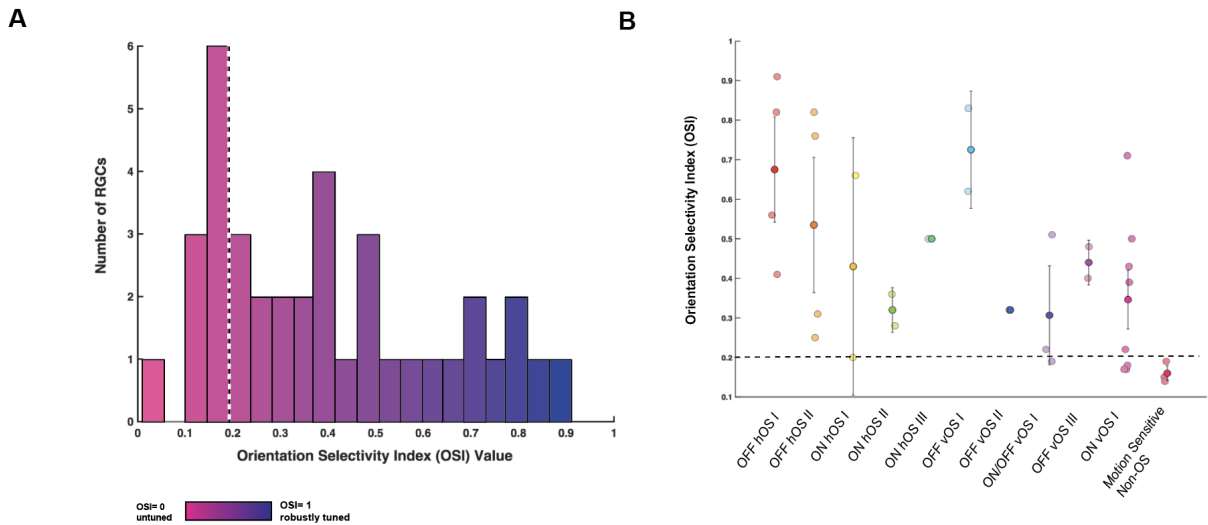


Figure 3.8 Targeted RGCs show a broad range of OS tuning strengths | (A) OSI value was obtained using the fluorescence response of individual cells (n=32 individual RGCs, n=28 mice) to the drifting grating stimulus. We used the formula $OSI = (R_{pref} - R_{orth}) / (R_{pref} + R_{orth})$. White dotted line indicates an OSI value of 0.2, our cutoff for an OS tuned cell (B) Individual markers indicate OSI values for individual cells in each group. Mean OSI values indicated with darker shading and black bars to denote standard deviation. Differences between groups were not significant (One-Way ANOVA; p=0.165). Black dotted line indicates an OSI value of 0.2, the cutoff for an OS cell.

Figure 3.9 Orientation Angle Preferences of RGC Groups | (A) Schematic of drifting grating stimulus and corresponding angle values. (B) Distribution of Orientation Angle Preferences determined with peak OSI angle, defined as the orientation where the sum of the response amplitudes to opposite drifting directions peaks. Individual RGC fluorescence responses from 28 mice (n=32 individual RGC responses). (C) Proportion of RGCs from each morphologically defined group that responded preferentially to a given angle. Preferred orientation was determined based on the maximum sum of oppositely moving drifting gratings.

with their preferred ON or OFF response reflected in the stratification of their dendrites in either the ON or OFF layers of the IPL. This was expected, because cell groupings were determined by stratification depth, which directly impacts the bipolar cells synapsing with the RGC dendrites and determining the polarity of a cell. The ON/OFF vOS type demonstrated possible ON/OFF properties, but did not cleanly respond to either flashing stimuli, similar to its EyeWire correlate, type 5to. As this type did not respond preferentially to any of the spot sizes presented in our light-step stimuli, it is likely that a larger stimulus size would elicit a stronger preference for light or dark stimuli, or more cleanly distinguish it as an ON/OFF cell. Until then, I remain agnostic to what the polarity of this type is, but for the sake of this study will refer to it as the ON/OFF vOS I type.

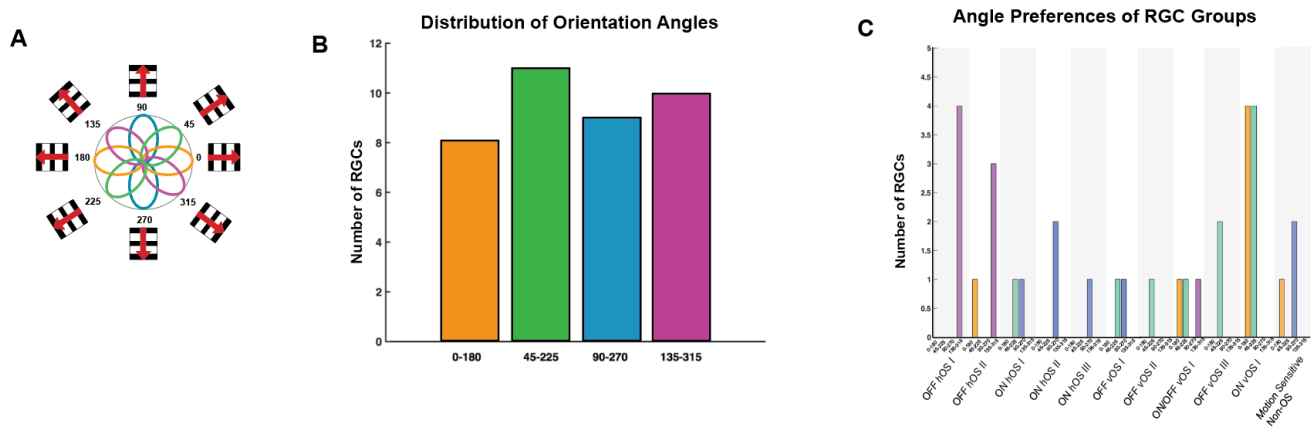


Figure 3.9 Orientation Angle Preferences of RGC Groups | (A) Schematic of drifting grating stimulus and corresponding angle values. (B) Distribution of Orientation Angle Preferences determined with peak OSI angle, defined as the orientation where the sum of the response amplitudes to opposite drifting directions peaks. Individual RGC fluorescence responses from 28 mice (n=32 individual RGC responses). (C) Proportion of RGCs from each morphologically defined group that responded preferentially to a given angle. Preferred orientation was determined based on the maximum sum of oppositely moving drifting gratings.

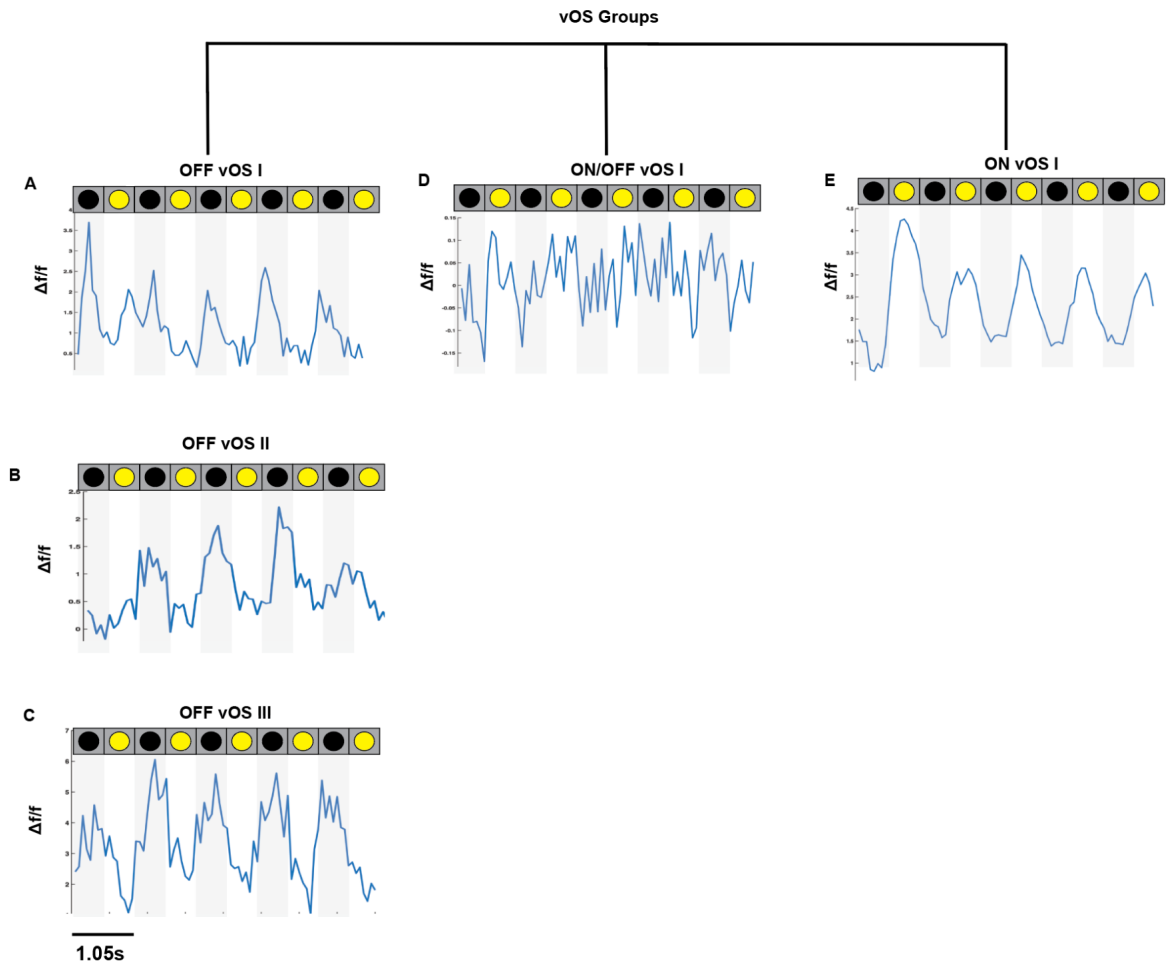


Figure 3.10 Contrast Polarity of vOS Type OS RGCs. RGC contrast polarity (ON/OFF) is readily resolved from the calcium response (A-E) Representative fluorescent tracings of individual RGCs in response to a flashing spot stimulus. The fluorescent response to the peak stimulus size response was used for each respective cell (from 33-666 μ m). A-C represent ON types. D represents an ON/OFF type. E represents an ON type.

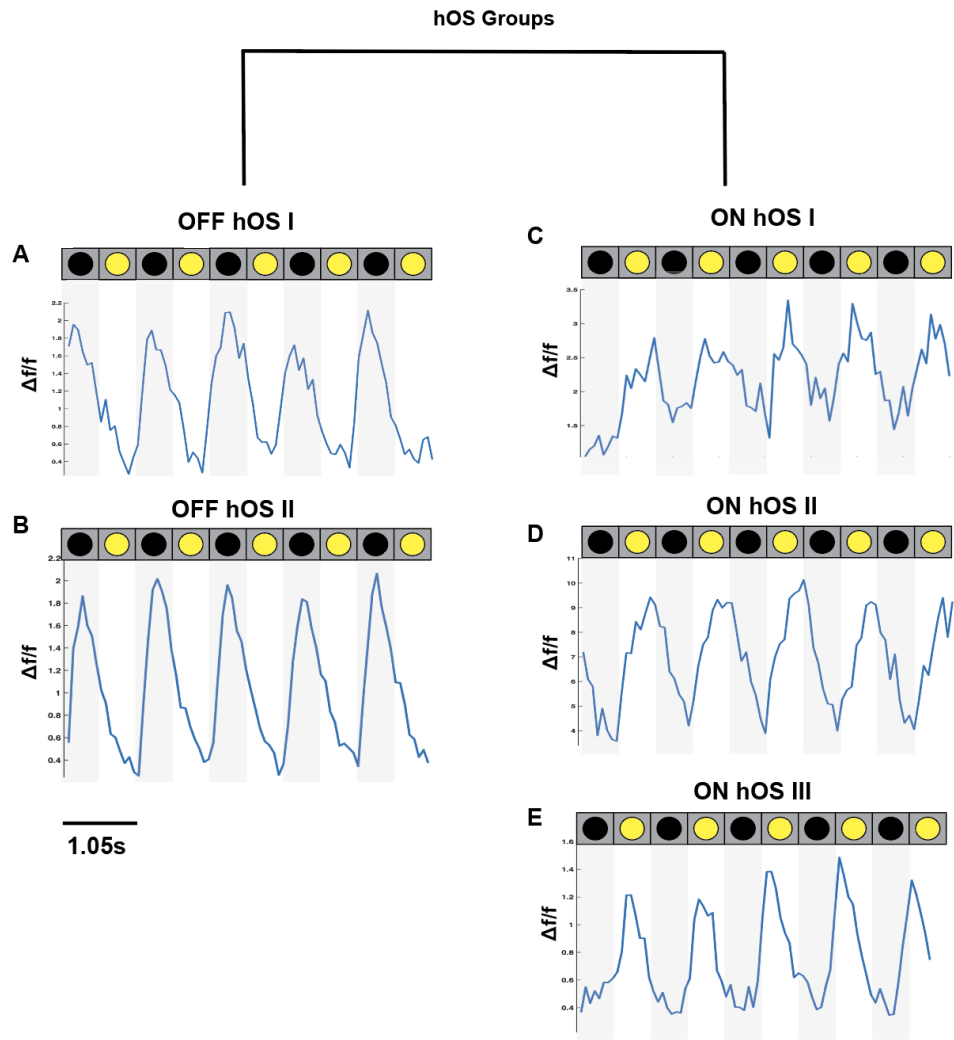


Figure 3.11 Contrast Polarity of hOS Type OS RGCs. RGC contrast polarity (ON/OFF) is readily resolved from calcium response] (A-E) Representative fluorescent tracings of individual RGCs in response to a flashing spot stimulus. The fluorescent response to the peak stimulus size response was used for each respective cell (from 33-666 μ m). A-B represent ON types. C-E represents an OFF types.

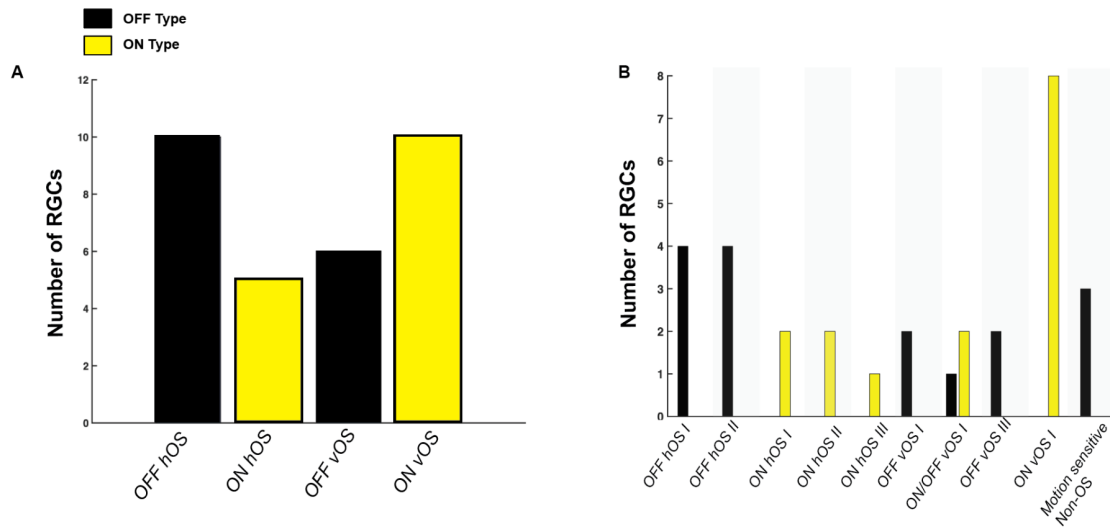


Figure 3.12 Distribution of RGC Type Contrast Polarity Preferences | (A) Proportion of ON and OFF vOS and hOS types determined by summation of combined responses to light increment and decrement stimuli. (B) Contrast polarity data for each morphological cell group (n=32 individual RGCs, n=28 mice).

3.4.4 Morphological Groups Demonstrate Heterogeneous Functional Responses

With information on stratification depth, contrast polarity, and orientation preference, I put together a dendrogram of types (Figure 3.13) and compared functional and morphological properties amongst cell groups. Within each group, cells were fairly consistent in their orientation preference. One exception was the ON/OFF vOS I type, which demonstrated a variety of orientation angles, but was named for its most prominent tuning properties.

When I compared OSI values across types, most cells were fairly variable in their tuning (Figure 3.8, B).

Within each RGC group there was a range of size tuning preferences (Figure 3.14). This is consistent with the findings from the large scale calcium imaging survey by Baden et al., (2016). They determined that their RGC clusters broadly span feature dimensions such as their preference for global versus local stimuli. The rgctypes.org site put together

by the Schwartz group as part of their multimodal RGC study includes information on receptive field sizes. There, too, most types span a wide range of preferences with a general trend for specific stimulus sizes. A higher n would likely elicit more reliable receptive field size preferences for each of our RGC groups.

I found that most cells preferred a temporal low frequency (1Hz) (Figure 3.15). The exception was the OFF vOS 1 type, which demonstrated a preference for a 1Hz and 10 Hz flashing spot. I note a robust preference for the 1Hz flashing spot as a hallmark of the ON vOS I type.

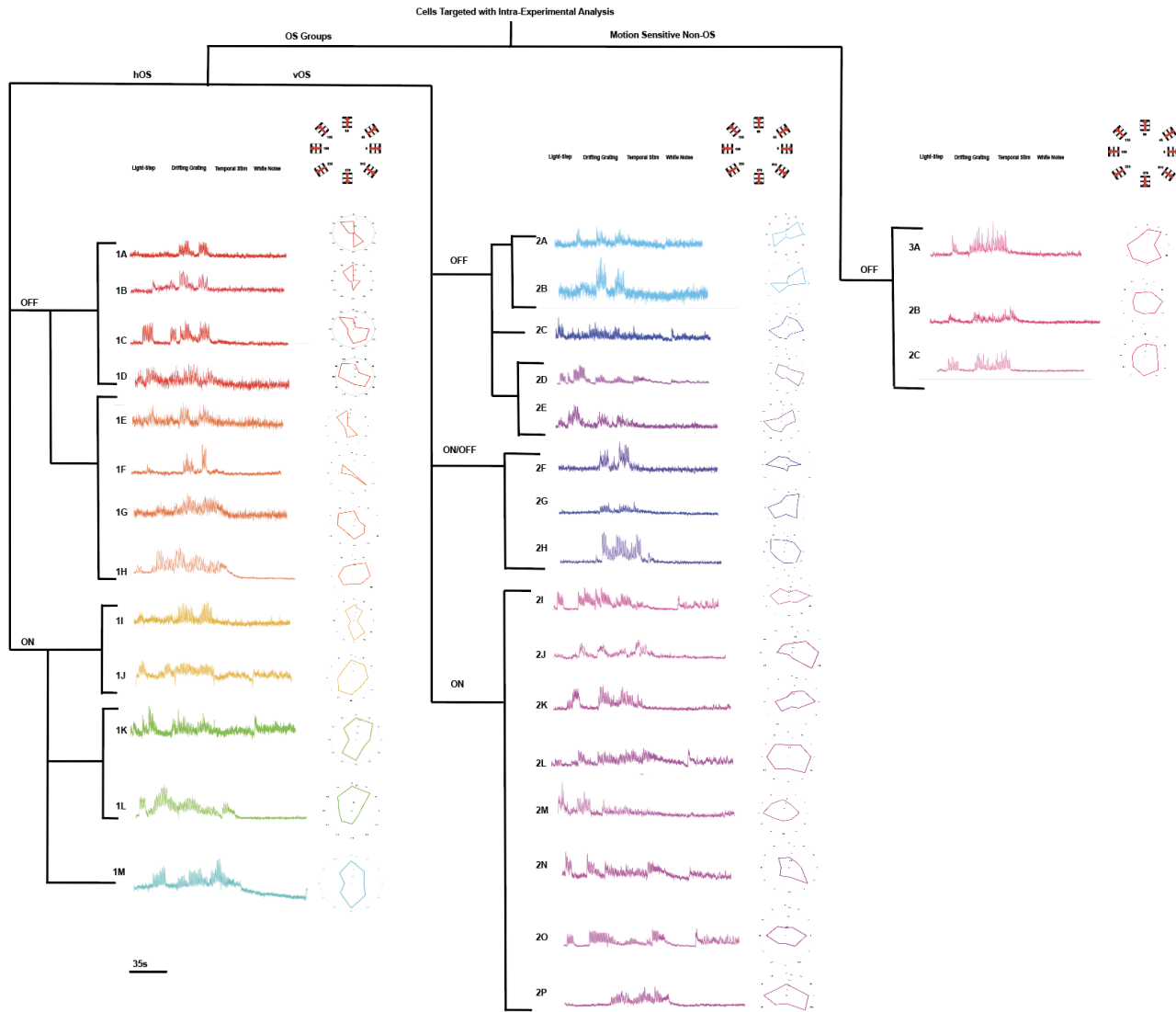


Figure 3.13 Dendrogram of RGC Functional Responses | Each trace represents the USTIM-evoked response of a single RGC (See Fig 2.4). Polar plots (right) show the modulation amplitude of the response to grating motion in each presented direction (n=32 individual RGC responses, n=28 mice). Each tracing represents an RGC targeted with the intraexperimental analysis described in Chapter II, falling into clusters 9,15, or 16 and is assigned a number that corresponds with a cell morphology of the same ID in Fig. 3.2. Polar plots to the right of each tracing are plotted by taking a fft of the average fluorescent response during that presented orientation of the drifting grating stimulus. Cells are grouped based on the stratification depth detailed in figure 3.6 and have been split up here by their polarity established in figures 3.10-2.12. 1A-1M represent hOS groups, 2A-2P represent vOS groups, and 3A-3C represent non-OS Motion sensitive cells that fell into OS clusters.

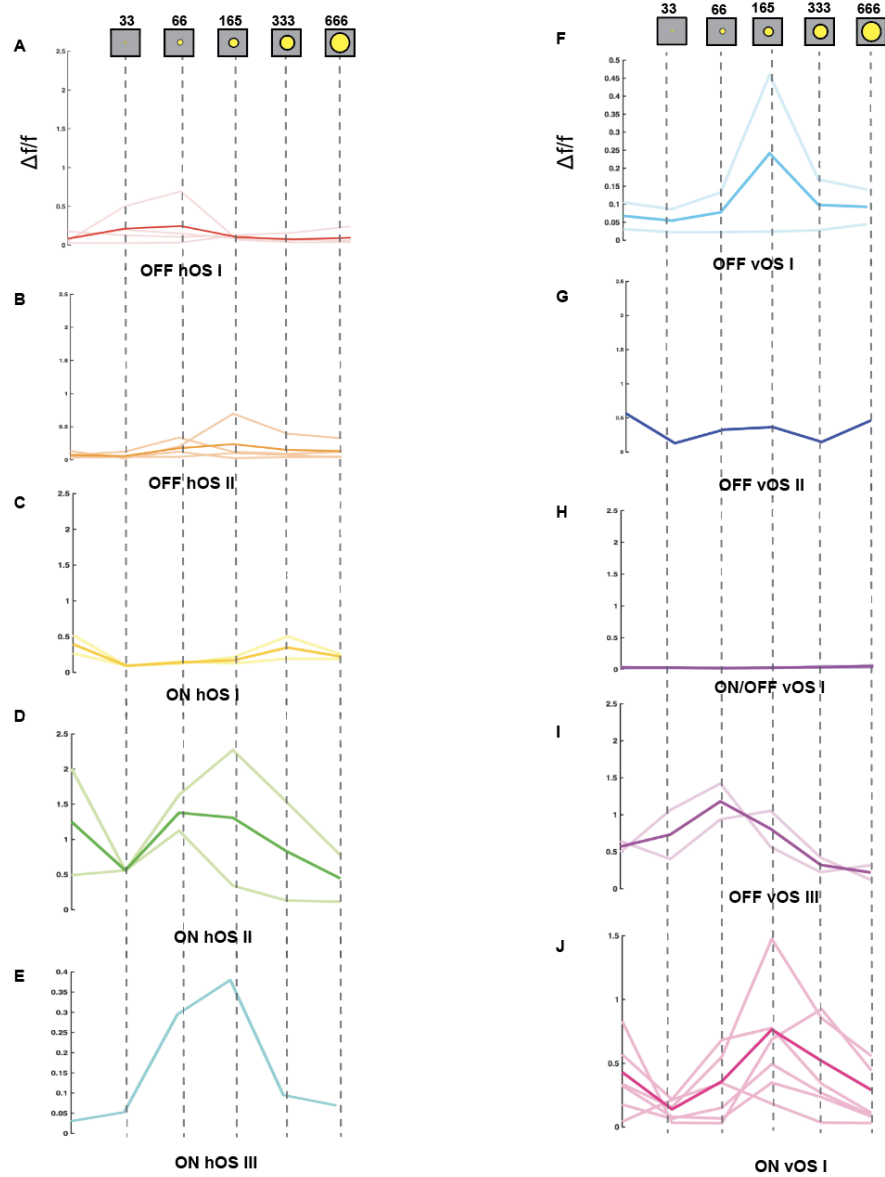


Figure 3.14 Size Tuning Functions of RGC Groups | (A-J) Size tuning functions were obtained with contrast-reversing spots of increasing diameter (33, 66, 165, 333, and 666 μm). Response is plotted as a fast fourier transform of the fluorescent response of the RGC during the time that the stimulus was presented. Darker lines with markers indicate the mean of all RGCs in that group (n=32 individual RGCs, n=28 mice).

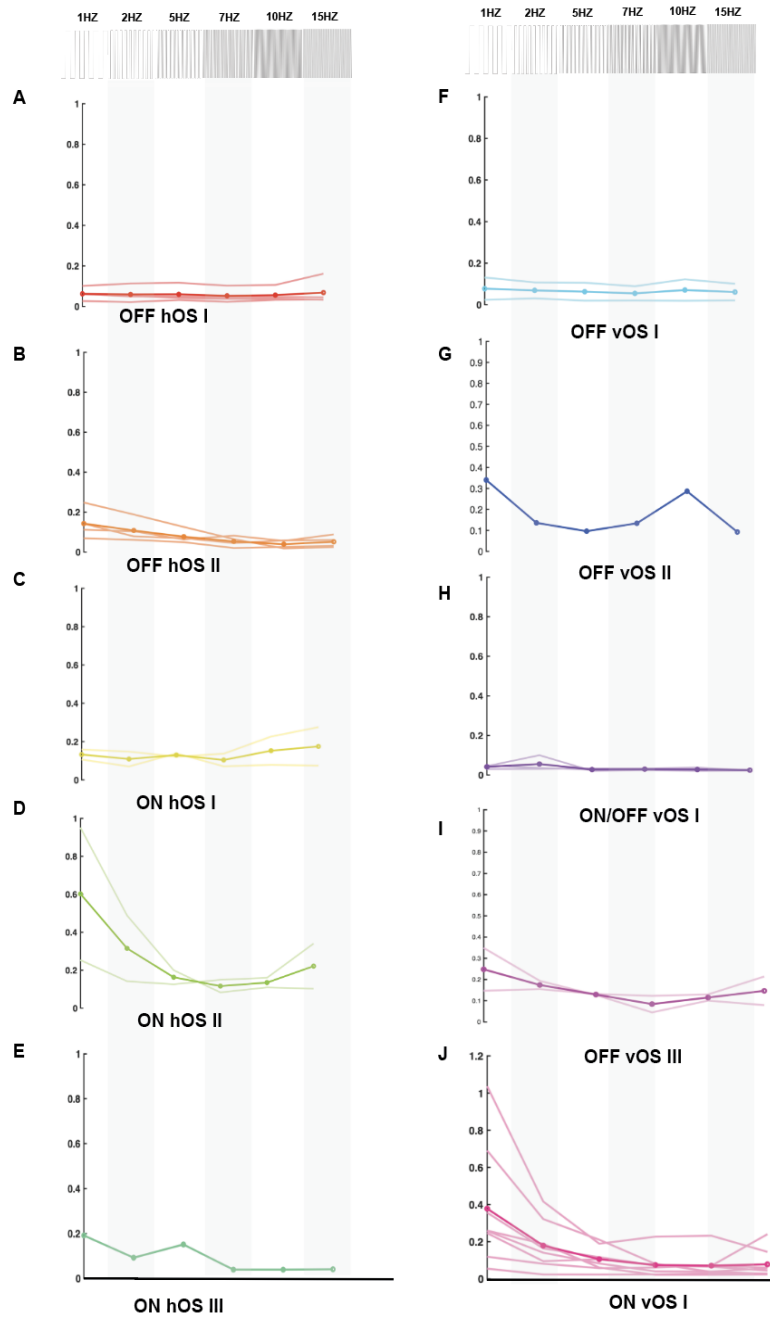


Figure 3.15 Temporal tuning functions of identified OS RGC groups | (A-J) Response amplitudes were measured as the response modulation amplitude computed using the Fast Fourier Transform of the response. Lightly shaded lines indicate individual RGC responses to temporal stimulus set at 1HZ, 2HZ, 5HZ, 7HZ, 10HZ, 15HZ. Darker lines with circular markers indicate mean fluorescent response of all RGCs in the group (n=33 individual RGCs, n=28 mice).

3.4.5 RGC Morphology Quantified with Imaris Analysis

Morphology was analyzed using Imaris Imaging Software. The Imaris Filament function was used to trace individual RGC dendrites semi-automatically (Figure 3.16, A). After the filament was completed (Figure 3.17) a series of anatomical quantifications were produced by the program, allowing us to compare morphological features amongst types. We know from the literature that tangential profile is not as reliable a predictor of a type as stratification depth (Sumbul et al., 2014), but I aimed to build out a profile for each cell that included potentially unique morphological features.

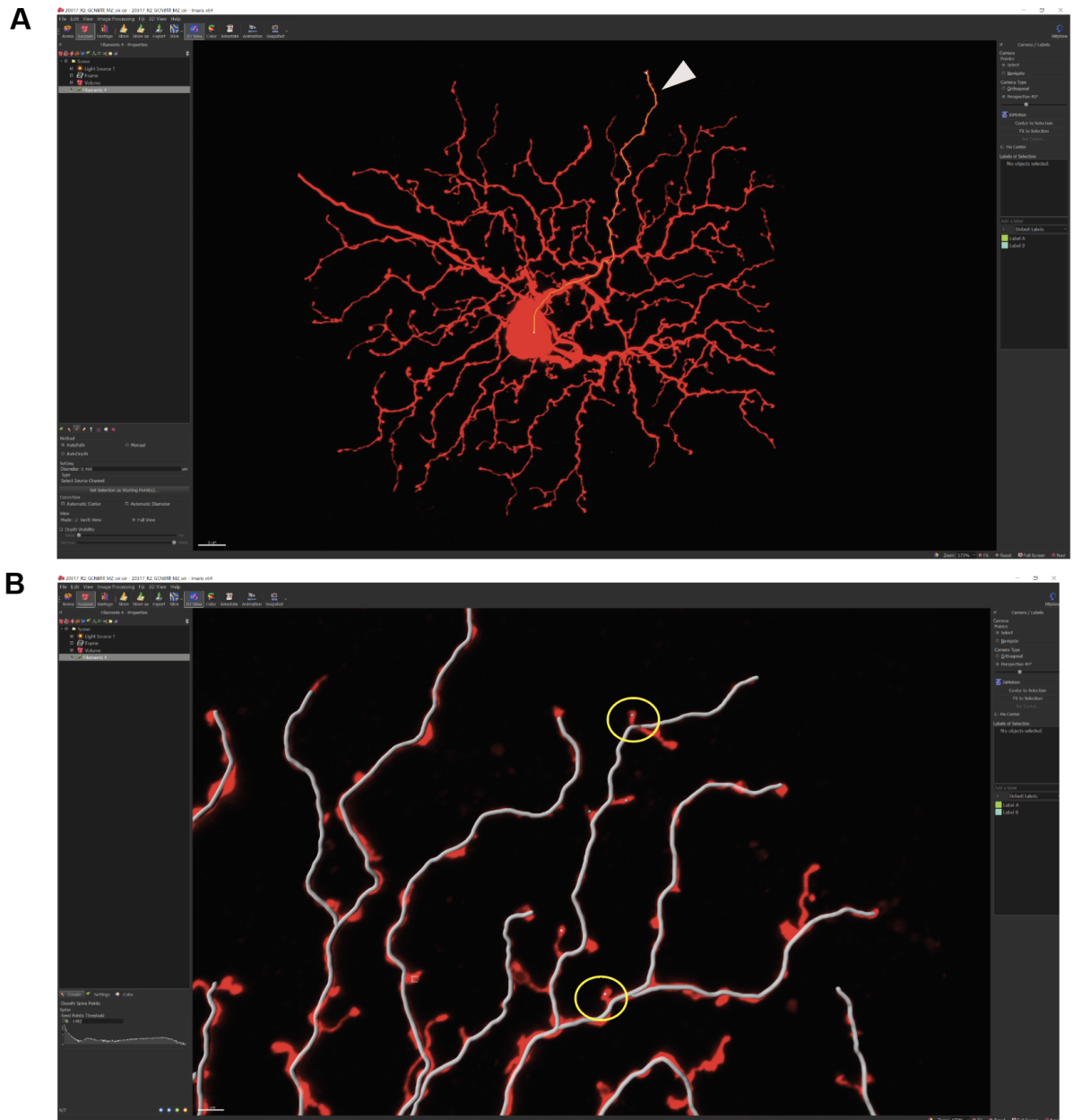


Figure 3.16 Imapris Filament and Spine Reconstruction | (A) Semi-automatic anatomical reconstruction of RGC (red) performed using the Filament Tool in Imapris. Individual filament (indicated with white arrow) is shown in yellow during reconstruction, from soma to the tip of the dendrite. (B) Spine reconstruction in Imapris using seed points (example spine with seed points indicated with yellow circles).

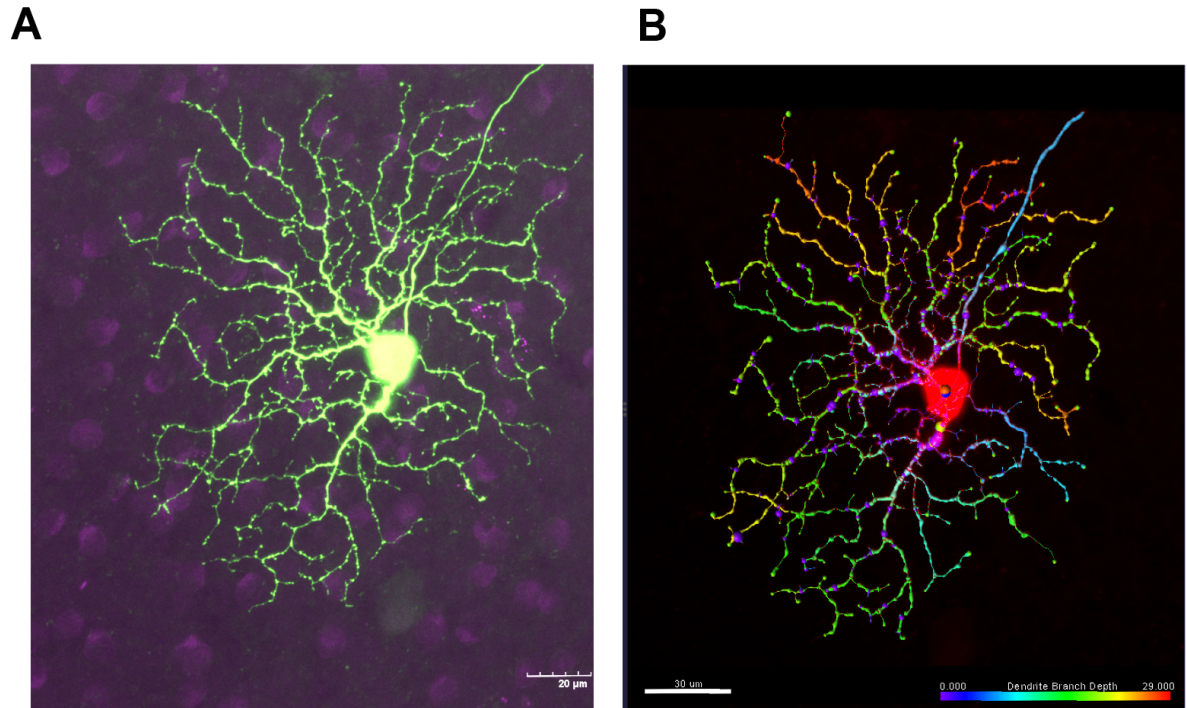


Figure 3.17 Quantitative Morphological Analysis of OS RGCs using Imaris Software | (A) Confocal z-projection of neurobiotin-filled OS cell (green) and choline acetyltransferase positive amacrine cells (magenta). (B) Cell morphology image generated in Imaris showing complete filament reconstruction of the RGC shown in (A). Colors indicate stratification depth.

3.4.6 Unique Morphological Features Observed Across Types

There was apparent variation across RGC groups when I quantified their total dendritic length (Figure 3.18, C). However, there was no significant difference observed with One-Way ANOVA ($p=0.0956$). I noted that the ON hOS II type demonstrated smaller dendritic area and length compared to the other types.

Dendritic complexity was a more polarizing feature across types. The OFF vOS III type, which did not demonstrate any remarkable difference in length compared to other types, exhibited the highest degree of dendritic complexity (Figure 3.18, D). Here, too, I

did not identify a significant difference in dendritic overlap using One-Way ANOVA ($p=0.075$).

While reconstructing RGCs, I noticed that several cells demonstrated the unique feature of dendritic spines. So, I used the Imaris program to annotate RGC spines (Figure 3.16, B). The most notable “spiny” cell types were the OFF hOS II type and ON/OFF vOS I type (Figure 3.19, A,B). When RGC spine count was analyzed, the OFF hOS II type had significantly more spines than the OFF hOS I and ON vOS I types, and the ON/OFF vOS I type had significantly more spines than the OFF hOS I and ON vOS I types (One-Way ANOVA; $p=0.00122$; Figure 3.19, A). When the same cell groups were analyzed for spine density, the ON/OFF vOS I type had significantly denser spines than the OFF hOS I and ON vOS I types (One-Way ANOVA; $p=0.0107$; Figure 3.19, B).

I also noticed that several cells possessed elongated dendritic arbors. Since there is precedent in the literature for elongated arbors corresponding with OS tuning (Antinucci et al., 2016; Nath & Schwartz, 2016; Bloomfield, 1991) I used Fiji (ImageJ; Schneider et al., 2012; Schindelin et al., 2012) to fit an ellipse to a polygon drawn around the dendritic field. I observed cells with remarkably elongated dendrites (Figure 3.20, A, C) but, surprisingly, did not find consistency in dendritic elongation within our morphologically defined types, or any significant difference across types (Figure 3.20, D; One-Way ANOVA, $p=0.1572$). While the occurrence of elongated arbors could indicate an anatomical substrate for OS tuning, I do not have enough information at this point to determine whether there is a direct correspondence between ellipticity and OS tuning in our dataset.

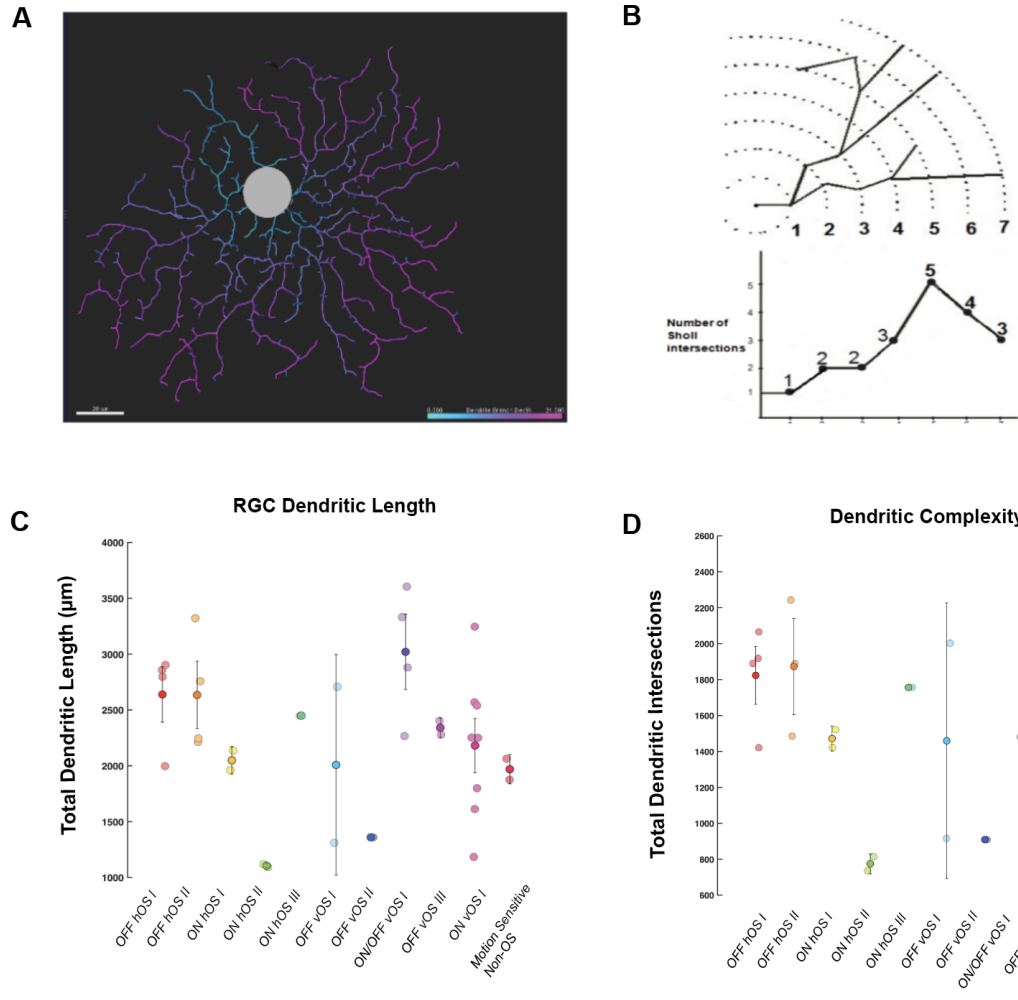


Figure 3.18 Quantifying OS RGC anatomical features using Imaris | (A) Filament reconstruction of RGC in Imaris; soma location denoted with grey circle. (B) From Imaris manual — Filament No. Sholl intersections is defined as the number of dendritic intersections on concentric spheres, defining dendrites spatial distribution as a function of the distance from the beginning point using 1µm step sizes. (A) Dendritic length in µm computed from the Imaris Filament reconstruction. Individual markers indicate dendritic length (µm) for each RGC. Darker shaded marker indicates mean with standard deviation. (B) Dendritic complexity determined by summing the area under the curve for sholl analyses for each individual RGC (individual markers). Mean shown in darker shade with standard deviation in black. There was no significant difference in dendritic length (One-Way ANOVA ; $p=0.0956$) or complexity (One-Way ANOVA; $p=0.075$) between groups.

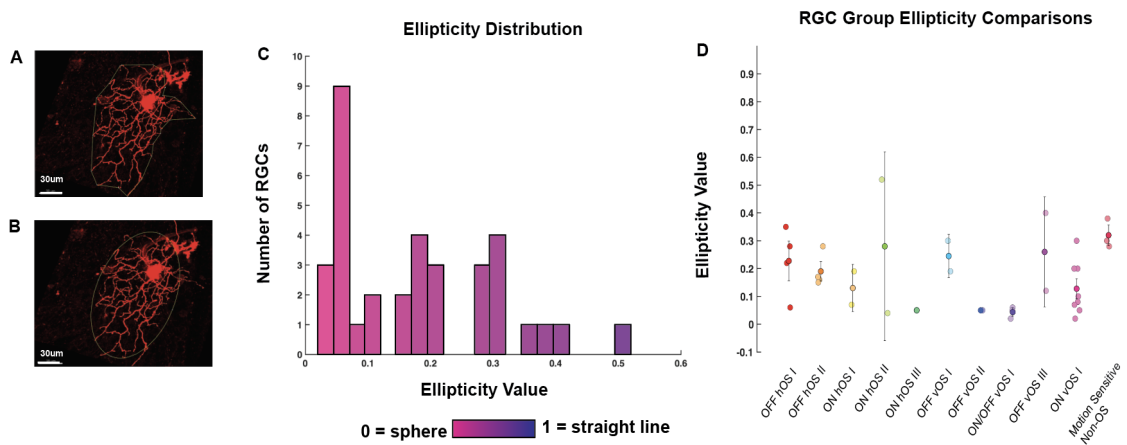


Figure 3.20 Ellipticity of RGC Arbors | (A-B) Z-projections of reconstructed RGCs. Image processing package Fiji was used to fit a polygon (A) and ellipse (B) to the reconstructed morphology to quantify the major and minor axis measurement which was used to calculate the ellipse value from 0-1 with 0 being a perfect sphere and 1 being a straight line. (C) Distribution of ellipticity values from reconstructed cells. (D) Comparison of ellipticity amongst cell groups with individual markers denoting individual cell ellipticity values from 0-1. Ellipticity values were not significantly different between groups (One-Way ANOVA; $p=0.1572$).

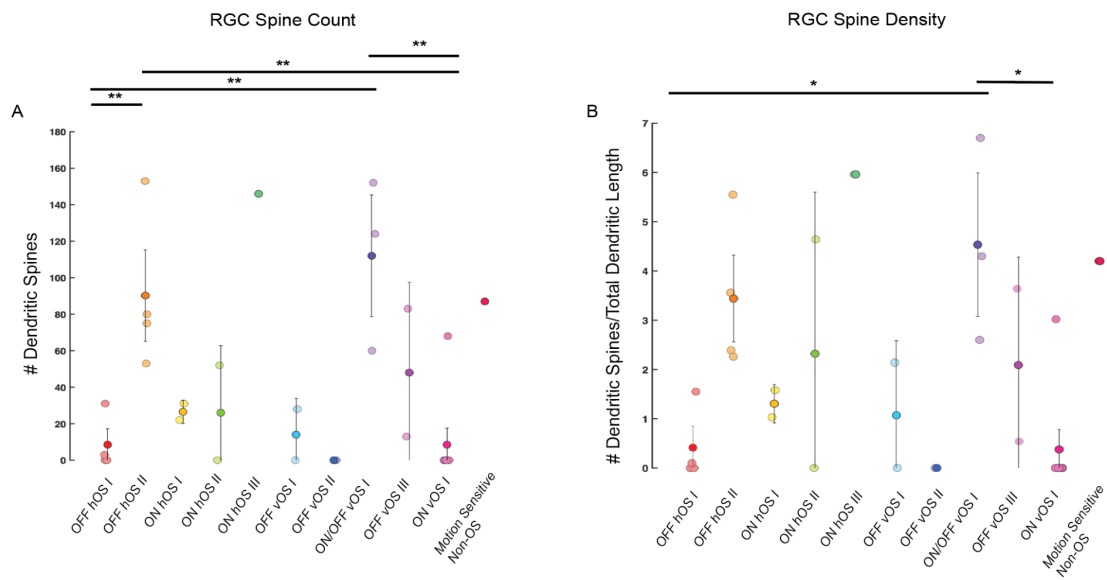


Figure 3.19 RGC Spine Count | (A) Total number of dendritic spines determined with Imaris Imaging Software. Individual markers indicate spine count for individual RGCs. Darker shaded marker for each respective group indicates mean spine count and standard deviation. (B) Total number of dendritic spines divided by the filament dendrite length. Individual markers indicate spine density for individual RGCs. Darker shaded marker for each respective group indicates mean spine density and standard deviation. ** $p<0.01$ * $p<0.05$ One-Way ANOVA

3.4.7 RGC Group Detailed Profiles

Using a combination of morphological and functional parameters, I was able to build out a profile for each OS group, describe their anatomical and functional features, and link them with types from the literature. Information for each individual cell can be found Table 1. I report on 10 morphologically distinct groups of cells demonstrating OS tuning, and 1 group that does not appear orientation tuned but is sensitive to directional motion:

1) OFF hOS I

I identified an OFF hOS type that consistently demonstrates OFF polarity and stratifies distal to the OFF ChAT band (n=4; normalized stratification depth = 1.13; Figure 3.6 A). I believe it corresponds with the 2i type from the EyeWire museum, which is functionally described on rgctypes.org as an OFF medium sustained cell type. It also likely corresponds with the OFF hOS type from Nath & Schwartz (2017), which also stratifies distal to the OFF ChAT band. Its OSI average was among the two highest groups, at OSI = 0.68 (SD=0.23; Figure 3.8, B).

2) OFF hOS II

I identified a second OFF hOS type whose dendrites were abutting the OFF ChAT band (n=4; normalized stratification depth = .79). This type consistently demonstrated OFF polarity. It likely corresponds with the 4i type from the EyeWire museum. This type has not been described in a previous discrete OS study, indicating that it may be a new OS type. The 4i type is described in rgctypes.org as an OFF transient small receptive field type. Our cell peaked at a 165um spot size, consistent with its apparent rgctype.org correlate.

This cell type demonstrates an OSI average of .54 (SD=0.3). I note the unique characteristic of prominent dendritic spines in this cell type.

3) *ON hOS I*

I identified an ON hOS type that was bistratified (n=2; normalized stratification depth = -0.19, 1.29) with dendrites laying against the outer edge of the ON and OFF ChAT band. It likely corresponds with the ON hOS type from Nath & Schwartz (2016). Due to the arrangement of its dendritic arbor, I believe it corresponds with type 27 from the EyeWire Museum. Type 27 is described as a sustained suppressed-by-contrast type in the rgctypes.org site. It has an average OSI value of 0.43 (SD=0.33).

4) *ON hOS II*

I also identified an ON hOS type that has not been described in a prior study. The cell stratifies proximal to the ON ChAT band (n=2; normalized stratification depth = -0.41). I believe it corresponds with type 9n from the EyeWire museum which is also called the PixON type (Johnson et al., 2018) a cell that encodes local image contrast. Total dendritic length was shorter than other types and demonstrated minimal dendritic overlap or complexity. It has an average OSI value of .32 (SD=0.06).

5) *ON hOS III*

I identified a cell that stratifies just distal to the ON ChAT band (n=1, normalized stratification depth = .19). It likely corresponds with the 6t type from the EyeWire museum. While the arrangement of its dendrites are very similar to the OFF hOS II group,

and it also demonstrates very prominent dendritic spines, its stratification depth and polarity placed it in a separate grouping. It is functionally described as an ON transient type. The OSI value for this cell is 0.5.

6) OFF vOS I

I identified an OFF vOS type that is likely the same OFF vOS type described in Nath & Schwartz (2017). The cell is stratified along the distal aspect of the OFF ChAT band (n=2; normalized stratification depth = 1.05). I believe this type likely corresponds with the 2aw type from the EyeWire Museum. I describe its dendrites as wavy and loosely stratified. It is also called the J-RGC type which is a cell that has been described as responding to upward motion (Nath & Schwartz, 2017; Kim In-Jung et al., 2008). It is functionally described as an OFF sustained type in the rgctypes.org database. The OSI average for this group was 0.73. (SD=0.15), placing it amongst the two most robustly OS tuned groups.

7) OFF vOS II

I identified an OFF vOS cell with dendrites stratified proximal to the ON ChAT band and some sparse dendritic stratification distal to the OFF ChAT band (n=1; normalized stratification depth = -.33, 1.5). This type likely corresponds with the 82wi type from the EyeWire museum and is described in rgctypes.org as an ON horizontal OS small receptive field type using data from Nath & Schwartz (2016).

8) OFF vOS III

I identified a second vOS type with preference for ON and OFF stimuli. It is very similar to the ON/OFF vOS I group but is more centrally stratified without multiple intensity peaks into the OFF ChAT band (n=2; normalized stratification depth = .63; Figure 3.6). I believe it corresponds with the 5so type from the EyeWire Museum. The 5so type is functionally described as an ON-OFF small RF type in rgctypes.org and is also described as an HD2 cell (Jacoby & Schwartz, 2017) a type tuned to object motion. The average OSI value for this type was 0.44 (SD=0.06).

9) ON/OFF vOS I

I identified a vOS type that has not been described in a prior OS study. The type had apparent ON and OFF responses. I believe it corresponds with the 5to type from the EyeWire Museum (n=3; normalized stratification depth = .69). Its spiny dendrites stratify in the central IPL and demonstrate several intensity peaks well into the OFF ChAT band. The EyeWire correlate for this type also demonstrates occasional ON and OFF tuning. The 5to type does not have a correlate in the rgctypes.org database. It is a unique cell type that did not respond to any of our light step stimuli, but still demonstrates robust activity in response to the drifting grating stimulus. It showed an average OSI value of 0.31 (SD = 0.18).

10) ON vOS I

I identified a bistratified ON vOS type (n=8) with dendrites stratifying along the ON and OFF ChAT bands with ON layer bias (n=4 quantified cells; normalized stratification depth

= -0.13, 0.93). I believe this type likely corresponds with 82wo from the EyeWire Museum. This type demonstrated an OSI average of 0.35 (SD = 0.2). Several cells demonstrated an OSI value under 0.2.

11) Motion Sensitive Non-OS Group

Our intraexperimental analysis identified a type with apparent motion sensitivity but below-threshold OSI average (Mean OSI = 0.16; SD = 0.16). This type likely corresponds with 5si from the EyeWire Museum and also is unique in its spiny arbor.

3.5 Summary & Discussion

The major goal of this aim was to construct a multimodal profile of OS Retinal Ganglion Cell Types using an intra-experimental analysis method to target cells via their functional response to a spatiotemporally diverse stimulus. The intra-experimental analysis was effective as it efficiently identified OS cells which could then be targeted for anatomical reconstruction. By analyzing stratification depth, I could split cells into different groups for further comparison. The results of Chapter III are summarized as a schematic in Figure 3.21. I sorted cells from OS clusters into 10 morphologically distinct types — and 1 non-OS type — based on our multimodal analysis. The summary of those cell types is as follows:

- 1) OFF hOS Type I** stratifies distal to the OFF ChAT band and likely corresponds with the 2i type from the EyeWire Museum.

- 2) **OFF hOS Type II** has spiny dendrites abutting the OFF ChAT band and likely corresponds with type 4i from the EyeWire Museum.
- 3) **ON hOS Type I** is characterized by its bistratified dendrites on either side of the ON and OFF bands in the marginal IPL. This type likely corresponds with Type 27 from the EyeWire Museum.
- 4) **ON hOS Type II** is defined by its dendrites stratifying proximal to the ON band. It likely corresponds with type 9n from the EyeWire Museum.
- 5) **ON hOS Type III** only presented as a single cell in our study and its spiny dendrites stratify just distal to the ON ChAT band. It may correspond with type 6t from the EyeWire Museum.
- 6) **OFF vOS Type I** stratifies in the OFF ChAT band and likely corresponds with type 2aw from the EyeWire Museum.
- 7) **OFF vOS Type II** consists of only one cell in our study and demonstrates slender dendrites that are bistratified. It likely corresponds with type 82wi from the EyeWire Museum.
- 8) **ON/OFF vOS Type I** has dendrites stratifying from central IPL past the OFF ChAT band with multiple intensity peaks. It likely corresponds with type 5to.
- 9) **OFF vOS Type III** stratifies centrally and likely corresponds with type 5so.
- 10) **ON vOS Type I** is bistratified with ON layer bias and likely corresponds with type 82wo from the EyeWire Museum.

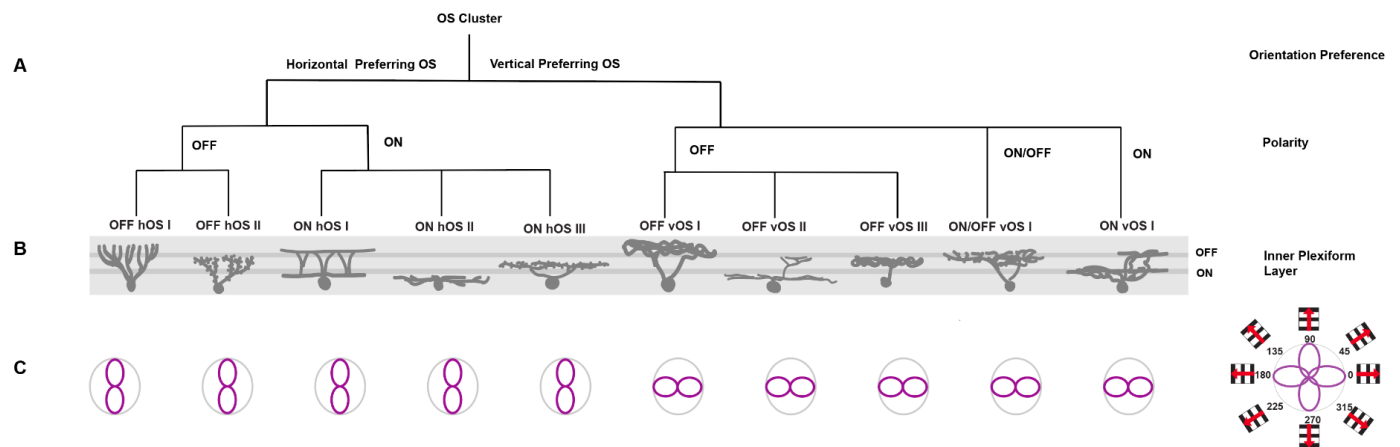


Figure 3.21 Overview of morphologically identified OS RGC Types | (A) Dendrogram of cell types guided by stratification depth. Dendrogram starts with cell responses assigned to an OS cluster. The dendrogram then splits groups by their averaged preference for horizontally or vertically oriented drifting gratings. Cells are split again by their preference for light or dark stimuli. (B) Schematic representations of stratification profiles for the defined set of OS RGC types. (C) Schematic representation of fluorescent response to drifting grating stimulus shown in purple.

I note that, within each template cluster (Figure 2.5, B;C), I identified multiple morphological types, indicating that each of our OS clusters contains multiple cell types. Forcing multiple cells into a type could be the reason for occasional non-OS cells getting grouped into that cluster. Changing the template to incorporate more cell types would likely circumvent this issue and allow for more targeted study of specific cell types using our novel method.

One of our objectives was to determine if there were OS RGC types that had not been previously described in detailed study. Our work indicates, firstly, that there are likely more than four RGC types that respond preferentially to oriented stimuli, as I observed 10 morphologically distinct RGC types with OS properties. For our cell types that have not

been described in a detailed OS study before, this presents an interesting avenue for future investigation into previously unknown OS cells.

While I also aimed initially to link morphological features with orientation tuning, the morphological data I gathered was insufficient to make any statement about whether there is definitively an anatomical substrate for orientation tuning. Previous work has described a morphological basis for orientation tuning (Antinucci & Hindges, 2013; Antinucci & Hindges, 2016; Nath & Schwartz, 2016; Bloomfield, 1994). While I did observe instances of apparent dendritic elongation (Figure 3.2, 1C; 2D; 3A; 1L) I did not observe any consistency in this feature within cell groupings (Figure 3.20).

I observed that many of the EyeWire correlates of our identified types that had been examined for their functional properties demonstrated variability in their apparent directional/orientation tuning. So, while this study has shed light on the diversity of cells that produce OS, it has also raised some questions about how and why so many different cell types have the capacity for OS tuning. There are a few possible explanations:

1) *A “Messy” Visual System*

I believe that some types may demonstrate OS tuning as a result of dedicated OS circuits, while others may occasionally produce an apparent OS response as a result of their dendritic structure. Why so many morphological types produce OS responses is an open conceptual question. Theoretically, all the OS information that is needed to be relayed to

downstream centers should be accomplished most efficiently with a few types — an ON and OFF type for horizontal and vertical orientations. Is there a purpose for multiple cells to produce OS, or is the mouse visual system just “messy”? Our intraexperimental analysis presents an efficient way to target cells based on OS response, but if a cell type that produces OS tuning as a by-product of dendritic arrangement in just a few instances of its development, we would capture it and only analyze the cells that have OS properties.

2) Some Cells May Be Selective for Axial Motion — Not OS.

Another potential explanation for our finding multiple morphological types is that some of the cells in our study are not OS, but may be selective for axial motion. Our drifting grating stimulus would not differentiate an axial motion selective cell from an OS cell. A potential future experiment could include presenting a more diverse stimulus set that includes a flashing bar, a moving bar, and a moving spot, thus determining whether the cell is truly OS, is responding to directional motion, or both.

3) Different OS Cells Are Projecting to Different Downstream Targets

While we don't yet know where OS cells project in downstream visual centers, it is possible that different types may be serving different purposes (For example, vision versus non-vision forming pathways). It makes sense conceptually that OS cells may project to areas with known OS tuning such as the dLGN and Superior Colliculus (Zhao et al., 2013; Piscopo et al., 2013), but other OS types could project to completely different targets such

as the paravigeminal nucleus or pulvinar.

The major findings of this first aim were that there are more than 4 OS types based on calcium imaging responses alone, and that those types can be reliably separated by their morphology and function. Because of the nature of the experimental analysis, function is prioritized and cells are targeted based on their drifting grating response. It is possible that cells that do not regularly demonstrate OS, but do so occasionally, would be targeted by our study as OS types. Detailed physiological analysis is necessary to determine if these cells have a distinct circuit responsible for generating the OS response.

CHAPTER IV- TARGETED ELECTROPHYSIOLOGICAL ANALYSIS OF ORIENTATION SELECTIVE GANGLION CELLS

4.1 Introduction & Background

In cell types without an elongated dendritic field — for which morphology cannot explain OS tuning, an integration of asymmetric synaptic inputs by amacrine cells and bipolar cells can contribute to the selective firing of OSGCs. Amacrine cell inhibition has been directly implicated in OS studies of rabbit, zebrafish, and mouse (Caldwell et al., 1978; Antinucci et al., 2016; Nath and Schwartz, 2016). Additionally, whole-cell voltage clamp recordings in rabbit, zebrafish, and mouse have produced examples of OSGCs types where both excitatory and inhibitory currents are tuned to the preferred and orthogonal orientation, respectively (Venkataramani and Taylor, 2010, Antinucci et al., 2016, Nath and Schwartz, 2016).

The objective of this aim was to determine the role of synaptic mechanisms in OS tuning of functionally identified OSGCs in our survey. Elongated receptive fields of OSGCs can arise from an asymmetric convergence of inputs. To create an orientation selective receptive field, there should be either inhibitory inputs during the orthogonal orientation, excitatory inputs during the preferred orientation, or both (Figure 4.1). I expected some combination of these mechanisms to be at play in target cells — *if they have a dedicated OS circuit*. I used the intra-experimental analysis approach described in Chapter II and III to target OSGCs for whole-cell voltage clamp recordings to isolate

excitatory and inhibitory currents to determine if they contribute to the cell's orientation tuning.

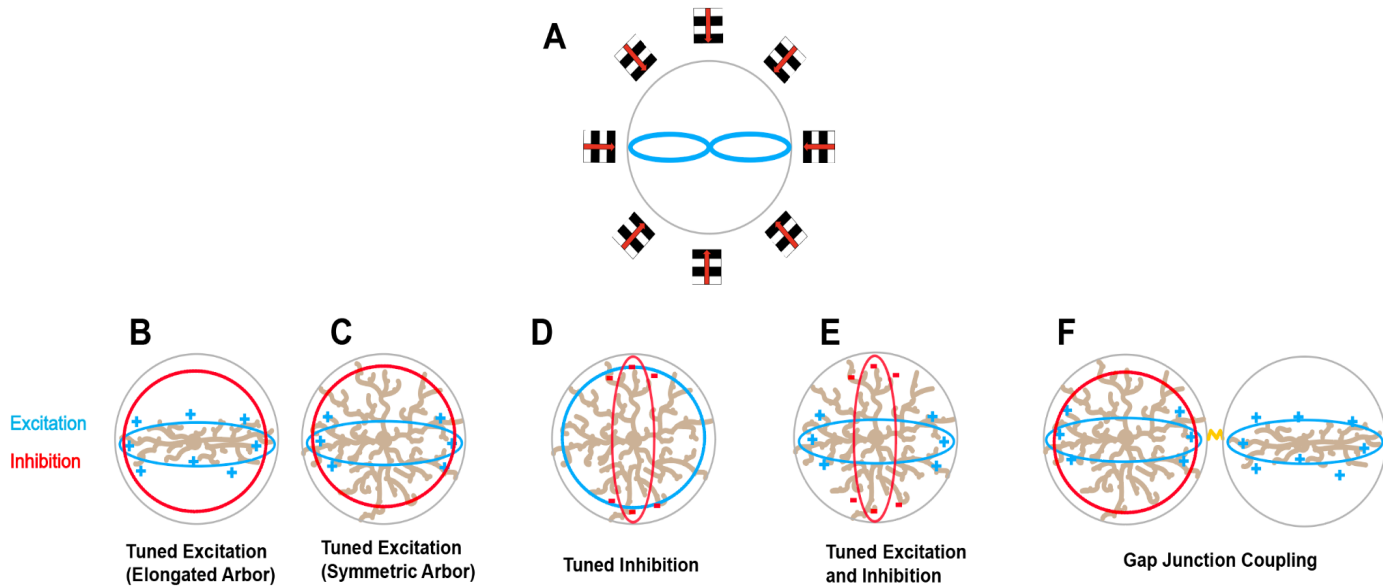


Figure 4.1 | Potential tuning mechanisms for Orientation Selective Cells. There are several ways to achieve an elongated receptive field associated with Orientation Selective Cells. **(A)** Example of a cell that responds preferentially to a vertically oriented stimulus moving horizontally across the visual field. **(B)** An elongated dendritic structure could create bias of excitatory responses along the oriented axis of the arbors. In this case, the dendritic field could directly provide the basis for an elongated receptive field. **(C)** In a cell with more symmetric dendritic arbors, tuned excitation during the preferred stimulus presentation could be the source of tuning. **(D)** Inhibition during the orthogonal presentation of the stimulus. **(E)** Excitation during the preferred and inhibition during the orthogonal. **(F)** Gap junction coupling of a cell with an orientation selective amacrine cell or ganglion cell could provide orientation selectivity.

4.2 Methods

4.2.1 Retinal Dissection

Retinal dissection is the same as described in Chapter II.

4.2.2 Two-Photon Calcium Imaging

Two-photon calcium imaging is the same as described in Chapter II.

4.2.3 Intraexperimental Analysis

Intraexperimental analysis is the same as described in Chapter III.

4.2.4 Targeted Electrophysiology

Cells were targeted for electrophysiological recording using the intra-experimental analysis method described previously. Borosilicate glass pipettes (typical impedance, 6-8mΩ) were filled with intracellular solution containing (in mM): 120 Cs-methanesulfonate, 5 TEA-Cl, 10 HEPES, 10 BAPTA, 3 NaCl, 2 QX 314-Cl, 4 ATP-Mg, 0.4 GTP-Na₂, and 10 phosphocreatine-Tris₂ (pH 7.3, 280 mOsm), and red fluorescent dye (Sulforhodamine 101). Voltage clamp recordings of ganglion cells were performed at the reversal potential for chloride and cations, respectively -60 mV and +15 mV.

4.2.5 Determining OSI Value for Electrophysiological Recordings

I quantified the computed OSI value for each cell using the following formula:

$$OSI = (R_{pref_ori} - R_{orth}) / (R_{pref_ori} + R_{orth})$$

Where R is the cell's electrophysiological response held at either reversal potential for excitation or inhibition. Pref_ori indicates the preferred orientation, and orth indicates the non-preferred orientation. The preferred orientation was defined by taking the maximum sum of two opponent directions that evoked the largest response. The null or "orthogonal" orientation is perpendicular to the preferred orientation.

4.3 Results

To assess how the synaptic inputs contribute to the orientation selective responses, OS cells were targeted for whole-cell voltage clamp electrophysiology. OSGCs were exposed to the same spatiotemporally diverse stimuli that was described in Chapter II. In voltage clamp recordings a ganglion cell was held at the reversal potential for cations, isolating inhibition (-60mV), and chloride, isolating excitation (+15 mV). I hypothesized, for each respective OSGC, that OS could be explained from either tuned excitation, tuned inhibition, or both. Cells were filled with sulforhodamine during whole cell voltage-clamp recordings to visualize penetration of the cell, and to acquire fluorescence image stacks to compare with prior morphological data (Chapter III).

After collecting about 30 (n=29) electrophysiological responses from 19 *Thy1*-GCaMP6f mice, I sorted them into groups based on their unique physiological properties. I grouped cells based on their: contrast polarity, orientation tuning preferences, response kinetics, and temporal tuning. I identified 5 major groups based on the electrophysiological data alone (n=21 individual RGCs, n=19 mice; Figure 4.2-4.6) and found that the different cells within each group showed strong similarity. I linked each of the five groups with our known functional/morphological types from Chapter III based on similarities within their calcium response. 8 cells did not fit into one of these 5 groups. Of these, several demonstrate tuning mechanisms consistent with OS, but were assigned an “unknown” category if they could not be cleanly sorted into one of the groups or grouped amongst each other (n=8).

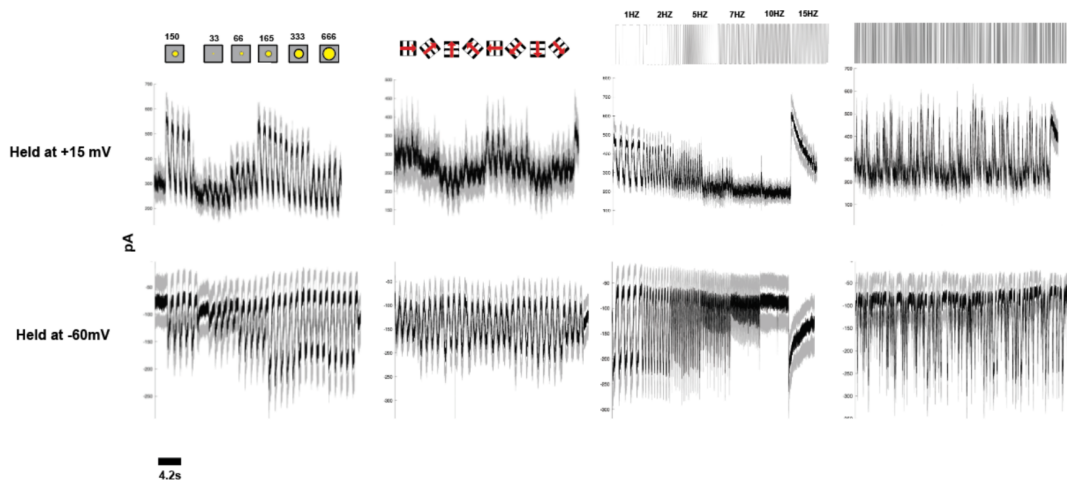


Figure 4.2 ON hOS I Electrophysiology | Whole-cell voltage recordings of target RGCs. Cells were held at reversal potential for chloride (-60mV) to isolate excitatory inputs and cations (+15 mV) to isolate inhibitory inputs. Individual cell responses are shown in grey; mean response is shown in black. (n=6 inhibition; n=7, excitation).

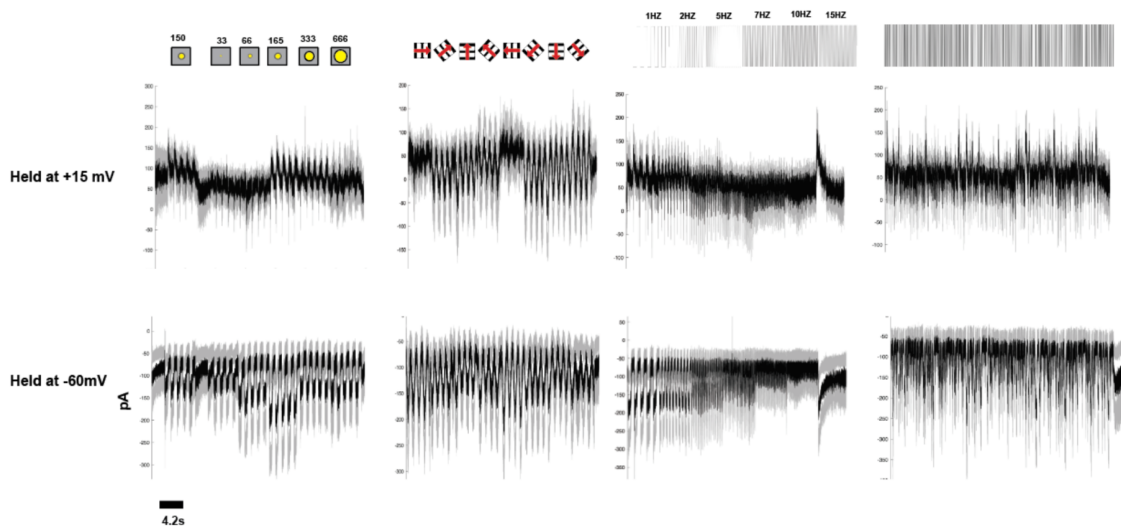


Figure 4.3 ON vOS I Electrophysiology | Whole-cell voltage recordings of target RGCs. Cells were held at reversal potential for chloride (-60mV) to isolate excitatory inputs and cations (+15 mV) to isolate inhibitory inputs. Individual cell responses are shown in grey; mean response is shown in black. (n=3, inhibition; n=3, excitation).

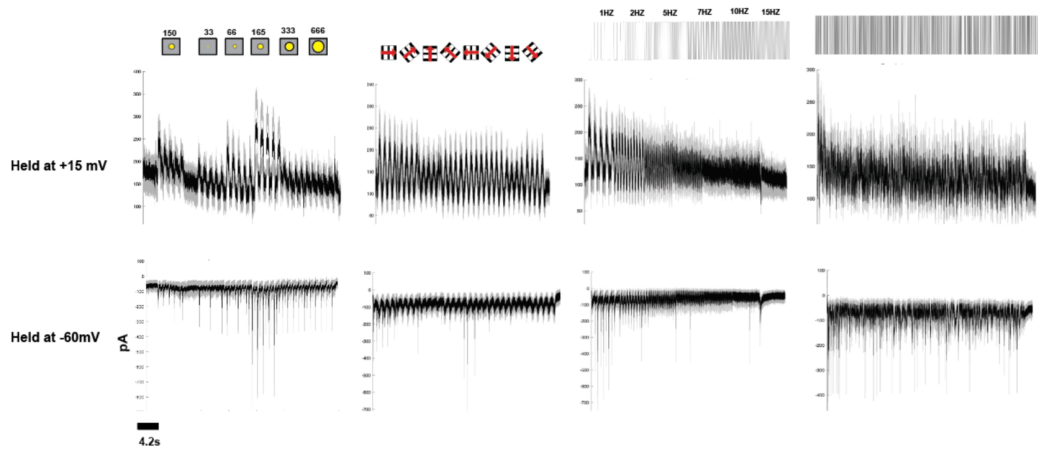


Figure 4.4 OFF vOS II Electrophysiology | Whole-cell voltage recordings of target RGCs. Cells were held at reversal potential for chloride (-60mV) to isolate excitatory inputs and cations (+15 mV) to isolate inhibitory inputs. Individual cell responses are shown in grey; mean response is shown in black. (n=5, inhibition; n=5 excitation).

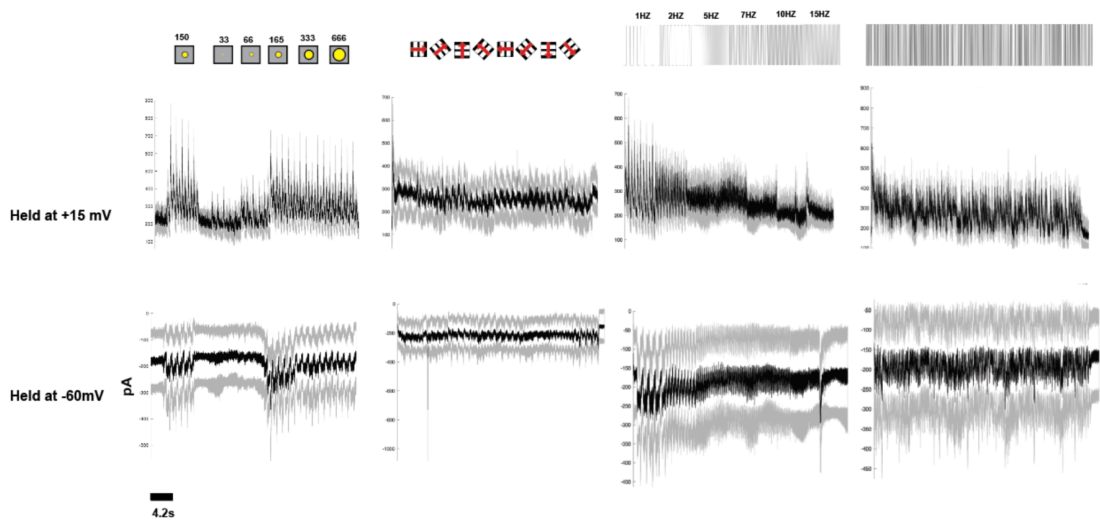


Figure 4.5 OFF vOS III Electrophysiology | Whole-cell voltage recordings of target RGCs. Cells were held at reversal potential for chloride (60mV) to isolate excitatory inputs and cations (+15 mV) to isolate inhibitory inputs. Individual cell responses are shown in grey; mean response is shown in black. (n=3 inhibition; n=3 excitation).

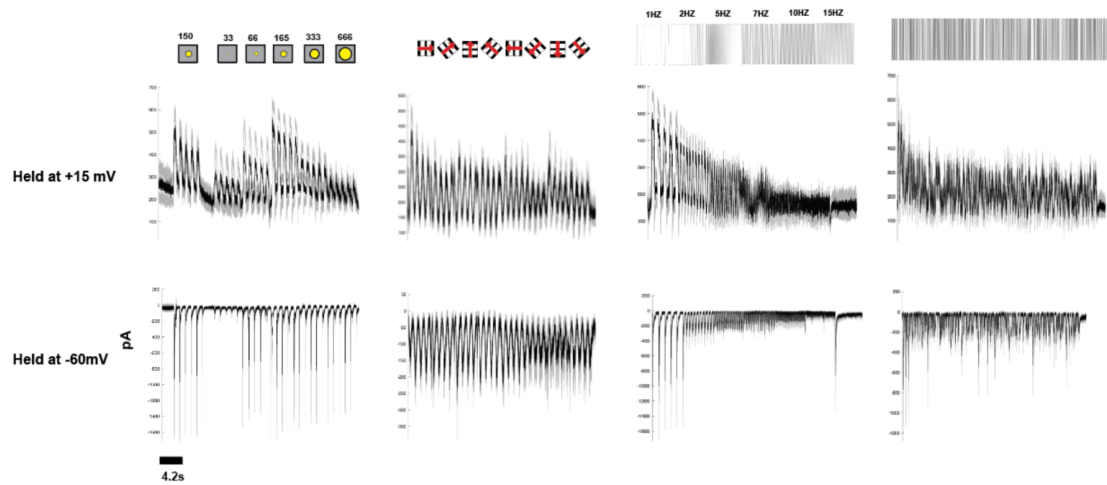


Figure 4.6 OFF hOS II Electrophysiology | Whole-cell voltage recordings of target RGCs. Cells were held at reversal potential for chloride (-60mV) to isolate excitatory inputs and cations (+15 mV) to isolate inhibitory inputs. Individual cell responses are shown in grey; mean response is shown in black. (n=3 inhibition; n=3 excitation).

The electrophysiological properties of the five groups are as follows:

4.3.1 ON hOS Type I Demonstrates Robustly Tuned Inhibition and Excitation

I observed a subset of hOS cells with robustly tuned excitation and inhibition (n=7 RGCs, mean excitation =0.26, mean inhibition = 0.42; Figure 4.7), indicating that OS in this cell type is driven by both excitation and inhibition. The inhibitory tuning was significantly stronger than the excitatory tuning, indicating that inhibition may be a stronger driver of the total OSI response (p=0.0155; Welch's T-test).

The excitatory responses were aligned with the preferred orientation of the cell — both the fluorescent response and excitatory response peaked primarily during the 90-270° presentation of the drifting grating stimulus (Figure 4.14). The inhibitory response was more spread out across the different presentations of the stimulus, and surprisingly the most

common inhibitory preferred orientation was not perfectly orthogonal to the preferred orientation; oblique orientations were more common.

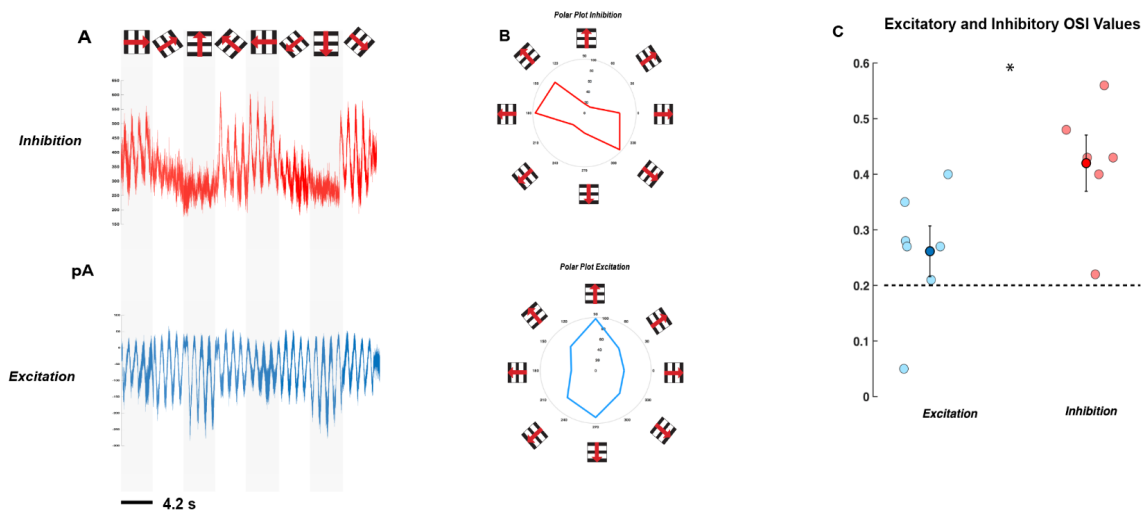


Figure 4.7 ON hOS Type I Demonstrates Robust Excitatory and Inhibitory Tuning | (A) Representative whole-cell voltage recordings. Below (blue) cell was held at reversal potential for chloride (-60mV) to isolate excitatory inputs. Above (red) cell was held at reversal potential for cations (+15) to isolate inhibitory inputs. Each presentation of the drifting grating stimulus lasts for a duration of 4.2 seconds. A fit of the each electrophysiological response to the individual drifting grating stimuli were plotted in (B) as representative polar plots for inhibition (OSI=0.59) and excitation (OSI=0.32). (C) OSI values for excitation (n=7, mean=0.26, n=7 mice) and inhibition (n=6, mean=0.42, n=6 mice) recorded from individual RGCs (n=7 RGCs, n=7 mice). The OSI value was calculated by taking the greatest summed value of two opposing drifting grating directions as the "preferred stimulus" and the sum of the perpendicular axis as the "non-preferred" orientation and applying the formula $OSI = (R_{pref-Rorth}) / (R_{pref+Rorth})$. Each marker denotes an individual recording, with the mean shown in a darker color with black bars to indicate standard deviation. The dotted line indicates an OSI value of 0.2. * $p < 0.05$; Welch's T-test.

4.3.2 ON vOS Type I Demonstrates Tuned Inhibition Only

A subset of vertical-prefering cells was identified with robustly tuned inhibition and negligible tuned excitation (n=3, mean excitation=0.14, mean inhibition =0.56; Figure 4.8); the inhibitory OSI response was significantly stronger than the excitatory OSI response (p=0.002; Welch's T-test). So, it appears that OS in this cell is driven by inhibition only. However, based on the preferred angle data for this cell type, there is apparent oppositely tuned inhibition and excitation (Figure 4.14). If excitation did not play a role in cell tuning,

it would be surprising for the excitatory preferred angle to be consistently opposite that of the inhibitory response. Thus, it appears that cells in this group are tuned through both excitation and inhibition, but the inhibitory mechanism is predominant.

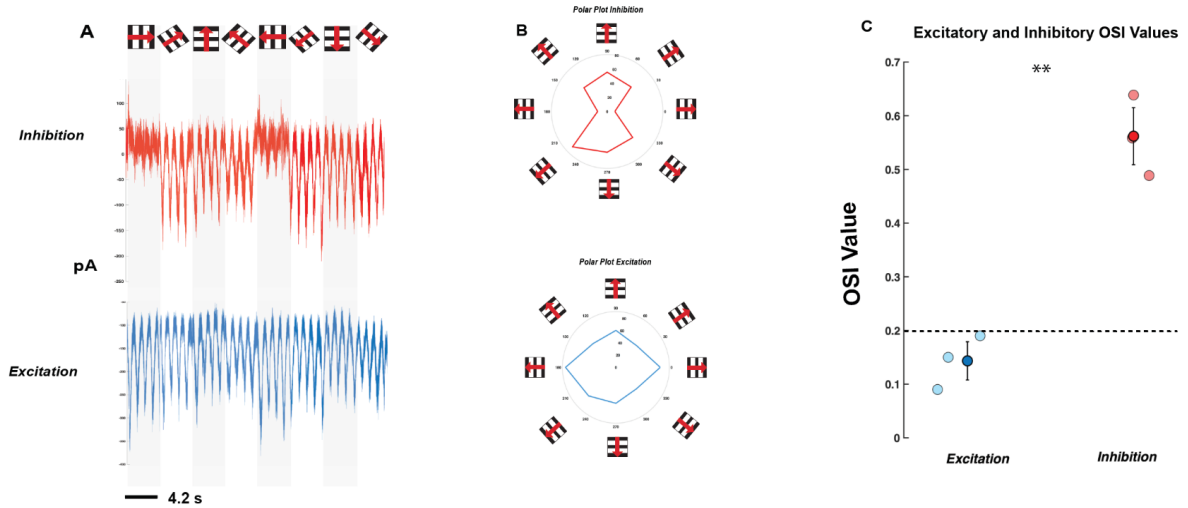


Figure 4.8 ON vOS Type I Demonstrates Inhibitory Tuning and Minimal Excitatory Tuning | (A) Representative whole-cell voltage recordings. Below (blue) cell was held at reversal potential for chloride, (-60mV) to isolate excitatory inputs. Above (red) cell was held at reversal potential for cations (+15) to isolate inhibitory inputs. Each presentation of the drifting grating stimulus lasts for a duration of 4.2 seconds. A fit of the each electrophysiological response to the individual drifting grating stimuli were plotted in (B) as representative polar plots for inhibition (OSI=0.64) and excitation (OSI=0.15). (C) OSI values for excitation (n=3, mean=0.14) and inhibition (n=3, mean=0.56) recorded from individual RGCs (n=3 RGCs, n=3 mice). The OSI value was calculated by taking the greatest summed value of two opposing drifting grating directions as the "preferred stimulus" and the sum of the perpendicular axis as the "non-preferred" orientation and applying the formula $OSI = (R_{pref} - R_{orth}) / (R_{pref} + R_{orth})$. Each marker denotes an individual recording, with the mean shown in a darker color with black bars to indicate standard deviation. The dotted line indicates an OSI value of 0.2. ** p<0.01; Welch's T-test.

4.3.3 OFF vOS Type II Demonstrates Matching Tuned Excitation and Inhibition

A subset of OFF vertical preferring cells that demonstrated surprising behavior was identified during electrophysiological recordings. There appeared to be slightly tuned excitation during the preferred stimulus (n=5, mean excitation = 0.19) with tuned inhibition matching the preferred excitatory angle of orientation (n=5, mean inhibition = 0.21) and no

significant difference between the two ($p=0.69$; Welch's T-test; Figure 4.9). During recordings to determine inhibition, the tuning was remarkably, and very consistently, matched to the angle of excitation (Figure 4.14). I believe this could be due to gap junction coupling, which has been reported previously in OS cells (Nath & Schwartz, 2017).

4.3.4 OFF vOS Type III Demonstrates Modest Excitatory Tuning

During recordings, I identified an OFF vOS cell type with modest excitatory tuning during

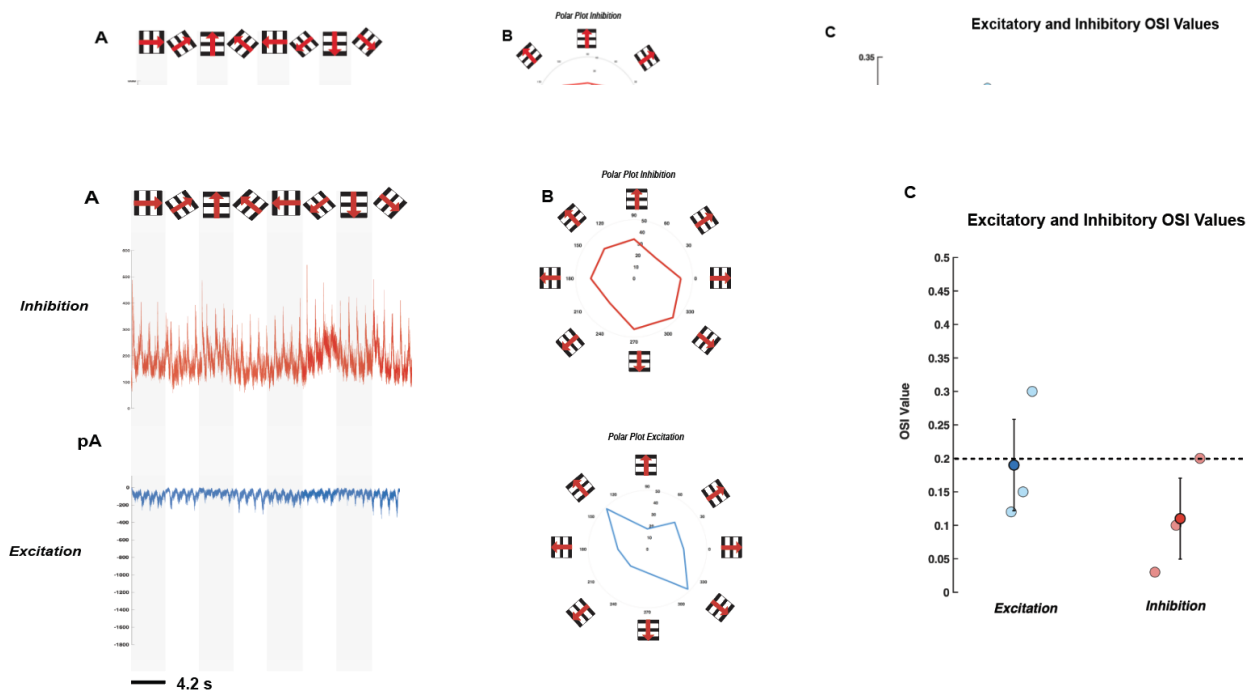


Figure 4.10 Off vOS Type III Demonstrates No Distinct OS Tuning | (A) Representative whole-cell voltage recordings. Below (blue) cell was held at reversal potential for chloride (-60mV) to isolate excitatory inputs. Above (red) cell was held at reversal potential for cations (+15) to isolate inhibitory inputs. Each presentation of the drifting grating stimulus lasts for a duration of 4.2 seconds. A fit of the each electrophysiological response to the individual drifting grating stimuli were plotted in (B) as representative polar plots for inhibition (OSI=0.13) and excitation (OSI=0.22). (C) OSI values for excitation (n=3, mean=0.19) and inhibition (n=3, mean=0.11) recorded from individual RGCs (n=3 RGCs, n=3 mice). The OSI value was calculated by taking the greatest summed value of two opposing drifting grating directions as the "preferred stimulus" and the sum of the perpendicular axis as the "non-preferred" orientation and applying the formula $OSI = (R_{pref} - R_{orth}) / (R_{pref} + R_{orth})$. Each marker denotes an individual recording, with the mean shown in a darker color with black bars to indicate standard deviation. The dotted line indicates an OSI value of 0.2. There was no significant difference between the two groups (Welch's T-test; $p=0.34$).

the preferred orientation and untuned inhibition (n=3, mean excitation = 0.19, mean

inhibition = 0.11), with no significant difference between the two ($p=0.34$; Welch's T-test; Figure 4.10).

4.3.5 OFF hOS Type 2 Demonstrates No Apparent OS Tuning Mechanism

When targeting cells that fell into the horizontal cluster, I identified a type with no apparent, consistent tuning for inhibition ($n=3$, $OSI=0.12$) or excitation ($n=3$, $OSI = 0.05$) with no significant difference between the two ($p=0.286$; Welch's T-test; Figure 4.11). This cell type also lacked consistency in its fluorescence response; while other aspects of the cell activity led it to be grouped together with the hOS cells, the response to the drifting grating stimulus — while most frequently preferring the horizontal presentation — also demonstrated an instance of preference for the vertical orientation (Figure 4.14).

4.3.6 Electrophysiological Tuning Corresponds with Fluorescent Responses

Several of the recorded cell types demonstrated little to no OS tuning when I isolated their excitatory and inhibitory inputs. I did note that the types with the most robust tuning in whole-cell recording — the ON hOS I type (Excitatory OSI = 0.26, n=7; Inhibitory OSI = 0.42, n=6) and ON vOS I type — also demonstrated the highest OSI values in their calcium responses (ON hOS I OSI = 0.58, ON vOS I OSI = 0.63; Figure 4.12; Figure 4.14). The cell with the lowest mean imaged OSI value (OFF hOS II; OSI = 0.37) demonstrated electrophysiological tuning below the cutoff for OS (excitation, OSI = 0.05, n=3; inhibition, OSI = .12, n=3).

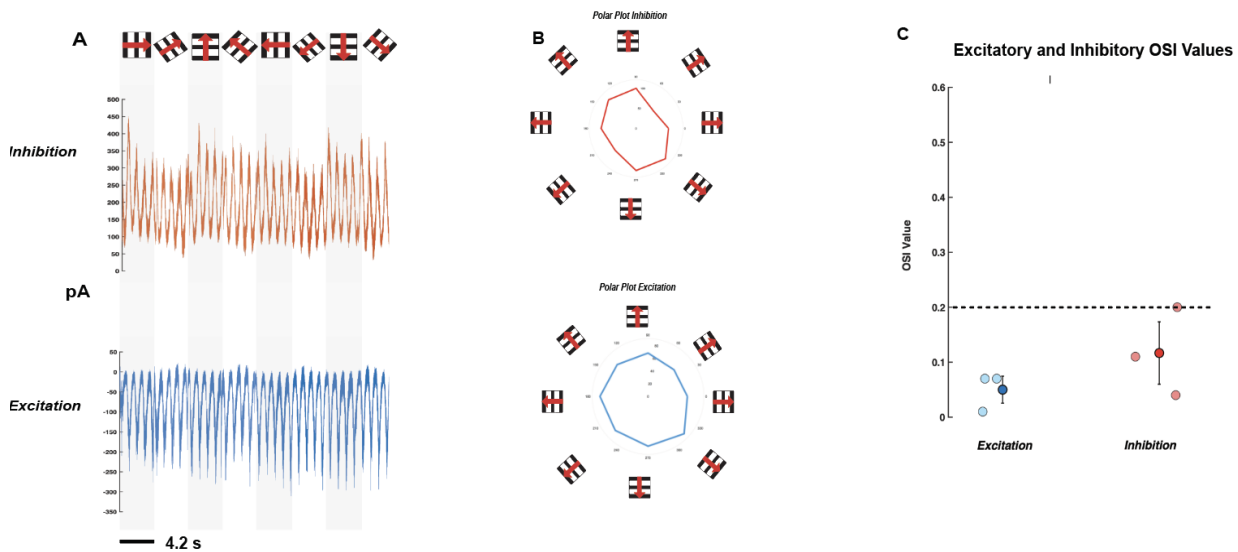


Figure 4.11 OFF hOS Type II Demonstrates No Apparent OS Tuning Mechanism | (A) Representative whole-cell voltage recordings. Below (blue) cell was held at reversal potential for chloride (-60mV) to isolate excitatory inputs. Above (red) cell was held at reversal potential for cations (+15) to isolate inhibitory inputs. Each presentation of the drifting grating stimulus lasts for a duration of 4.2 seconds. A fit of the each electrophysiological response to the individual drifting grating stimuli were plotted in (B) as representative polar plots for inhibition (OSI=0.11) and excitation (OSI=0.7). (C) OSI values for excitation (n=3, mean=0.05, n=3 mice) and inhibition (n=6, mean=0.12, n=6 mice) recorded from individual RGCs (n=3 RGCs, n=3 mice). The OSI value was calculated by taking the greatest summed value of two opposing drifting grating directions as the "preferred stimulus" and the sum of the perpendicular axis as the "non-preferred" orientation and applying the formula $OSI = (R_{pref} - R_{orth}) / (R_{pref} + R_{orth})$. Each marker denotes an individual recording, with the mean shown in a darker color with black bars to indicate standard deviation. The dotted line indicates an OSI value of 0.2. There was no significant difference between the two groups (Welch's T-test; p=0.286)

4.3.7 Inhibition, Not Excitation, Divides Cell Types

I compared electrophysiological OSI values across RGC groups. When I compared excitatory tuning I did not observe a significant difference in the tuning strength (OSI) of different RGC types ($p=0.07567$; One-Way ANOVA; Figure 4.12). However, I did observe a robust and significant difference when I compared inhibitory tuning across types. Both the ON hOS I and ON vOS I type demonstrated significantly stronger inhibitory tuning than the remaining three types — OFF vOS II, OFF vOS III, and OFF hOS II ($p=0.00002$; One-Way ANOVA; Figure 4.12). The ON hOS I and ON vOS I types did not demonstrate any difference when compared to each other; likewise the three remaining types also did not demonstrate any difference amongst each other.

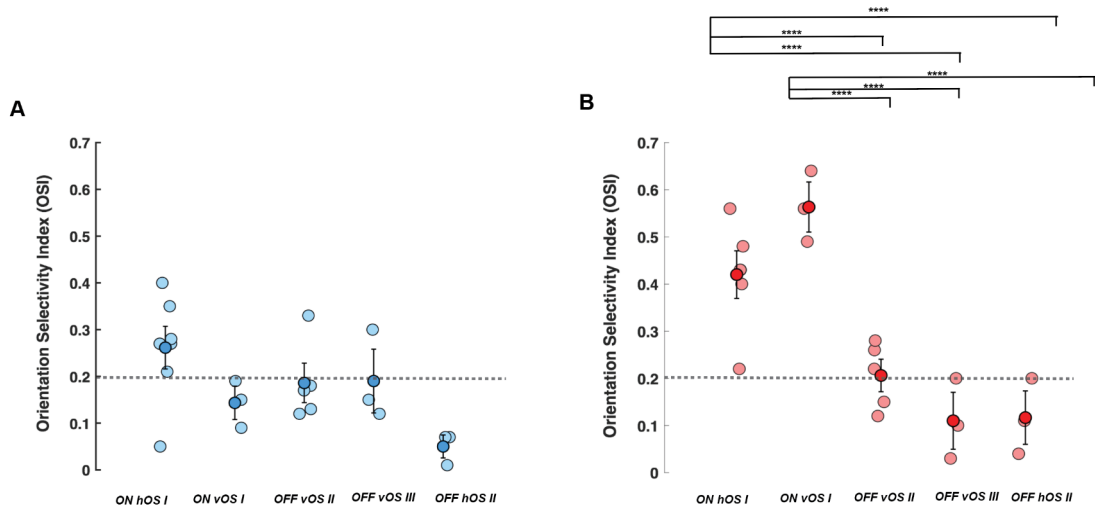


Figure 4.12 Comparing OS Tuning Across RGC Groups | Individual RGC whole-cell voltage recordings held at reversal potential for chloride (-60mV) to isolate excitatory inputs (A) and cations, +15 to isolate inhibitory inputs (B). Individual cell responses indicated with blue (excitatory) and red (inhibitory) circular markers. Mean for excitatory responses and inhibitory responses shown in darker blue and red, respectively, with standard deviation shown with black bars (n=21 RGCs; n=19 mice). Dotted lines indicate an OSI value of 0.2. OSI determined using the formula $OSI = (R_{pref}-R_{orth})/(R_{pref}+R_{orth})$. *** p<0.001; One-Way ANOVA.

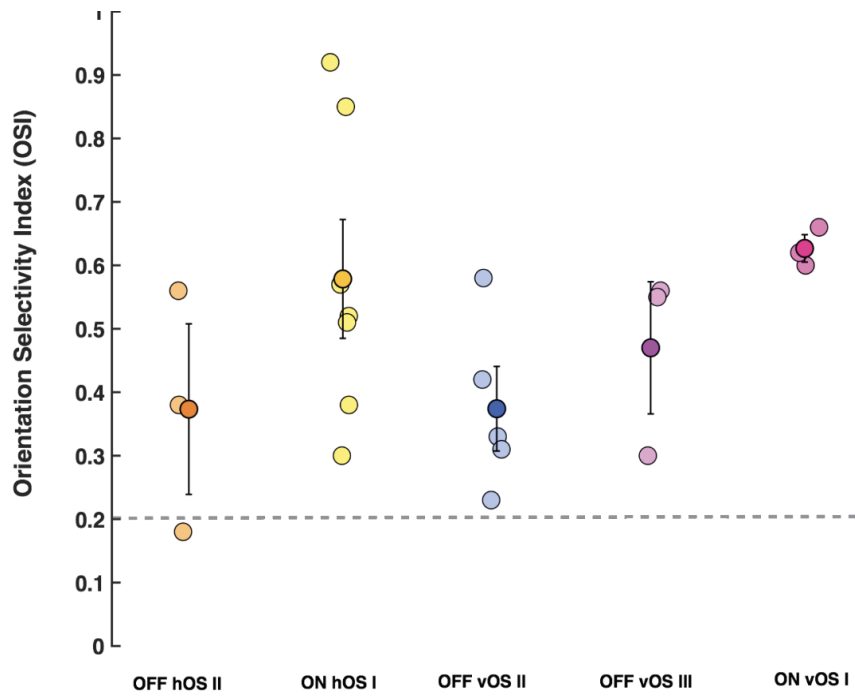


Figure 4.13 Comparison of calcium imaging-based OSI values across RGC types | (A) OSI Value was obtained using the fluorescent response of individual RGCs (n=21 RGCs, n=19 mice) to the drifting grating stimulus. We used the formula $OSI = (R_{pref}-R_{orth})/(R_{pref}+R_{orth})$. Dotted line indicates an OSI value of 0.2, our cutoff for an OS tuned cell. Individual markers indicate OSI values for individual cells in each group. Mean OSI values indicated with the darker respective color and black bars denote standard deviation. There was no significant difference between the RGC groups (One-Way ANOVA: n=0.189)

4.3.8 Fluorescence OSI Does Not Explain Difference in Tuning

To explain the robust difference in tuning, I looked to the OSI values for corresponding fluorescence responses of these cells. Surprisingly, the fluorescence OSI value for each cell group does not fully explain the differences in electrophysiological tuning. When calcium imaging and electrophysiological responses were compared, there was no significant difference between the five groups ($p=0.18915$; One-Way ANOVA, Figure 4.13).

Considering the diversity of tuning mechanisms amongst types, and the robust differences in tuning, I remain unsure as to why the integrated excitatory and inhibitory mechanisms do not result in a difference in OSI value.

4.3.9 Cell Morphology Accurately Predicts Response Kinetics and Contrast Polarity

By linking electrophysiologically recorded cells with the morphological types established in Chapter III, I was able to correlate morphological features with response features from our electrophysiological recordings, which are more spatiotemporally precise than calcium imaging data. Because of the higher spatiotemporal resolution of electrophysiology, I was able to assess the transient/sustained properties of OS types. I know from the literature that centrally stratifying cells generally express transient properties, while cells stratifying in the inner or outer margins of the IPL are more likely to exhibit sustained kinetics (Bae et al., 2017). I expected that the stratification profiles of our types would match up with the recorded response properties.

The OFF hOS II type demonstrates robust transient excitation in response to a dark spot, and, as predicted, stratifies more centrally in the IPL (Figure 4.15). The ON hOS I type is stratified in the inner and outer margins of the IPL, and also exhibits sustained

inhibition and excitation. Also, as predicted, the OFF vOS III type demonstrates transient excitation and inhibition and is centrally stratified. The ON vOS I type demonstrates excitation and inhibition and is centrally stratified. The ON vOS I type demonstrates sustained properties, and has arbors in the outer ON layer. The only cell that did not fit the profile was the OFF vOS II type. With arbors in the outermost portions of the IPL, I expected sustained response kinetics, but instead found transient excitation and sustained inhibition.

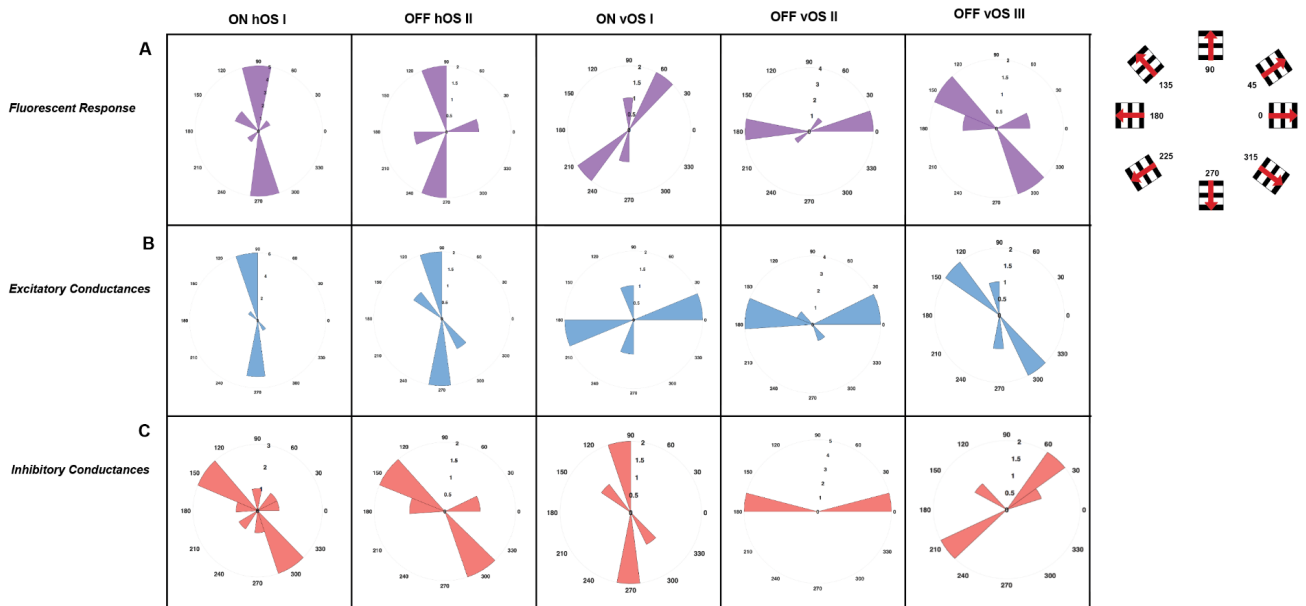


Figure 4.14 Orientation Angle Preference Distributions of Physiologically Recorded Cells | Polar Histograms of cell type orientation angle preferences. Preferred angle taken as the maximum sum of two oppositely moving gratings during the presentation of the drifting grating stimulus. (A) Polar histograms of cell group taken from the fluorescent response of the cell. (B) Polar histograms (purple) of preferred orientations during isolation of the excitatory inputs from whole-cell voltage clamp experiments held at -60mV (blue). (C) Polar histograms of cell groups during whole-cell voltage recordings held at +15mV to isolate inhibitory inputs to cell tuning (red). Angle preferences plotted by converting degree of orientation to radians with deg2rad function in MATLAB.

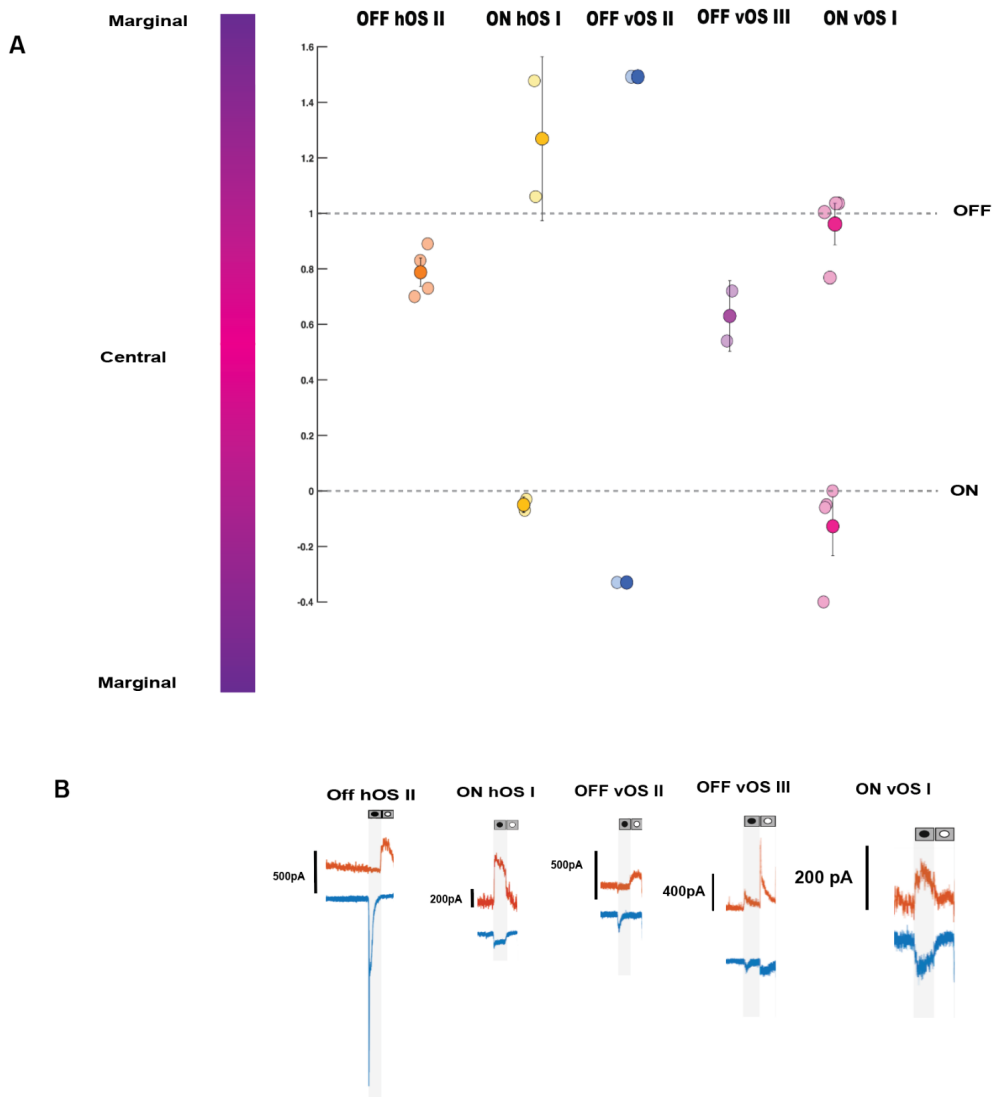


Figure 4.15 Cell Morphology Accurately Predicts Response Kinetics and Contrast Polarity | (A) Quantified stratification depths of OS types at normalized IPL depths — 0 indicates ON CHAT band and 1 indicates OFF CHAT band. Individual colored markers indicate individual cells. Mean indicated with darker shading and standard deviation is indicated with black bars. (B) Corresponding representative whole-cell voltage clamp responses to cell types paired with morphologies in (A) in response to an ON and OFF flashing spot stimulus.

4.4 Summary and Discussion

I used the intra-experimental analysis method that developed in Chapter II and III to target OSGCs for detailed electrophysiological study. The method of targeting cells via their calcium imaging responses — and analyzing those responses live — proved effective in targeting OS cells for electrophysiology. The cells that were targeted for electrophysiology made up a subset of all apparent OS tuned cells from our calcium imaging survey. Future experiments will be needed to elucidate the tuning mechanisms of all OS RGC groups identified in our study

In summary, I examined the underlying tuning mechanisms of 5 cell types — 3 of which demonstrated apparent dedicated OSI tuning mechanisms when their excitatory and inhibitory electrophysiological contributions were analyzed. The electrophysiologically defined groups identified in this chapter are as follows:

- 1) ***ON hOS I*** Demonstrates Robust Excitatory and Inhibitory Tuning
- 2) ***ON vOS I*** Demonstrates Robust Inhibitory Tuning
- 3) ***OFF vOS Type II*** Demonstrates Matching, Moderately Tuned Excitation and Inhibition
- 4) ***OFF vOS Type III*** Demonstrates Minimally Tuned Excitation
- 5) ***OFF hOS Type II*** Demonstrates No Apparent OS Tuning Mechanism in its Synaptic Currents

I believe that the diversity of tuning, or lack thereof in some, lends to a theory I postulated in the chapter III — some cells have dedicated OS circuits and some merely produce OS as a by-product of “accidental” tuning. The OFF hOS II type, for example,

showed an average OSI value of 0.37 when its fluorescence response was analyzed. But I did not find any considerable OS tuning at the level of its synaptic currents. However, their electrophysiological response was also not consistent with what I would expect from an untuned cell, as there was some regularity in the response to directional grating stimuli. Potentially, there is some selectivity of this cell type to a feature of the drifting grating stimulus during isolated inhibitory recordings that — when integrated with excitatory information — produces a response that is measurably OS. Additional stimulus parameters may better describe why the cell has this response to the drifting grating stimulus.

The fluorescence response data for the physiologically investigated types indicate that the ON hOS I, OFF vOS II, and ON vOS I type demonstrate the most consistency in their angles or orientation (Figure 4.14) and demonstrate a clear tuning mechanism when considering excitatory and inhibitory magnitude and angle preference (Figure 4.12; Figure 4.14). The remaining types demonstrated some inconsistency in their preferred orientation, and lacked a clear tuning mechanism for generating an OS response. However, I note that with the OFF vOS III type, the

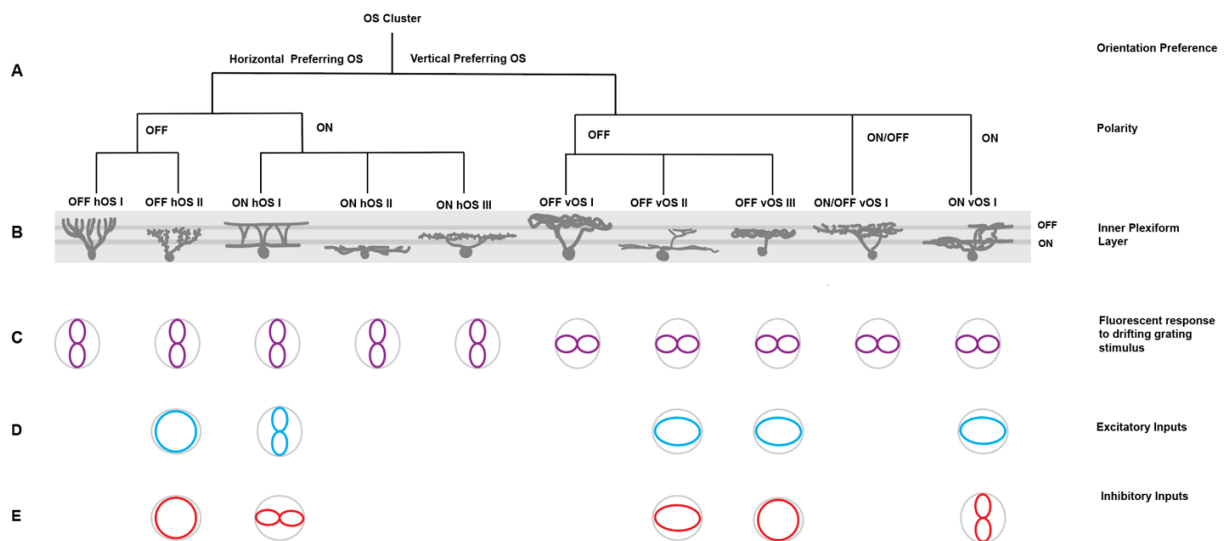


Figure 4.17 Dendrogram of OSGC Types with Tuning Profiles | (A) Cells were targeted if they were sorted into OS clusters. They were split up by their preference for horizontal or vertical orientations. They were then split by their polarity. (B) Stratification profiles for OS types. Representative illustrations for each type shown. (C) Fluorescent response to drifting grating stimulus shown in purple. (D) Schematic representation of excitatory inputs shown in blue. (E) Schematic representation of inhibitory inputs shown in red.

excitatory and inhibitory responses are oppositely aligned, indicating a potential mechanism for OS tuning. It is possible that, although the individual conductances were not robust, their combined, modest amplitude is sufficient to produce an OS signal.

Alternatively, it is possible that the OFF hOS II type and OFF vOS III type are not dedicated OS cells, while the ON hOS I, ON vOS I, and ON vOS II type have dedicated OS circuits. For the two former types, it is still unclear what role these cells play in the retina. For example, they may respond to our stimulus set because they are tuned to object motion. Or they may be truly untuned to orientation and motion, but some arrangement of their dendrites produces a response to the stimulus that cannot be explained with

electrophysiological recording or our morphological analysis. Additional experiments will be necessary to resolve these questions.

For the clearly tuned types, analyzing their circuit level properties would be a necessary next step in deciphering the *source* of tuning. For cell types in which there is measurable orientation tuning in their inhibitory and excitatory contributions, I can speculate as to how that tuning arises:

For cell types in which there is tuned inhibition, the inhibition likely arises due to inhibitory contacts during the null or orthogonal presentation of the drifting grating stimulus, likely through Amacrine Cell release of inhibitory neurotransmitters GABA or glycine. Pharmacological loss-of-function experiments would further distinguish the amacrine cell types responsible for inhibition, and whether that inhibition arises from Wide-Field GABAergic amacrine cells (the likely candidate as they have the spatial extent necessary to produce orientation tuning) or Narrow-Field Glycinergic Amacrine cells.

For cell types in which there is tuned excitation, the origin of that tuning would arise from tuned glutamate release. This could happen through a few different mechanisms:

1) OS information could potentially be relayed directly through tuned glutamate release via OS Bipolar Cell Types. Incidences of directional tuning in bipolar cells have been reported (Matsumoto et al., 2021). More recently, OS tuned glutamate release from a centrally stratifying BC5 bipolar cell type has been reported (Hanson et al., 2023). For our RGC types that stratify in central IPL, such as the ON/OFF vOS I, OFF vOS III, and Motion-Sensitive Non-OS types, tuned glutamate release from BC5 cells could potentially play a role in their tuning, and present an interesting avenue for future investigation.

2) A glutamate-releasing Amacrine Cell could relay tuned excitatory signals. A vGluT3-expressing amacrine cell type has been reported in mouse retina and has been implicated in motion selective circuits (Lee et al., 2014).

3) Selective contacts of bipolar cells onto RGC dendrites could result in an integration of excitatory inputs that generates tuned excitation. This mechanism has been reported in rabbit retina (Bloomfield, 1991). Our study identified several highly elongated RGCs, which have also been reported in Nath & Schwartz's study (2016). While a direct anatomical synaptic connection has not been tested to prove an anatomical substrate for excitatory OS tuning in mouse, this reflects an interesting opportunity for future study.

Interestingly, while I did observe an apparent correlation between the magnitude of OSI tuning in the fluorescence response and electrophysiological responses, I did not observe any significant difference in OSI values between groups (See Results Section 4.3.8). I am uncertain as to the cause of discrepancy between the electrophysiological signatures of these cells and their corresponding fluorescence responses.

The results of the electrophysiological studies, combined with the morphological analysis, functional imaging, and review of the literature, are consolidated in a summary schematic (Figure 4.16). Ultimately, these electrophysiological experiments have helped us determine whether certain cells are OS types with apparent dedicated OS presynaptic circuits. We have a better understanding now of how many OS types there are, and what the OS output from the retina looks like. The next major question is where these cells project, and how these OS features contribute to tuning in downstream visual centers.

CHAPTER V- RETINORECIPIENT TARGETS OF ORIENTATION SELECTIVE TYPES

5.1 Introduction and Background

A major question in the field of visual neurobiology is how projections from retina contribute to computations in downstream visual centers. When retinal direction selectivity is disrupted in the mouse, there is a reduction in motion-preferring cortical cells in layer 2/3 of V1 (Hillier et al., 2017). This suggests that there is “periphery dependent” visual motion in the cortex. It is reasonable to speculate that some degree of orientation tuning is inherited from the retina as well.

The dLGN acts as a relay between the retina and the visual cortex. It can be subdivided into two regions, core and shell. The shell consists of the thin, dorsolateral region of dLGN, adjacent to the optic tract (Grubb and Thompson, 2004). The shell and core are anatomically and biochemically distinct (Grubb and Thompson, 2004). Connectomic differences have also been discovered between the two regions. For example, specific subsets of genetically identified RGCs have been mapped to specific dLGN areas, demonstrating type-specific projections to different regions of dLGN (Martersteck et al., 2017). Tectogeniculate inputs vary between the two regions as well, for example, inputs from the Superior Colliculus are restricted to the shell region of dLGN (Bickford, 2015).

Recent studies have also identified functional differences between dLGN neurons in shell and core regions. Notably, DS and OS responses are biased to the shell of dLGN (Piscopo et al., 2013).

It is important to understand the contributions of OSGCs to tuning in downstream visual areas, but information on retinorecipient targets of OSGCs is lacking. The objective of these experiments was to identify retinorecipient targets of OSGCs that are labeled by retrograde trans-synaptic circuit tracing from shell and core dLGN regions. Since the lateral shell of dLGN contains direction and orientation tuned cells, I hypothesized that OSGCs innervate the dLGN shell. I tested this in collaboration with the Bickford lab at UofL. To restrict the spread of virus to one synapse, and identify projections of RGCs to specific regions of dLGN, I used the rabies g-deletion method (Figure 5.1). In a series of tests, I used state-of-the-art retrograde rabies tracing in CRHR-Cre mice to test for OSGC inputs to the region of dLGN (Figure 5.2). In a second set of experiments, I tested for OSGC inputs to the shell region of dLGN (Figure 5.3). Calcium imaging surveys of ganglion cells in both approaches were used to determine the proportion of OS cell types that target either the shell or core of dLGN. The rationale for these experiments was that successful completion of the proposed work would contribute to a critical missing element of OSGC characterization. Since OS tuned cells have been found in dLGN shell (Piscopo et al., 2013), our expectation was that OSGCs would innervate the shell of dLGN. This would be the first study to directly implicate specific, functionally-identified OSGC types within target regions of dLGN, contributing to information on how dLGN might utilize inputs from retina to generate its tuned responses.

Rabies G-Deletion Method

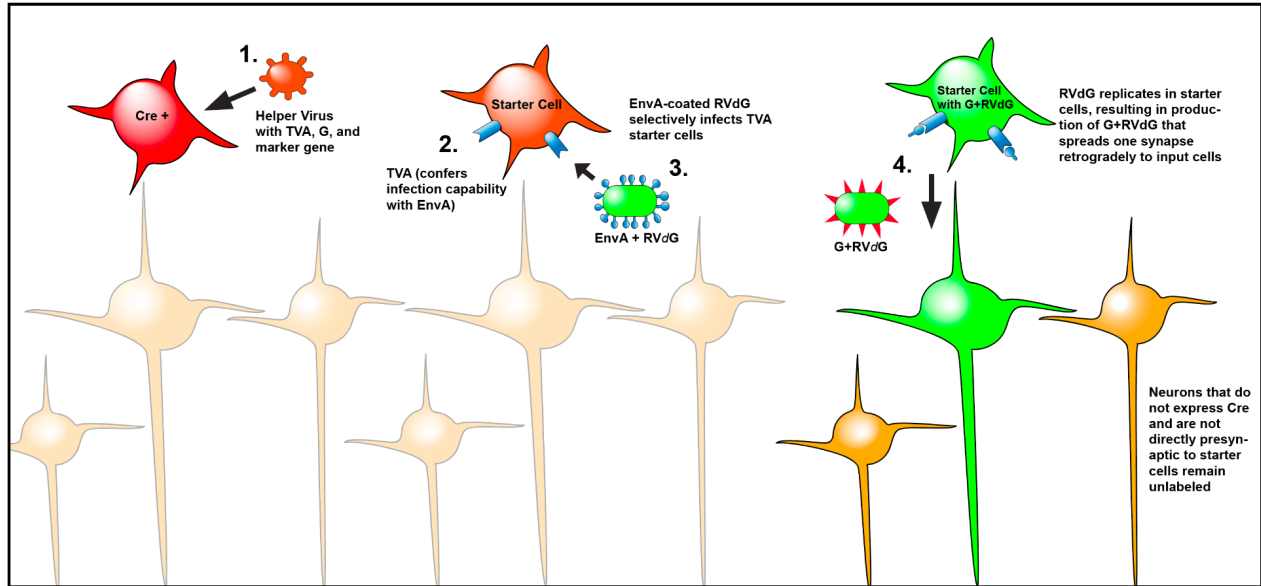


Figure 5.1 | Illustration of the G-deleted Rabies tracing method (1) The target area (dLGN or SC) is injected with a virus that expresses avian receptor protein (TVA), G, and marker gene in a Cre-dependent manner, resulting in expression of TVA, G, and marker gene exclusively in cells that express Cre (shown in red) (2) After sufficient time for accumulation of TVA and G (3 weeks), EnvA-coated RVdG is injected in the target retinorecipient area (3) This selectively infects the TVA starter cells (shown in orange). The EnvA + RVdG contains the coding sequence for GCaMP6s or a marker gene, resulting in expression in the starter cells. The RVdG replicates in the starter cells, resulting in the production of G + RVdG that spreads trans-synaptically to input cells (4) Input cells will express GCaMP6s or the marker gene (shown in green). Other neurons that do not express Cre and are not directly presynaptic to starter cells remain unlabeled (yellow).

Monosynaptic Circuit Tracing Method to Identify Shell-Projecting RGCs

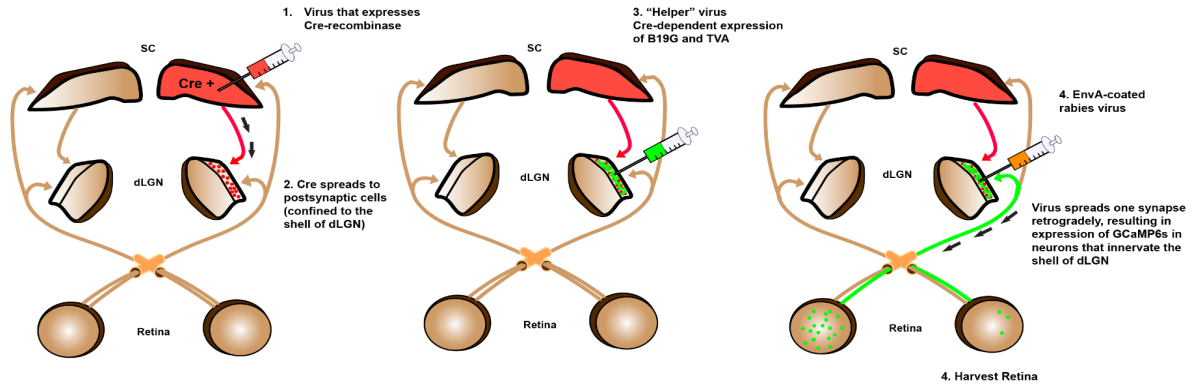


Figure 5.2 | Diagram of Monosynaptic Circuit Tracing Method to identify Projections of RGCs to dLGN 'Shell' (1) Inject SC of WT mice with a virus that will (2) express Cre-recombinase in postsynaptic cells (confined to the shell of dLGN). (3) In the same surgery as step number 1, we inject the dLGN with a "helper" virus that expresses- in a Cre dependent manner- rabies glycoprotein B19G and avian receptor protein (TVA). TVA confers infection capability to rabies glycoprotein B19G and avian sarcoma leucosis virus glycoprotein EnvA (4) 3 weeks later, inject dLGN with EnvA-coated rabies virus coding for GCaMP6s. The helper virus will allow to starter cells to spread one synapse retrogradely, which will result in (5) expression of GCaMP6s in only neurons that innervate cells in the shell of dLGN. (6) 1 week after the rabies injection, harvest the retina and collect ganglion cell functional responses with two-photon fluorescence calcium imaging to determine which ganglion cell types project to dLGN shell.

Monosynaptic Circuit Tracing Method to Identify Core-Projecting RGCs

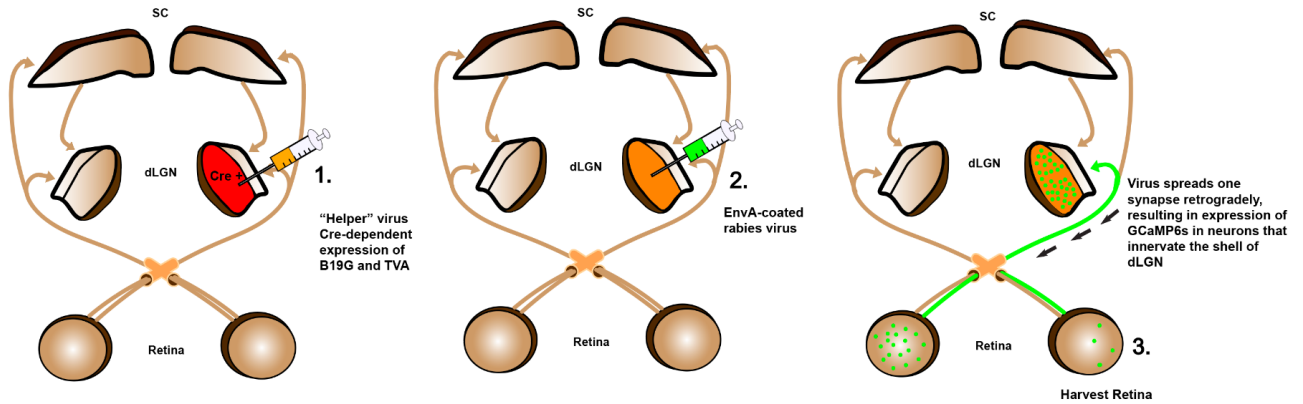


Figure 5.3 | Diagram of Monosynaptic Circuit Tracing Method to identify Projections of RGCs to dLGN 'Core' (1) In CRHR-cre mice ("Core-cre" mice), the dLGN is injected with a "helper" virus that expresses, in a cre dependent manner, the rabies glycoprotein B19G and the avian receptor protein (TVA- that confers infection capability to rabies virus pseudotyped with the avian sarcoma leucosis virus glycoprotein EnvA. (2) Three weeks later, the dLGN is injected with EnvA-coated rabies virus coding for GCaMP6s. The helper virus allows the virus to spread one synapse retrogradely, which results in expression of GCaMP6s in all neurons that project to the core of dLGN. (3) One week after rabies injection, the retinas are harvested for two-photon calcium imaging

5.2 Methods

5.2.1 Stereotaxic Virus Injections in SC and dLGN

In preparation for surgery, adult mice were anesthetized with ketamine (100-150 mg/kg) and xylazine (10-15 mg/kg), and were also injected with analgesic meloxicam (5mg/kg). Mice were then positioned in a stereotaxic apparatus (Angle Two Stereotaxica, Leica, Wetzlar, Germany) and the scalp was incised. Next, a small hole was drilled into the skull covering the primary visual cortex (2.75 mm caudal to Bregma, 0.6 mm lateral to midline, 1.3 mm ventral to Bregma). Virus was injected unilaterally or bilaterally in SC. Viruses were delivered with a 34-gauge needle attached to a Nanofil syringe inserted in an ultramicropump. Once the needle was lowered into the SC, the viral solution at a volume of

70-120nL was injected at a rate of 30 nL/min. Following injection, the pipette was removed and the scalp was sealed with n-butyl cyanoacrylate. Animals were then placed on a heating pad until normal mobility returned, and were monitored for healing for 48 h. For dLGN injections, a stereotaxic apparatus was used to guide a Hamilton syringe (World Precision Instruments) to the dLGN (-2.3 mm AP, 2.2 mm ML, -2.8 mm DV from bregma).

5.2.2 Rabies Tracing Method dLGN ‘Shell’

To selectively target cells projecting to the dLGN shell, the superior colliculus of adult C57BL/6J mice was injected with 200nL of Cre-dependent AAV (trans-Cre), with the purpose of expressing Cre-recombinase in postsynaptic cells confined to the shell of dLGN. In the same surgery, the superior colliculus was injected with 200nL of flex-TVA-helper virus (helper virus) that expressed, in a Cre-dependent manner, the rabies glycoprotein B19G and avian receptor protein (TVA). Three weeks later, the dLGN was injected with an EnvA-coated rabies virus coding for GCaMP6s. The helper virus allowed the rabies virus to spread one synapse retrogradely, resulting in expression of GCaMP6s in all neurons that innervate cells located in the shell of dLGN. To target cells projecting to dLGN core, we utilized CRHR-Cre mice (or “Core-Cre” mice). The dLGN of adult “Core-cre” mice was injected with 150nL of flex-TVA-helper, conferring infection capability to EnvA, but only for cells in the core of dLGN. Three weeks later, the dLGN was injected with the EnvA-coated rabies virus coding for GCaMP6s.

5.2.3 Retinal Dissection

Mouse euthanasia, retinal dissection and mounting is the same as described in Chapter II.

5.2.4 Histology

After the eyes were removed from the animal, the whole brain was removed and postfixed overnight in 4% PFA in a .1 M phosphate buffer. The brains were then washed with PBS. They were then cut into 70 um-thick sections along the coronal plane using a vibratome (Leica VT1000S).

5.2.5 Two-Photon Fluorescence Calcium Imaging

Two photon calcium imaging and subsequent analysis is the same as described in Chapter II. To efficiently locate RGCs while reducing the possibility of exclusion, cells were targeted by following their axons from the center of the tissue outward.

5.2.6 Confocal Imaging

Confocal imaging methods for the retina are the same as described in Chapter III.

5.2.7 Determining the DSI Value for Each Cell

To quantify direction tuning, I computed for each cell the DSI using the formula:

$$DSI = (R_{pref} - R_{null}) / (R_{pref} + R_{null})$$

Where *pref* indicates the preferred direction — determined by finding the fft of the highest response to the drifting grating stimulus. *Null* indicates the direction opposite that of that with the highest magnitude.

5.2.8 Determining the OSI Value for Each Cell

To determine the OSI value for each cell I used the following formula:

$$OSI = (R_{pref_ori} - R_{orth}) / (R_{pref_ori} + R_{orth})$$

Where R is the cell's fluorescent response, and pref_or_i indicates the preferred orientation, and orth indicates the non-preferred orientation. I determine the preferred orientation by taking the maximum combination of the response to two oppositely moving gratings with matching orientation. The orthogonal orientation is just as described, the orientation that is offset to the preferred orientation by 90°.

5.3 Results

5.3.1 Monosynaptic Circuit Tracing Method Reproduces Previous Study in WFV-Cre Mice

Before we investigated the projections of RGCs to the dLGN, we performed, as a control experiment, the monosynaptic circuit tracing method in NTSR1-Cre (WFV-Cre) mice, to replicate the study by Reinhard et al., (2019). To identify RGCs projecting to Wide Field Vertical Cells we injected the SC of WFV-mice (mice that express Cre in Wide Field Vertical cells) with a flex-TVA-helper virus. Three weeks later, the SC was injected with an EnvA-coated rabies virus coding for GCaMP6s. This retrogradely labeled RGC's that target the SC. 8 days after the second injection, the retinas were excised and the ganglion

cell layer was surveyed using the method described in Chapter II. Somas of labeled cells were located by following the axons from the center of the retinal explant outward. I observed strong labeling of RGCs with the green fluorescent GCaMP6s under two-photon imaging (Figure 5.4, C). Under confocal imaging I observed RGCs well-filled with tracer, with dendrites clearly visible (Figure 5.4, A-B). Using light stimulation I observed robust calcium imaging responses in cells expressing GCaMP6s (Figure 5.5).

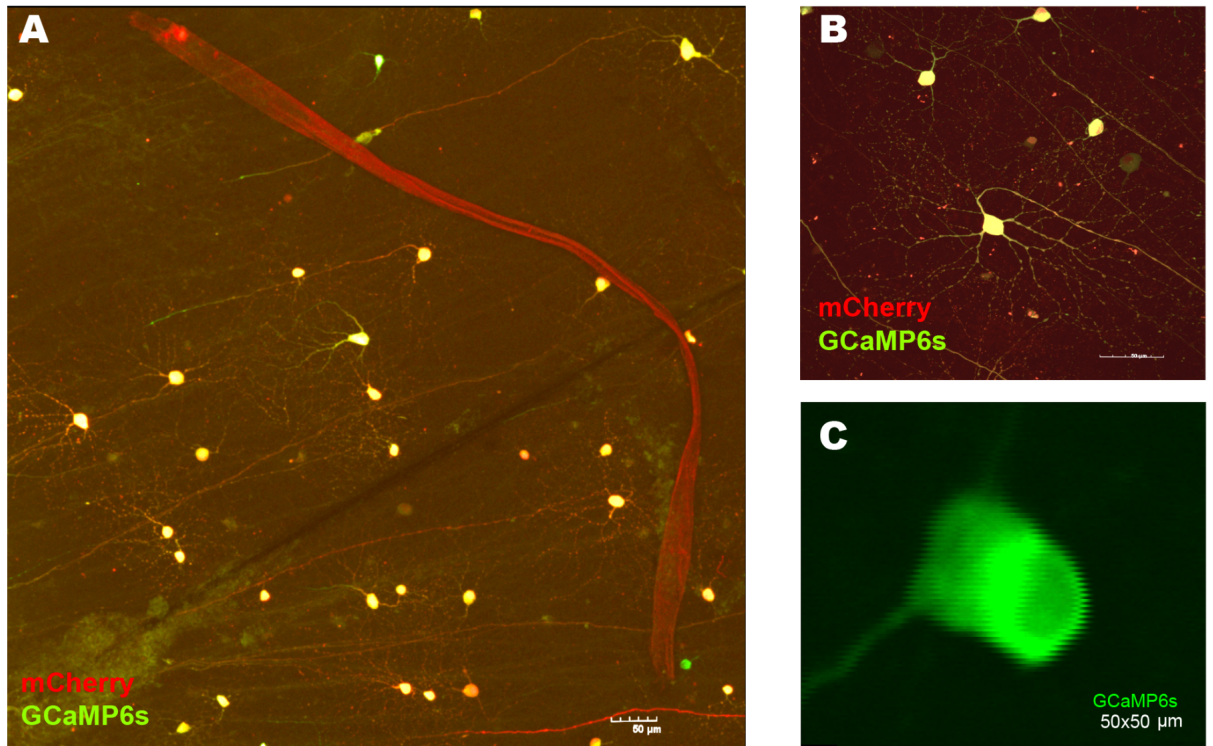


Figure 5.4 Retrograde Tracing in WFV-Cre Mice | (A) Confocal fluorescence image of ganglion cell layer (10x, Olympus FV1000NA objective) Example RGCs are indicated with white arrows. Tracer-filled RGCs project to WFV-cre cells in Superior Colliculus. (B) 40x confocal Z-projection of RGC retrogradely traced from SC. (C) Two-photon scan image window. Green indicates GCaMP6s.

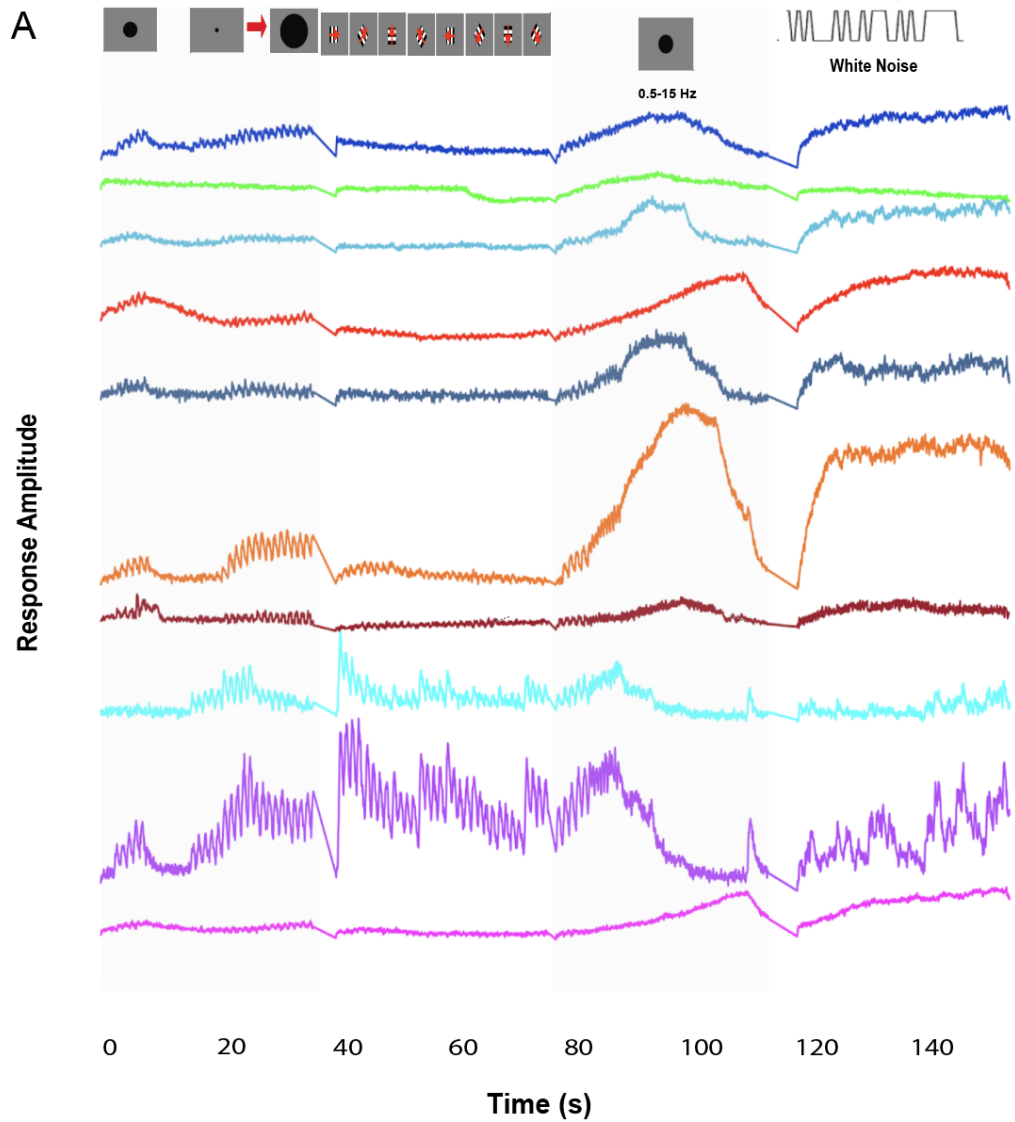


Figure 5.5 USTIM-Evoked calcium responses shown diverse visual function of WFV-projecting RGCs in WFV-Cre Mice (A) Example calcium responses of WFV-projecting RGCs. Mice were injected with rabies virus coding for calcium indicator GCaMP6s.

5.3.2 Retrograde Tracing from Shell Identifies DS and OS RGC Responses

Once we established that the monosynaptic circuit tracing method was efficacious, we moved on to retrogradely labeling RGCs projecting to dLGN regions. To identify projections to dLGN shell, we injected the Superior Colliculus (SC) of wild-type (WT) mice with a virus that is transported transynaptically. The virus induces the expression of Cre-recombinase in postsynaptic cells — confined to the shell of dLGN. In the same surgery, we subsequently injected the dLGN with a “helper” virus that expresses — in a Cre-dependent manner — the rabies glycoprotein B19G and the avian receptor protein, TVA. TVA is a binding partner of EnvA. Thus, TVA confers infection capability to rabies virus pseudotyped with the avian sarcoma leucosis virus glycoprotein (EnvA). Since TVA is not present in mouse unless injected, the rabies virus is capable of infecting only cells expressing the EnvA binding partner, TVA (Callaway, 2010).

The dLGN was injected two weeks later with a rabies virus coding for GCaMP6s (EnvA-SADΔG-GCaMP6s). The helper virus allows the rabies virus to spread one synapse retrogradely. This resulted in the expression of GCaMP6s only in RGCs innervating the shell of dLGN (Figure 5.6, A-C).

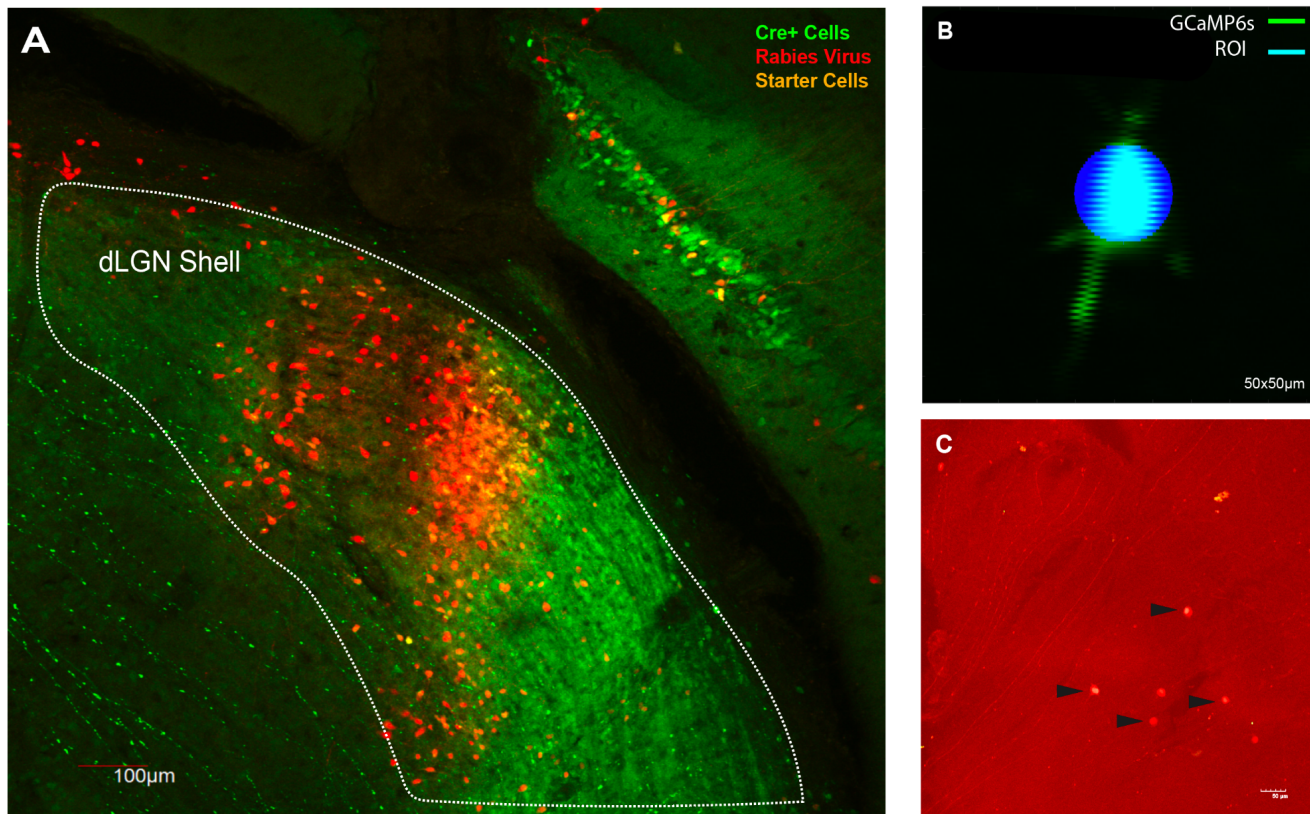


Figure 5.6 Retrogradely Labeling Shell-Projecting RGCs | (A) 2 micron thick optical confocal image of dLGN in Thy1 GCaMP6f mouse. Cre + cells anterogradely labeled from Superior Colliculus shown in green. EnvA-coated rabies virus shown in red. Starter cells expressing both shown in yellow. **(B)** Scan field with RGC ROI masks, during two-photon imaging of RGC expressing GCaMP6s from experiment using WT animal. **(C)** 10X confocal image of ganglion cell layer. Somas of RGCs retrogradely labeled from dLGN shell indicated by black arrows.

I isolated the retinae of injected mice and performed calcium imaging of RGCs expressing GCaMP6s with the goal of harvesting fluorescent responses and developing a library of light-evoked RGC response vectors for dLGN shell. The goal was then to analyze functional light-step responses and link cells from the dLGN shell-survey with our retinal RGC survey in *Thy1-GCaMP6f* mice. I expected to find OSGCs in our survey of dLGN shell-projecting ganglion cells.

The first three cohorts, imaged at 8 days post-rabies injection, showed a high proportion of cell death and lacked all light-evoked calcium responses. In response, we

shortened the duration of the rabies virus incubation to five days and observed healthier cells with GCaMP6s expression, but no light-evoked responses, indicating that there was no functional activity. When I recorded the light-evoked responses, I observed virtually no functional activity. After several more failed cohorts, I decided to use a different approach and injected *Thy1*-GCaMP6f mice with a rabies virus encoding DsRed. I was able to survey the ganglion cell layer and only harvest the responses of cells that co-expressed green fluorescent GCaMP6f and the DsRed tracer. Here, I observed robust functional responses. In total, I observed colabeling of 133 cells across 4 *Thy1*-GCaMP6f animals (n=6 retinas). To rule out cells that lacked OS or DS tuning due to unhealthy responses, I sorted cells based on the variance of their fluorescence response, then excluded all cells with aberrant fluorescence responses including: apparent photobleaching and excessive calcium sequestering. More than half of the recorded cells were precluded due to apparent unhealthy or abnormal responses, leaving 41 “healthy” cells. I believe this high number of aberrant cells could be due to toxicity from the rabies virus.

I analyzed the fluorescent responses of individual shell-projecting RGCs to determine their OSI and DSI values and plot the distributions of each (Figure 5.7, A-B), with the occurrence of both indicating projections of OS and DS cells to dLGN shell. Because of the nature of the OS and DS calculation, there was considerable overlap between cells that could be considered OS and those that were DS (Figure 5.7, C).

Cells were identified as OS or DS-responding based on which value was more prominent. For example, a cell with a DSI value of 0.81 and an OSI value of 0.28 would be considered DS. I will refer to cells in their respective categories as DS or OS, but note that

I cannot be completely certain that they are discrete OS or DS types with unique OS tuning mechanisms based on their OSI/DSI value alone.

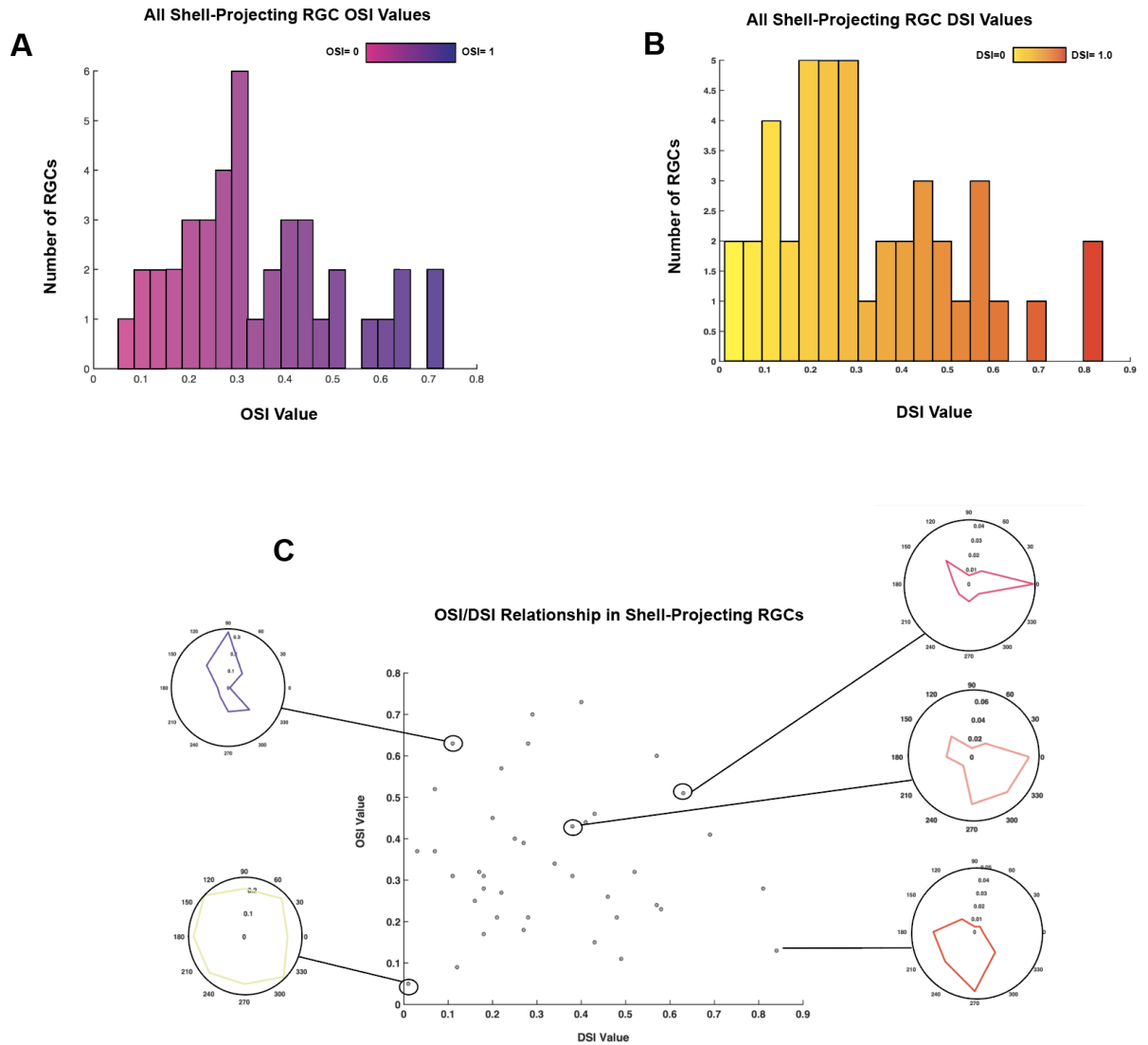


Figure 5.7 Survey of Shell-Projecting RGCs Identifies DS and OS Responses | (A) and (B) distributions of respective OSI and DSI values of shell-projecting RGCs (n=41 RGCs; n=4 mice). OSI determined by taking the maximum sum of the fluorescent response of two oppositely moving gratings during the drifting grating portion of the stimulus. DSI determined by taking the maximum fluorescent response to a drifting grating direction. (C) Scatterplot of DSI values plotted against OSI values for individual shell-projecting RGCs in survey. Example RGCs circled correspond with connected polar plots to demonstrate the relationship between the DSI/OSI value.

5.3.3 Shell-Projecting OS RGCs Encompass hOS and vOS types

In our survey of shell-projecting RGCs, I identified 24 cells with OSI responses over 0.2 that were determined to be healthy (Figure 5.8). OSI values ranged from 0.21 to 0.73 (mean=0.429; n=24; Figure 5.9, A). I identified both ON and OFF cell types representing both cardinal orientations and oblique orientations (Figure 5.9, B, C). I believe this implicates OS RGCs in projections to dLGN shell specifically. These results show that both ON and OFF hOS and vOS types project to the dLGN shell region. However, I do not have sufficient data to determine if specific OS types project to dLGN shell.

Shell-Projecting OS RGCs

ON | OFF

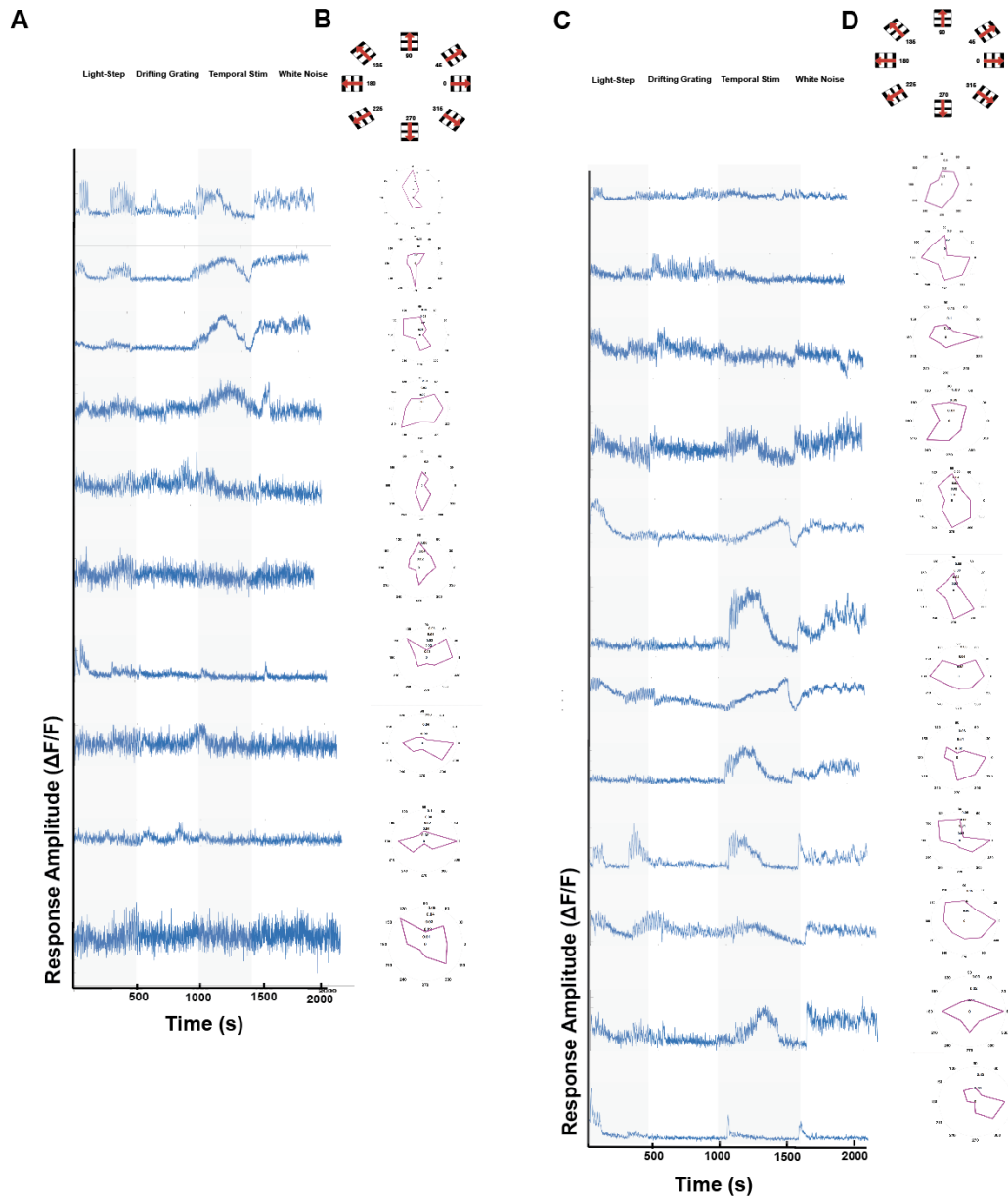


Figure 5.8 USTIM-evoked calcium responses of Shell-Projecting RGCs | Calcium responses of ON (A) and OFF (C) shell-projecting RGCs (n=24 RGCs, n=3 mice) with corresponding polar plots (B) and (D) in response to the drifting grating stimulus.

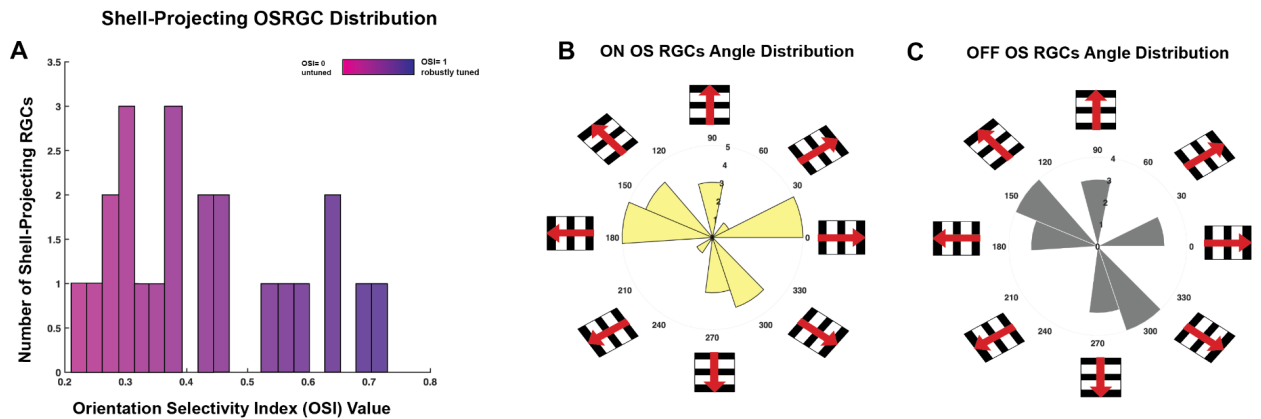


Figure 5.9 Shell-Projecting RGCs Include Diverse OS Types | (A) Distribution of individual shell-projecting RGC types with OSI over 0.2 calculated using the formula $(R_{pref}-R_{orth})/(R_{pref}+R_{orth})$. Responses were determined by analyzing the fluorescent responses of RGCs ($n=23$ individual RGCs; $n=3$ *Thy1-GCaMP6f* mice). (B) and (C) are polar histograms of respective ON ($n=13$) and OFF ($n=10$) shell-projecting RGCs with OSI values greater than 0.2. Preferred angle of individual RGCs was determined by analyzing the fluorescent response of individual RGCs and taking the maximum sum of two oppositely moving gratings.

5.3.4 ON and ON/OFF DS Types Project to dLGN shell

As expected from the literature, I identified DSGCs in our shell-projecting RGC survey. I identified 14 cells with a DSI value over 0.2, at a range of 0.28-0.84 (Figure 5.10 A; mean = 0.52; $n = 14$). Upward, downward, rostral, and nasal directions were each represented in our survey (Figure 5.10 B, C).

5.3.5 Identifying RGC Projections to dLGN Core

I next sought to determine the incidence of orientation-tuned cells that projected to the dLGN core to compare with the results of the previous experiments. We injected the dLGN of CRHR-cre, “Core-cre” mice with a “helper” virus that expresses rabies glycoprotein B19G in a Cre-dependent manner and avian receptor protein TVA (Figure 5.3). Two weeks later, we injected the dLGN with EnvA-coated rabies virus that allows the rabies virus to

spread one synapse retrogradely, which results in the expression of GCaMP6s in all RGCs innervating core of dLGN (Figure 5.11, A-C).

I used the same approach described in Chapter II to image ganglion cells in retinal explants. Since OS tuning has not been implicated in Core-residing dLGN cells, I expected a lower proportion of OSGCs in core-projecting ganglion cell populations when compared to shell-projecting ganglion cell populations.

As with the WT mice from the shell-projecting experiments, I observed apparent aberrant functional responses or no functional responses in cells that expressed GCaMP6s. However, confocal imaging showed retrogradely labeled RGCs strongly filled with tracer and dendrites were well resolved. I used these morphologies to link cells with corresponding types from the literature.

I observed multiple occurrences of a cell type with a highly elongated primary dendrite and distinct dendritic swelling at the soma, resulting in a tapered soma appearance (Figure 5.12, A). I believe this type corresponds with the 7ir sustained-ON DS type from the Eyewire Museum. This type is an ON DS sustained type (Dhande et al., 2013). This was an interesting finding, since DSGC types participate in circuits specific to dLGN ‘Shell’, but not dLGN Core. The dLGN Shell also demonstrates proportionally more DS tuned cells than Core (Piscopo et al., 2013), and receives inputs from DS RGCs (Bickford et al., 2015). Work with Cre lines and viral tracings to map projections from retina have identified CART expressing RGCs — known ON-OFF DSGCs (Sanes & Masland, 2015) — as having retinorecipient targets in dLGN shell (Martersteck et al., 2017). ON DSGCs do not express CART, and would therefore be excluded. Why ON DSGCs would project to Core of dLGN is an open question and an interesting avenue for future investigation.

I further identified a type that likely corresponds with type 25 from the Eyewire Museum — characterized by its highly overlapped “bushy” dendrites and two primary dendrites emerging from the soma (Figure 5.12, B). This type is bistratified, with bias towards the OFF layer. In the EyeWire dataset, this type demonstrates a high degree of variability in its directional response.

A third type I observed was an Alpha type (Figure 5.12, C) — but I cannot be certain which Alpha RGC type without functional data or precise quantification of stratification depth, which was lacking in these experiments.

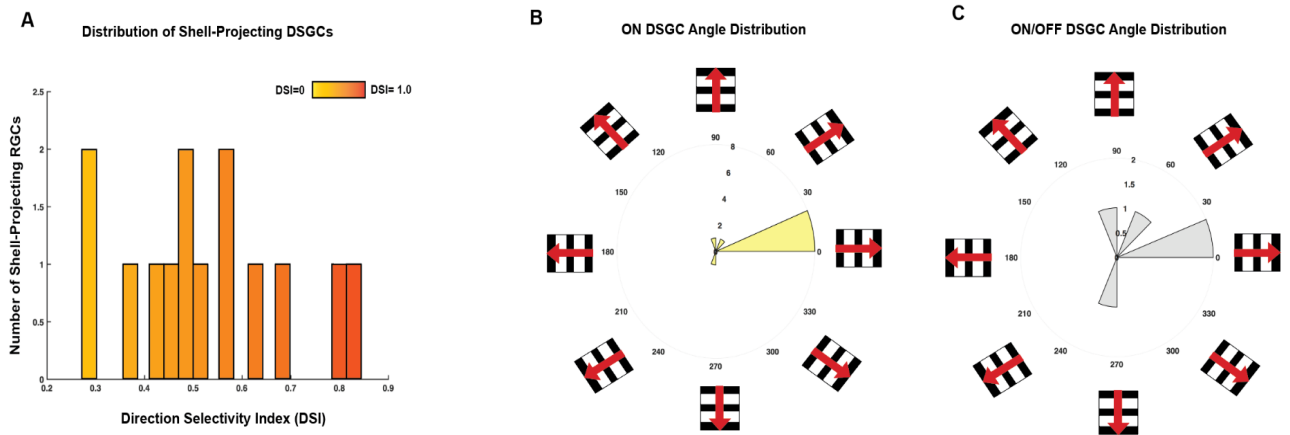


Figure 5.10 Distribution of Shell-Projecting DS Cells | (A) Distribution of individual shell-projecting RGC types with DSI over 0.2 calculated using the formula $(R_{pref}-R_{null})/(R_{pref}+R_{null})$. Responses were determined by analyzing the fluorescent responses of RGCs (n=14 individual RGCs; n=4 *Thy1-GCaMP6f* mice). (B) and (C) are polar histograms of respective ON (n=9) and ON/OFF (n=5) shell-projecting RGCs with DS values greater than 0.2. Preferred angle of individual RGCs was determined by analyzing the fluorescent response of individual RGCs and taking the maximum response to the drifting grating stimulus.

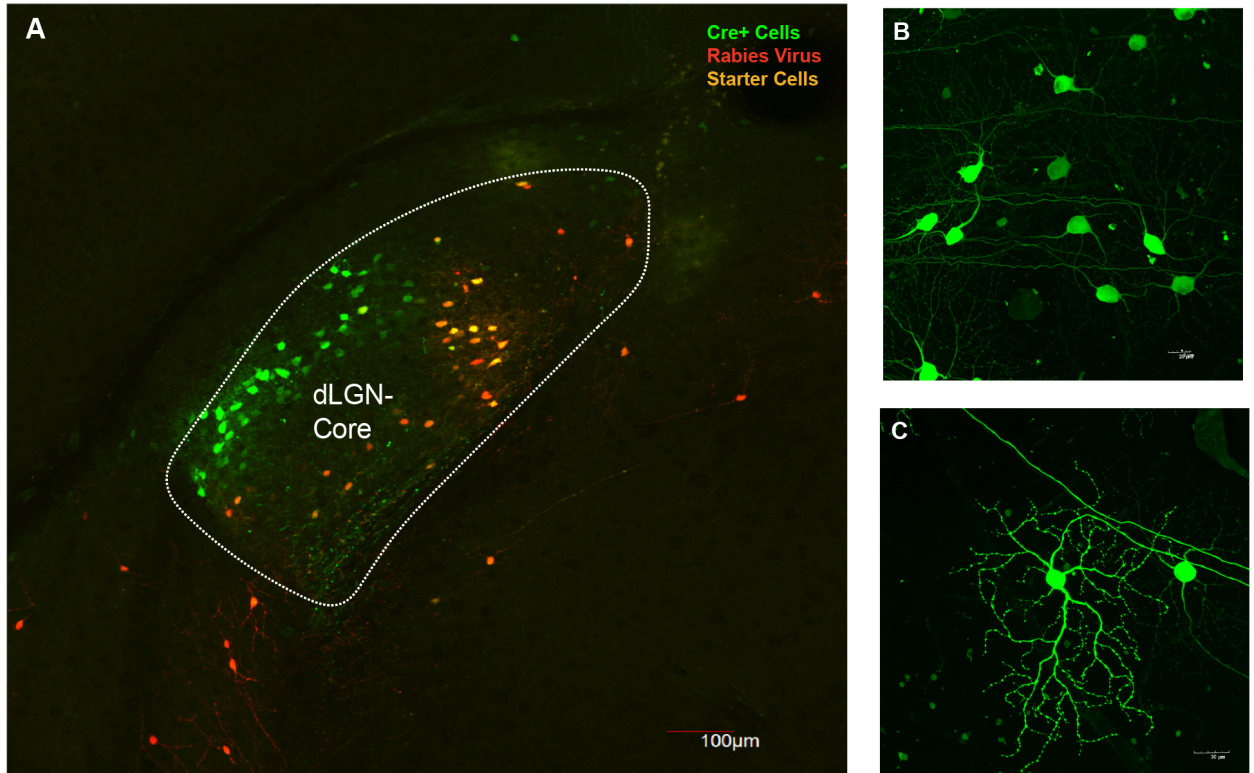


Figure 5.11 Monosynaptic Circuit Tracing to Retrogradely Label Core-projecting RGCs | (A) 2 micron thick optical confocal image of dLGN in Core-cre⁺ mouse. Cre⁺ cells expressing helper virus shown in green. EnvA-coated rabies virus shown in red. Starter cells expressing both shown yellow. (B) 40X confocal image of Core-cre fixed retina. Green indicates RGCs that have been retrogradely labeled with green GCaMP6s. Multiple RGC morphologies are represented. (C) 40X confocal image of two RGCs in green, retrogradely traced from dLGN core.

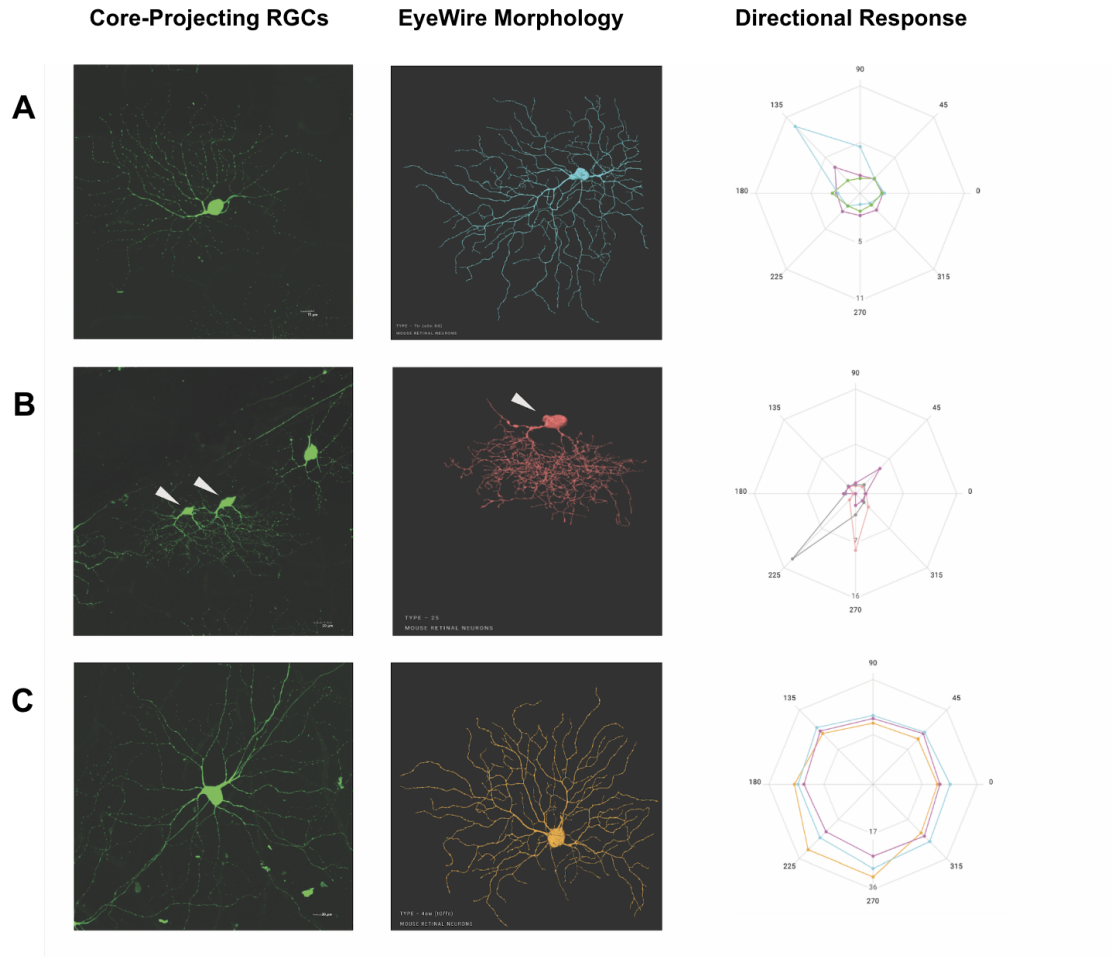


Figure 5.12 Core-Projecting RGC Morphologies | (A) Z-stack projections of representative RGCs retrogradely labeled from dLGN core. (B) EyeWire Data of potential corresponding RGCs with their directional response (C).

Summary & Discussion

Because OS tuning has been reported specifically in the dLGN shell, I expected a portion of the retrogradely traced RGCs to demonstrate OS tuning. As predicted, I identified OS cell types representing multiple orientation preferences in our experiments identifying projections to dLGN shell. The incidence of orientation tuned cells aligns with our prediction that OS cells project to dLGN shell. More experiments will be needed to determine the specific types projecting to dLGN shell, whether there is any bias towards

hOS or vOS types, and what the morphological correlates of those types are. While I do not have direct evidence that these projections generate the OS tuning observed in dLGN shell, I believe this data supports the idea that some level of OS may be inherited from retina. I was not able to compare and contrast functional responses to Core-projecting RGCs. Future studies will be needed to fully address the question of whether OS cells also project to Core regions, and if there is a significantly higher proportion of OS cells projecting to Shell regions when compared to Core regions.

I am uncertain as to why the calcium imaging was successful in our WFV-cre control experiment but not in our shell and core projecting RGC experiments. I speculate that the number of required injections could be responsible. With each additional injection required, there is a greater possibility of missing the target area, thus resulting in a lower n value. Even in successful experiments, where the calcium signal was robust and healthy in many cells, I observed that a large portion of the cells were still completely unresponsive. In our WFV cre experiments, there was a large portion of cells that were nicely filled with GCaMP6s. Our n was much lower in our other experiments, making it difficult to ascertain whether the cells had unhealthy responses because of the experiment conditions, or if it was due to probability. It is also notable that in the initial study by Reinhard et al., (2019) — even though the RGCs were retrogradely traced with GCaMP6s — the cells were still investigated for their functionality via whole-cell patch clamp recording. It is possible that the accumulation of rabies and DsRed in retrogradely traced RGCs resulted in aberrant calcium responses that may be circumvented if cells were recorded using patch clamp. Future experiments should also include morphological reconstruction of retrogradely filled cells to more accurately link types with those in the literature.

I believe our findings present the necessary preliminary data to justify the rabies g-deletion method as a suitable avenue for investigating projections of functional OS types. Identifying cell-type specific projections will be a critical step forward in identifying the contribution of OSGCs to downstream OS tuning. I think our studies indicate a potential contribution of OS cell types to OS tuning in dLGN shell that is worth investigating further.

CHAPTER VI- SUMMARY, DISCUSSION, & FUTURE DIRECTIONS

Definitive classification of RGC types remains a major goal in the field of neuroscience. Relatively little is known about Orientation Selective Ganglion Cells when compared to other feature-detecting RGCs such as Directionally Selective Ganglion Cells. The goal of this study was to 1) develop a method to efficiently identify OSGCs in mouse retina; 2) generate a multimodal classification of OSGC types; 3) identify which OSGCs correspond with types from the literature — and which are novel; and 4) identify retinorecipient targets of OSRGCs.

Because there are currently no known molecular markers for OSRGCs, our first goal was to develop a method to effectively target these cell types in the mouse retina. Our calcium imaging survey and subsequent cluster analysis reliably and efficiently identified OS types. We developed an intra-experimental analysis method that permitted live targeting of cells based on their functional profile.

For multimodal analysis of RGC types, I collected functional and morphological data for each cell type. Based on morphology, I identified 10 distinct RGC types with OS tuning by using the intra-experimental analysis method and targeted morphological reconstruction. I also identified 1 type with mild but subthreshold OS tuning as the result of our analysis. The latter type was consistently assigned an OS group in the cluster analysis, but this grouping was based on other aspects of the response such as temporal tuning and contrast polarity, rather than just the oriented grating-evoked response.

Successful application of this technique presents a new proof of concept and provides opportunities for studying OS RGC types with a focus on “function-first” typology, and establishes precedent for studying other RGC types as well as cell types in other parts of the CNS.

After developing the intra-experimental analysis method and classifying cells based on their calcium imaging responses and morphology, I investigated cells for their synaptic properties using targeted whole-cell electrophysiology. I combined the collected morphological, functional, and electrophysiological data and compared it against typologies reported in the literature to build out a profile for different OS cell types. The resulting summarized types are as follows:

- 1) OFF hOS I** stratifies in the outer IPL margins and likely corresponds with the 2i type from the EyeWire Museum. I believe this type may also correspond with the OFF hOS type from Nath & Schwartz (2017).
- 2) OFF hOS II** has unique spiny, complex dendrites that stratify in the outer central IPL. This cell most closely matches type 4i from the Eyewire museum. Whole-cell recordings did not identify a discrete OS tuning mechanism for this type.
- 3) ON hOS I** is bistratified in the outer and inner margins of the IPL. This cell type likely corresponds with type 27 from the EyeWire Museum, and exhibits robust, oppositely tuned inhibitory and

excitatory conductances that shape its OS response. I believe this cell is also the ON hOS type from Nath & Schwartz (2016).

- 4) **ON hOS II** stratifies in the inner margins of the IPL and likely corresponds with type 9n from the EyeWire Museum.
- 5) **ON hOS III** was identified with one morphological reconstruction and has spiny dendrites that stratify in the inner central IPL. It matches the 6t type from the EyeWire Museum.
- 6) **OFF vOS I** stratifies in the outer marginal IPL and likely corresponds with type 2aw from the EyeWire Museum.
- 7) **OFF vOS II** has sparse dendrites that stratify in the inner marginal IPL with dendritic projections distal to the OFF ChAT band. This type likely corresponds with 82wi from the EyeWire Museum. Electrophysiological recordings identified modest, matching excitatory and inhibitory tuning.
- 8) **OFF vOS III** is centrally stratified in the IPL and closely matches type 5so from the EyeWire Museum. Electrophysiological recordings did not identify discrete OS tuning mechanisms for this cell type.
- 9) **ON/OFF vOS I** is centrally stratified with multiple dendritic stratification peaks in the outer central and inner marginal IPL. It likely corresponds with type 5to from the EyeWire Museum.
- 10) **ON vOS I** is a bistratified type with dendrites arborizing along the ON and OFF ChAT bands, with ON layer bias. It likely corresponds

with type 82wo from the EyeWire Museum and demonstrates robustly tuned inhibition and untuned excitation.

While the ON hOS I and OFF hOS I type are likely the same as those described in previous detailed studies (Nath & Schwartz, 2016; 2017), I also identified apparent “novel” OS types that have not been previously described. One of the cell types is the ON/OFF vOS I, 5to type. This type was likely missed in prior surveys due to its complete lack of light step response at up to a 666 μ m spot size. The benefit of our intraexperimental analysis method is that all aspects of the functional response were taken into account when aligning new responses with our response template, which led to its inclusion and description here. While I do not think this cell was one of the types investigated in our electrophysiological experiments, I believe it should be investigated in future studies for its circuit-level properties to determine whether this cell has distinct OS tuning mechanisms.

Close scrutiny of our recorded set supports that a few of the types I identified are not discrete OS types — evidenced by our electrophysiological recordings of cell inhibitory and excitatory inputs. The OFF hOS II and OFF vOS III types did not have detectable tuning mechanisms for OS, leading us to believe that these types may not represent discrete OS groups. However, their fluorescence OSI tuning profiles were not significantly different from other electrophysiologically investigated types. I am uncertain as to why their calcium imaging responses showed OS in the absence of a tuning mechanism. These cells should be investigated with a variety of stimuli to ascertain whether there is some other aspect of the drifting grating stimulus they are responding to, and what their preferred stimulus set is.

I also sought to identify projections of OSRGCs to dLGN. A study identifying projections to shell versus core regions of dLGN had not yet been performed, although OS cell types have been implicated in projections to dLGN at large. Using rabies virus-mediated monosynaptic circuit tracing, we expressed GCaMP6s in RGCs projecting to the dLGN shell. This method did not prove to be effective in preserving the health of the RGCs, so we used as an alternative the same injection method in our *Thy1*-GCaMP6f mice and used DsRed to co-label with green fluorescent-expressing RGCs. This preserved the apparent health of the cells and proved an effective method for imaging calcium responses in RGCs projecting to the dLGN shell. When I analyzed the responses of cells that were retrogradely labeled, I identified ON and OFF RGCs with preferences for both horizontal and vertical orientations. However, I do not have enough data to confidently claim any type-specific projections. The question of which specific OS types project to specific regions of dLGN is still an avenue of investigation.

Since I could not utilize transgenic GCaMP in Core-Cre mice, and experiments using the tracer GCaMP6s were ineffective, I was unable to analyze healthy responses from Core-projecting RGCs. So I could not contrast and compare with responses from shell-projecting RGCs. A possible next step would be to take *Thy1*-GCaMP6f mice and cross these with CRHR-Cre mice to label cells in the same manner as the shell experiments.

The question of OSRGC classification remains, “where do these cells project and how do they contribute to OS tuning in higher-order visual centers?” Orientation Selectivity is found in Primary Visual Cortex, Superior Colliculus, and dLGN (Wang et al., 2010; Ahmadlou and Heimel, 2015; Zhao et al., 2013; Piscopo et al., 2013; Suresh et al., 2016) and is highly conserved across species (Fisher et al., 2015; Passaglia et

al., 2002; Maturana and Frenk, 1963; Levick and Thibos, 1980; Bloomfield, 1991; Antinucci et al., 2016). However, we still do not understand how Orientation Selectivity in the Retina contributes to tuning in thalamus and cortex. Additional, robust surveys of shell and core projecting RGCs and targeted loss-of-function experiments to selectively perturb OS signaling from the retina will be needed to answer this question. Eventual molecular identification of OS types would be ideal for genetic perturbation of the retinogeniculate circuitry to more directly implicate OS RGC contributions to thalamic OS tuning.

There are a few additional questions that still need to be answered for us to better understand orientation selectivity in mouse. 1) What are the discrete OS types? 2) Why is there a high degree of variability amongst OS types 3) How does retinal OS contribute to downstream tuning?

Establishing how many discrete OS types there are turned out to be a more convoluted task than determining discrete DS types. ON-OFF DS types have similar bistratified dendrites, express neuropeptide CART, synapse with Starburst Amacrine Cells, and are implicated in specific thalamic circuits (Sanes & Masland, 2015, Bickford et al. 2015). When I look up ON-OFF DS types in the EyeWire museum, I can find remarkable consistency in the directional response and stratification patterns (Bae et al., 2017). Conversely, there are many types in our study — and other OS studies — that identify correlates with the EyeWire museum that demonstrate a high degree of variability in their tuning. For example, the 9n morphological type from the EyeWire museum, a type that has not yet been described in detailed OS study, appears to exhibit DS and OS properties in

response to a moving bar stimulus. Is it possible that some cells are definitively OS, and that others produce an apparent OS response as an occasional byproduct of their specific morphology or circuit connectivity? Studies have implicated offset dendrites (stratifying in the OFF and ON layer) as causing a directional response. For example, offset ON and OFF receptive fields appear to demonstrate mild DS and OS properties when presented with certain stimuli (Cooler & Schwartz, 2020). More studies, with a variety of stimuli, will be needed to determine why certain cells demonstrate mild OS tuning without dedicated circuits, and what their purpose is. Furthermore, analysis of cell type distribution across the ganglion cell layer would help parse whether cells are distinct types with regular overlap, or if they should be regrouped to form a regularly spaced mosaic.

For types in which there are clear inhibitory and excitatory mechanisms for tuning, such as our ON hOS I type and ON vOS I type, the next major steps are to dissect those circuits, and to pinpoint the cell types that contribute to the tuning. For DS cells, SACs are responsible for excitatory and inhibitory DS tuning, and bipolar cell types 7 and 2 have been implicated in DS-tuned glutamate release onto SAC terminals (Matsumoto et al., 2021). The next major goal in retinal circuit research will hopefully involve a push towards a comparable understanding of OS circuits. A key area of investigation could be type 5A (BC5A) bipolar cells which demonstrated apparent OS-tuned glutamate release (Hanson et al., 2023).

This work has provided new insight into the diversity of morphological RGC types that exhibit OS properties, and how some of those types generate an OS response. The findings have also provoked additional questions to explain why so many different types

produce an apparent OS response. I have identified OS-responding cells in projections to dLGN shell. *Additional studies will be necessary to confidently establish the full complement of OS types in the retina and their detailed circuit-level mechanisms, synaptic partners, molecular profiles, and retinofugal projections.*

REFERENCES

- Amthor, F.R., Takahashi, E.S. and Oyster, C.W. (1989), Morphologies of rabbit retinal ganglion cells with complex receptive fields. *J. Comp. Neurol.*, 280: 97-121.
- Amthor, F.R., Takahashi, E.S. and Oyster, C.W. (1989), Morphologies of rabbit retinal ganglion cells with concentric receptive fields. *J. Comp. Neurol.*, 280: 72-96.
- Antinucci, P., Nikolaou, N., Meyer, M. P., and Hindges, R. (2013). Teneurin-3 specifies morphological and functional connectivity of retinal ganglion cells in the vertebrate visual system. *Cell Rep.* 5, 582–592. doi: 10.1016/j.celrep.2013. 09.045
- Antinucci, P., Suleyman, O., Monfries, C., and Hindges, R. (2016). Neural mechanisms generating orientation selectivity in the retina. *Curr. Biol.* 26, 1802–1815. doi: 10.1016/j.cub.2016.05.035
- Baden T., P. B. (2016, January 21). The functional Diversity of Retinal ganglion cells in the mouse. *nature*, 529.
- Bae JA, Mu S, Kim JS, et al. Digital Museum of Retinal Ganglion Cells with Dense Anatomy and Physiology. *Cell*. 2018;173(5):1293-1306.e19.

doi:10.1016/j.cell.2018.04.040

Barlow, H. C.J. Barnstable, U.C. Dräger, Thy-1 antigen: A ganglion cell specific marker in rodent retina, *Neuroscience*, Volume 11, Issue 4, 1984, Pages 847-855, ISSN 0306-4522, [https://doi.org/10.1016/0306-4522\(84\)90195-7](https://doi.org/10.1016/0306-4522(84)90195-7).

Baylor D. How photons start vision. *PNAS*. 1996;93:560–65. B., Hill, R. M., & Levick,

W. R. (1964). Retinal Ganglion Cells responding selectively to direction and speed of image motion in the rabbit. *The Journal of physiology*, 173(3), 377–407. <https://doi.org/10.1113/jphysiol.1964.sp007463> Berson, D.M., F.D., & M.T. (2002) Phototransduction of Retinal Ganglion Cells That Set the Circadian Clock. *Science*, 295(5557), 1070-1073

Bickford M., Zhou N., Krahe T.E., Govindaiah G., Guido W., (2015). Retinal and

Tectal “Driver-Like” Inputs Converge in the Shell of the Mouse Dorsal Lateral Geniculate Nucleus. *Journal of Neuroscience* 22 July 2015, 35 (29) 10523-10534; DOI: 10.1523/JNEUROSCI.3375-14.2015

Boycott, B. B., & Wässle, H. (1974). The morphological types of ganglion cells of the

domestic cat's retina. *The Journal of physiology*, 240(2), 397–419.

Bloomfield, S. (1991). Two types of orientation-sensitive responses of amacrine cells in

the mammalian retina. *Nature*, 350, 347–350 <https://doi.org/10.1038/350347a0>.

Bloomfield, S. A. (1994, May). Orientation-Sensitive Amacrine and Ganglion Cells in the

Rabbit Retina. *Journal of Neurophysiology*, 71(5).

Brown SP, He S, Masland RH. Receptive field microstructure and dendritic geometry of retinal ganglion cells. *Neuron*. 2000;27(2):371-383. doi:10.1016/s0896-6273(00)00044-1

Cajal, R. y. (1899). *Textura del Sistema Nervioso del Hombre y de los Vertebrados*. New York: Springer-Verlag, 86-90.

Qian Chen, Joseph Cichon, Wenting Wang, Li Qiu, Seok-Jin R. Lee, Nolan R.

Campbell, Nicholas DeStefino, Michael J. Goard, Zhanyan Fu, Ryohei Yasuda, Loren L. Looger, Benjamin R. Arenkiel, Wen-Biao Gan, Guoping Feng, Imaging Neural Activity Using Thy1-GCaMP Transgenic Mice, *Neuron*, Volume 76, Issue 2, 2012, Pages 297-308, ISSN 0896-6273, <https://doi.org/10.1016/j.neuron.2012.07.011>.

Chen TW, Wardill TJ, Sun Y, Pulver SR, Renninger SL, Baohan A, Schreiter ER, Kerr RA, Orger MB, Jayaraman V, Looger LL, Svoboda K, Kim DS. Ultrasensitive fluorescent proteins for imaging neuronal activity. *Nature*. 2013 Jul 18;499(7458):295-300. doi: 10.1038/nature12354. PMID: 23868258; PMCID: PMC3777791.

Cleland BG, Enroth-Cugell C. Quantitative aspects of sensitivity and summation in the cat retina. *J Physiol*. 1968;198(1):17-38. doi:10.1113/jphysiol.1968.sp008591

- Cooler, S., Schwartz, G.W. An offset ON–OFF receptive field is created by gap junctions between distinct types of retinal ganglion cells. *Nat Neurosci* 24, 105–115 (2021). <https://doi.org/10.1038/s41593-020-00747-8>
- Creutzfeldt, B. S. (1970). Sensitivity distribution and spatial summation within receptive-field center of retinal on-center ganglion cells and transfer function of the retina. *Journal of Neurophysiology*.
- Cruz-Martín, A., El-Danaf, R., Osakada, F. *et al.* A dedicated circuit links direction-selective retinal ganglion cells to the primary visual cortex. *Nature* **507**, 358–361 (2014).
- Dhande OS, Estevez ME, Quattrochi LE, El-Danaf RN, Nguyen PL, Berson DM, Huberman AD. Genetic dissection of retinal inputs to brainstem nuclei controlling image stabilization. *J Neurosci*. 2013 Nov 6;33(45):17797-813. doi: 10.1523/JNEUROSCI.2778-13.2013. PMID: 24198370; PMCID: PMC3818553.
- Della Santina L, Inman DM, Lupien CB, Horner PJ, Wong RO. Differential progression of structural and functional alterations in distinct retinal ganglion cell types in a mouse model of glaucoma. *J Neurosci*. 2013;33(44):17444-17457.
- Della Santina L, Ou Y. Who's lost first? Susceptibility of retinal ganglion cell types in

experimental glaucoma. *Exp Eye Res.* 2017;158:43-50.

doi:10.1016/j.exer.2016.06.006

Demb JB, Singer JH. Functional Circuitry of the Retina. *Annu Rev Vis Sci.* 2015 Nov

24;1:263-289. doi: 10.1146/annurev-vision-082114-035334. PMID: 28532365;

PMCID: PMC5749398.

Ecker JL, Dumitrescu ON, Wong KY, et al. Melanopsin-expressing retinal ganglion-cell

photoreceptors: cellular diversity and role in pattern vision. *Neuron.*

2010;67(1):49-60.

Euler T., K. L. (2011, May). Bulk electroporation and population calcium imaging in

the adult mammalian retina. *Innovative Methodology.*

Euler T, Haverkamp S, Schubert T, Baden T. Retinal bipolar cells: elementary building

blocks of vision. *Nat Rev Neurosci.* 2014;15:507–19.

Famiglietti E.V., H. K. (1976, October 8). Structural basis for ON-and OFF-center

responses in retinal ganglion cells. *Science*, 194(4261), 193-195.

Farrow K, Masland RH. Physiological clustering of visual channels in the mouse

retina. *J Neurophysiol.* 2011;105(4):1516-1530. doi:10.1152/jn.00331.2010

Feinberg EH, Meister M. Orientation columns in the mouse superior colliculus.

Nature. 2015 Mar 12;519(7542):229-32. doi: 10.1038/nature14103. Epub

2014 Dec 17. PMID: 25517100.

Jacoby J., Schwartz GW., (2017) Three Small-Receptive-Field Ganglion Cells in the Mouse Retina Are Distinctly Tuned to Size, Speed, and Object Motion. *J Neurosci* 37:610-625

Jillian Goetz, Zachary F. Jessen, Anne Jacobi, Adam Mani, Sam Cooler, Devon Greer, Sabah Kadri, Jeremy Segal, Karthik Shekhar, Joshua R. Sanes, Gregory W. Schwartz, Unified classification of mouse retinal ganglion cells using function, morphology, and gene expression, *Cell Reports*, Volume 40, Issue 2, 2022, 111040, ISSN 2211-124. doi.org/10.1016/j.celrep.2022.111040

Johnson KP, Zhao L, Kerschensteiner D. A Pixel-Encoder Retinal Ganglion Cell with Spatially Offset Excitatory and Inhibitory Receptive Fields. *Cell Rep.* 2018 Feb 6;22(6):1462-1472. doi: 10.1016/j.celrep.2018.01.037. PMID: 29425502; PMCID: PMC5826572.

Hartline, H. K. (1938). The response of single optic nerve fibers of the vertebrate eye to illumination of the retina. *The American Journal of Physiology*.

Hattar S., H. W. (2002, February 8). Melanopsin-containing retinal ganglion cells: architecture, projections, and intrinsic photosensitivity. *Science*, 295(5557), 1065-70.

Hillier, D., Fiscella, M., Drinnenberg, A., Trenholm, S., Rompani, S. B., Raics, Z.,

Katona, G., Juettner, J., Hierlemann, A., Rozsa, B., & Roska, B. (2017). Causal evidence for retina dependent and -independent visual motion computations in mouse cortex. *Nature neuroscience*, 20(7), 960–968.

<https://doi.org/10.1038/nn.4566>

Kim IJ, Zhang Y, Yamagata M, Meister M, Sanes JR. Molecular identification of a retinal cell type that responds to upward motion. *Nature*. 2008 Mar 27;452(7186):478-82. doi: 10.1038/nature06739. PMID: 18368118.

Hanson L, Ravi-Chander P, Berson D, Awatramani GB. Hierarchical retinal computations rely on hybrid chemical-electrical signaling. *Cell Rep*. 2023 Jan 24;42(2):112030. doi: 10.1016/j.celrep.2023.112030. Epub ahead of print. PMID: 36696265.

Hubel, D. H., & Wiesel, T. N. (1962). Receptive fields, binocular interaction and functional architecture in the cat's visual cortex. *The Journal of physiology*, 160(1), 106–154. <https://doi.org/10.1113/jphysiol.1962.sp006837>

Jacoby J., Zhu Y., DeVries S. H., Schwartz G. W. (2015). An amacrine cell circuit for signaling steady illumination in the retina. *Cell Rep*. 13, 2663–2670. 10.1016/j.celrep.2015.11.062

Jacoby J, Schwartz GW. Typology and Circuitry of Suppressed-by-Contrast Retinal

Ganglion Cells. *Front Cell Neurosci.* 2018;12:269. Published 2018 Aug 27.
doi:10.3389/fncel.2018.00269

Kameneva T., Hamish M., Burkitt A.N. (2011) Modeling intrinsic electrophysiological properties of ON and OFF retinal ganglion cells. *J Comput Neurosci.* 31:547-561

Kim IJ, Zhang Y, Yamagata M, Meister M, Sanes JR. Molecular identification of a retinal cell type that responds to upward motion. *Nature.* 2008;452(7186):478-482. doi:10.1038/nature06739

Kolb, H. (n.d.). Morphology and Circuitry of Ganglion Cells by Helga Kolb. Kong JH, Fish DR, Rockhill RL, Masland RH. Diversity of ganglion cells in the mouse retina: unsupervised morphological classification and its limits. *J Comp Neurol.* 2005;489(3):293-310. doi:10.1002/cne.20631

Krieger B, Qiao M, Rousso DL, Sanes JR, Meister M (2017) Four alpha ganglion cell types in mouse retina: Function, structure, and molecular signatures. *PLoS ONE* 12(7): e0180091. <https://doi.org/10.1371/journal.pone.0180091>

Kuffler, S. W. (1953). Discharge Patterns and Functional Organization of Mammalian Retina. *John Hopkins Hospital and University.*

La Chioma A, Bonhoeffer T, Hübener M. Area-Specific Mapping of Binocular Disparity

across Mouse Visual Cortex. *Curr Biol.* 2019;29(17):2954-2960.e5.

doi:10.1016/j.cub.2019.07.037

Lee S, Chen L, Chen M, Ye M, Seal RP, Zhou ZJ. An unconventional glutamatergic

circuit in the retina formed by vGluT3 amacrine cells. *Neuron.* 2014 Nov

19;84(4):708-15. doi: 10.1016/j.neuron.2014.10.021. Epub 2014 Nov 6. PMID:

25456497; PMCID: PMC4254642.

Levick WR. Receptive fields and trigger features of ganglion cells in the visual streak of

the rabbit's retina. *J Physiol.* 1967;188(3):285-307.

doi:10.1113/jphysiol.1967.sp008140

Luo X, Lambrou GN, Sahel JA, Hicks D. Hypoglycemia induces general neuronal death,

whereas hypoxia and glutamate transport blockade lead to selective retinal

ganglion cell death in vitro. *Invest Ophthalmol Vis Sci.* 2001;42(11):2695-2705.

Marshel JH, Kaye AP, Nauhaus I, Callaway EM. Anterior-posterior direction opponency

in the superficial mouse lateral geniculate nucleus. *Neuron.* 2012;76:713–720.

doi: 10.1016/j.neuron.2012.09.021.

Martersteck, E. M., Hirokawa, K. E., Evarts, M., Bernard, A., Duan, X., Li, Y., Ng, L.,

Oh, S. W., Ouellette, B., Royall, J. J., Stoecklin, M., Wang, Q., Zeng, H., Sanes,

J. R., & Harris, J. A. (2017). Diverse Central Projection Patterns of Retinal

Ganglion Cells. *Cell reports*, 18(8), 2058–2072.

Matsumoto A, Agbariah W, Nolte SS, Andrawos R, Levi H, Sabbah S, Yonehara K.

Direction selectivity in retinal bipolar cell axon terminals. *Neuron*. 2021 Sep 15;109(18):2928-2942.e8. doi: 10.1016/j.neuron.2021.07.008. Epub 2021 Aug 13. Erratum in: *Neuron*. 2021 Dec 1;109(23):3895-3896. PMID: 34390651; PMCID: PMC8478419.

Mazurek M, Kager M, Van Hooser SD. Robust quantification of orientation selectivity and

direction selectivity. *Front Neural Circuits*. 2014 Aug 6;8:92. doi: 10.3389/fncir.2014.00092. PMID: 25147504; PMCID: PMC4123790.

Masland, R. H. (2013, October 18). The Neuronal Organization of the Retina. *Neuron*,

76(2), 266-280.

Michal Rivlin-Etzion, . K. (2011, June 15). Transgenic Mice Reveal Unexpected

Diversity of On-Off Direction-Selective Retinal Ganglion Cell Subtypes and Brain Structures Involved in Motion Processing. *The Journal of Neuroscience*, 31(24), 8760-8769.

Morgans CW, Zhang J, Jeffrey BG, Nelson SM, Burke NS, et al. TRPM1 is required

for the depolarizing light response in retinal ON-bipolar cells. *PNAS*. 2009;106:19174–78.

Morin LP, Studholme KM. Retinofugal projections in the mouse. *J Comp*

Neurol. 2014;522(16):3733-3753. doi:10.1002/cne.23635

- Murphy-Baum, B. L., & Taylor, W. R. (2015). The Synaptic and Morphological Basis of Orientation Selectivity in a Polyaxonal Amacrine Cell of the Rabbit Retina. *The Journal of neuroscience : the official journal of the Society for Neuroscience*, 35(39), 13336– 13350.
- Nath, A., and Schwartz, G. W. (2016). Cardinal orientation selectivity is represented by two distinct ganglion cell types in mouse retina. *J. Neurosci.* 36, 3208–3221.
- Nath, A., and Schwartz, G. W. (2017). Electrical synapses convey orientation selectivity in the mouse retina. *Nat. Commun.* 8:2025.
- O'Brien, B.J., Isayama, T., Richardson, R. and Berson, D.M. (2002), Intrinsic physiological properties of cat retinal ganglion cells. *The Journal of Physiology*, 538: 787-802. doi:10.1113/jphysiol.2001.013009
- Onkar S. Dhande, M. E.-D. (2013, November 6). Genetic Dissection of Retinal Inputs to Brainstem Nuclei Controlling Image Stabilization. *Journal of Neuroscience*, 33(45), 17797-17813.
- Purves D., G. J.-S. (2017, October). *Neuroscience 6th Edition*. Oxford University Press.
- R. Nelson, E. V. (1978, March). Intracellular staining reveals different levels of stratification for on- and off-center ganglion cells in cat retina. *Journal of*

Neurophysiology, 41(2).

Rheaume, B.A., Jereen, A., Bolisetty, M. *et al.* Single cell transcriptome profiling of retinal ganglion cells identifies cellular subtypes. *Nat Commun* **9**, 2759 (2018).

Román Rosón M, Bauer Y, Kotkat AH, Berens P, Euler T, Busse L. Mouse dLGN Receives Functional Input from a Diverse Population of Retinal Ganglion Cells with Limited Convergence. *Neuron*. 2019;102(2):462-476.e8.
doi:10.1016/j.neuron.2019.01.040

Passaglia, C. L., Troy, J. B., Ruttiger, L., and Lee, B. B. (2002). Orientation sensitivity of ganglion cells in primate retina. *Vis. Res.* 42, 683–694. doi: 10.1016/S0042- 6989(01)00312- 1

Sanes J. R., R. H. (2015, March 31). The types of Retinal Ganglion Cells: Current status and implications for neuronal classification. *Reviews in Advance*.

Schindelin J, Arganda-Carreras I, Frise E, Kaynig V, Longair M, Pietzsch T, Preibisch S, Rueden C, Saalfeld S, Schmid B, Tinevez J-Y, White DJ, Hartenstein V, Eliceiri K, Tomancak P, Cardona A. Fiji: an open-source platform for biological-image analysis. *Nat. Methods*. 2012;9:676–82.

Schneider CA, Rasband WS, Eliceiri KW. NIH Image to ImageJ: 25 years of image analysis. *Nat. Methods*. 2012;9:671–5.

- Scholl B, Tan AY, Corey J, Priebe NJ (2013) Emergence of orientation selectivity in the Mammalian visual pathway. *J Neurosci* **33**:10616–10624.
- Scholl B., J. B. (2013, June 15). Binocular integration and disparity selectivity in mouse primary visual cortex. *Journal of Neurophysiology*, *109*(12), 3013-3024.
- Sherman SM, Guillery RW. On the actions that one nerve cell can have on another: distinguishing "drivers" from "modulators". *Proc Natl Acad Sci U S A*. 1998;95(12):7121-7126. doi:10.1073/pnas.95.12.7121
- Sanes, M. (2015, March 31). The types of retinal ganglion cells: Current status and implications for neuronal classification. *Reviews in Advance*, *12*(21), 221-246.
- Satoru Kondo, K. O. (2016). Laminar differences in the orientation selectivity of geniculate afferents in mouse primary visual cortex. *Nature Neuroscience*, *19*(2).
- Seabrook T.A., T. J. (2017). Architecture, Function, and Assembly of the Mouse Visual System. *Annu. Rev. Neurosci.*, 499-538.
- Sümbül, U., Song, S., McCulloch, K. *et al.* A genetic and computational approach to structurally classify neuronal types. *Nat Commun* **5**, 3512 (2014).
- Suresh V, Çiftçioğlu UM, Wang X, Lala BM, Ding KR, Smith WA, Sommer FT, Hirsch

JA. Synaptic Contributions to Receptive Field Structure and Response Properties in the Rodent Lateral Geniculate Nucleus of the Thalamus. *J Neurosci*. 2016 Oct 26;36(43):10949-10963. doi: 10.1523/JNEUROSCI.1045-16.2016. PMID: 27798177; PMCID: PMC5098835.

Thoreson WB, Mangel SC. Lateral interactions in the outer retina. *Prog Retin Eye Res*. 2012;31:407–41.

Tien N.-W., Pearson J. T., Heller C. R., Demas J., Kerschensteiner D. (2015). Genetically identified suppressed-by-contrast retinal ganglion cells reliably signal self-generated visual stimuli. *J. Neurosci*. 35, 10815–10820. 10.1523/JNEUROSCI.1521-15.2015

Tsukamoto Y, Omi N. Classification of Mouse Retinal Bipolar Cells: Type-Specific Connectivity with Special Reference to Rod-Driven AII Amacrine Pathways. *Front Neuroanat*. 2017 Oct 24;11:92. doi: 10.3389/fnana.2017.00092. PMID: 29114208; PMCID: PMC5660706.

Vanessa Lanoue, H. M. (2019). Branching mechanisms shaping dendrite architecture. *Developmental Biology*, 451, 16-24.

Venkataramani, S. A. (2016). Synaptic mechanisms generating orientation selectivity in the on pathway of the rabbit retina. *J. Neurosci*, 36, 3336-3349.

Vlasits AL, Euler T, Franke K. Function first: classifying cell types and circuits of the

retina. *Curr Opin Neurobiol.* 2019;56:8-15. doi:10.1016/j.conb.2018.10.011

Völgyi, B., Chheda, S., & Bloomfield, S. A. (2009). Tracer coupling patterns of the ganglion cell subtypes in the mouse retina. *The Journal of comparative neurology*, 512(5), 664–687. <https://doi.org/10.1002/cne.21912>

Wässle H, Boycott BB. Functional architecture of the mammalian retina.

Physiol Rev. 1991;71(2):447-480. doi:10.1152/physrev.1991.71.2.447

Wässle, H., Peichl, L., & Boycott, B. B. (1981). Dendritic territories of cat retinal ganglion cells. *Nature*, 292(5821), 344–345.

<https://doi.org/10.1038/292344a0>

Wen Q, Chklovskii DB. A cost-benefit analysis of neuronal morphology. *J*

Neurophysiol. 2008;99(5):2320-2328. doi:10.1152/jn.00280.2007

Wiesel, H. a. (1959). Receptive Fields of Single Neurones In The Cat's Striate

Cortex. *J. Physiol.*, 148, 574-591.

Yang, G., & Masland, R. H. (1994). Receptive fields and dendritic structure of

directionally selective retinal ganglion cells. *The Journal of neuroscience : the official Journal of the Society for Neuroscience*, 14(9), 5267–5280.

Yang, G., & Masland, R. (1992). Direct Visualization of the Dendritic and Receptive

Fields of Directionally Selective Retinal Ganglion Cells. *Science*, 258(5090), 1949-1952.

Ya-tang Li, . B.-h.. (2015, August 5). Synaptic Basis for Differential Orientation Selectivity between Complex and Simple Cells in Mouse Visual Cortex. *J Neurosci.*, 35(31), 11081- 11093.

Yoshida K, Watanabe D, Ishikane H, Tachibana M, Pastan I, Nakanishi S. A key role of starburst amacrine cells in originating retinal directional selectivity and optokinetic eye movement. *Neuron*. 2001;30(3):771-780. doi:10.1016/s0896-6273(01)00316-6

Yvonne Ou, R. E. (2016, August 31). Selective Vulnerability of Specific Retinal Ganglion Cell Types and Synapses after Transient Ocular Hypertension. *Journal of Neuroscience* , 36(35), 9240-9252.

Zhang C, McCall MA. Receptor targets of amacrine cells. *Vis Neurosci*. 2012;29(1):11–29.

Zhao X, Chen H, Liu X, Cang J. Orientation-selective responses in the mouse lateral geniculate nucleus. *J Neurosci*. 2013 Jul 31;33(31):12751-63. doi: 10.1523/JNEUROSCI.0095-13.2013. PMID: 23904611; PMCID: PMC3728687.

Zylerberg, J. (2018). The role of untuned neurons in sensory information coding. *BioRxiv*.

APPENDIX A: ABBREVIATIONS

ANOVA	Analysis of Variance
ATP	Adenosine Triphosphate
bGH	Bovine Growth Hormone
CaM	Calcium-binding Protein Calmodulin
CART	Cocaine and Amphetamine Regulated Transcript
ChAT	CholineAcetyltransferase
cpGFP	Circularly Permuted Green Fluorescent Protein
dLGN	Dorsolateral Geniculate Nucleus
DRD4	Dopamine Receptor 4
DSGC	Direction Selective Ganglion Cell
DSI	Direction Selectivity Index
EnvA	Avian Sarcoma Leucosis Virus Glycoprotein
GABA	Gamma-Aminobutyric Acid
GCaMP6f	Green Fluorescent Calcium Indicator
GFP	Green Fluorescent Protein
hOS	Horizontal Orientation Selective
IPL	Inner Plexiform Layer
JAM-B	Junctional Adhesion Molecule B
LP	Lateral Posterior Nucleus
ooDSGC	ON/OFF Direction Selective Ganglion Cell
OS	Orientation Selective
OSGC	Orientation Selective Ganglion Cell
OSI	Orientation Selectivity Index
PBS	Phosphate Buffered Saline
PFA	Paraformaldehyde
RGC	Retinal Ganglion Cell
RMSD	Root-Mean-Square Deviation

SC	Superior Colliculus
TRHR	Thyrotropin-Releasing Hormone Receptor
TVA	Avian Receptor Protein
V1	Primary Visual Cortex
vOS	Vertical Orientation Selective
WPRE	Woodchuck Hepatitis Virus Posttranscriptional Regulatory Element
WFV	Wide Field Vertical
WT	Wild Type

APPENDIX B: Tables

Table 1

Morphology ID	Cell ID	Polarity	Eyewire correlate	Peak RF (um ²)	OSI	DSI	OSI Angle	NSD	Morphology
1A	22330 R1	OFF	2i	33	0.41	0.14	135-315	1.14	smooth
1B	19n06 R1	OFF	2i	666	0.91	0.14	135-315	1.11	smooth
1C	20317 R4	OFF	2i	165	0.82	0.23	135-315	1.09	smooth
1D	20508 R1	OFF	2i	66	0.56	0.06	135-315	1.16	smooth
1E	19904 R1	OFF	4i	66	0.76	0.17	135-315	0.73	spiny
1F	20526 R2	OFF	4i	66	0.82	0.2	135-315	0.83	spiny
1G	21809 R1	OFF	4i	165	0.31	0.23	135-315	0.89	spiny
1H	20520 R1	OFF	4i	165	0.25	0.18	0-180	0.7	spiny
1I	19612 R2	ON	27	333	0.66	0.12	90-270	-0.07, 1.07	smooth
1J	19o23 R2	ON	27	165	0.2	0.01	45-225	-0.3, 1.5	smooth
1K	19521 R1	ON	9n	66	0.36	0.1	90-270	-0.43	smooth
1L	19402 R2	ON	9n	165	0.28	0.26	90-270	-0.38	spiny
1M	20318 R1.1	ON	6t	165	0.5	0.11	90-270	0.19	spiny
2A	19n06 R2	OFF	2aw	66	0.62	0.16	90-270	1.03	spiny
2B	20820 R2	OFF	2aw	666	0.83	0.27	45-225	1.06	smooth
2C	19605 R1	OFF	82wi	666	0.32	0.02	45-225	-0.33, 1.5	smooth
2D	20909 R2	OFF	5so	165	0.4	0.15	45-225	0.72	spiny
2E	19n06 R3	OFF	5so	66	0.48	0.09	45-225	0.54	smooth
2F	20313 R1	ON	5to	165	0.51	0.14	45-225	0.48	spiny
2G	20609 R1	ON	5to	333	0.19	0.04	135-315	0.69	spiny
2H	20609 R2	OFF	5to	666	0.22	0.1	0-180	0.9	spiny
2I	20220 R1	ON	82wo	333	0.71	0.12	45-225	-0.4, 0.97	spiny
2J	19319 R1	ON	82wo	165	0.39	0.35	0-180	0, 1	smooth
2K	20617 R2	ON	82wo	66	0.43	0.17	0-180	-0.05, 0.75	smooth
2L	22113 R3	ON	82wo	165	0.17	0.13	45-225		smooth
2M	19516 R1	ON	82wo	333	0.18	0.13	0-180	-0.06, 1	smooth
2N	22104 R2	ON	82wo	165	0.17	0.13	45-225		smooth
2O	21o13 R1	ON	82wo	165	0.5	0.04	0-180		smooth
2P	21o14 R2.2	ON	82wo	333	0.22	0.08	45-225		smooth
3A	20218 R2	OFF	5si	165	0.15	0.02	90-270		
2B	20826 R1	OFF	5si	66	0.19	0.28	0-180	0.44	smooth
3C	20317 R2	OFF	5si	66	0.14	0.23	90-270	0.57	spiny

Table 2

Cell ID	DSI	OSI	DSI angle	OSI angle	x-coordinate	y-coordinate
22620_LE_04	0.61	0.21	270	90-270	-693	-679
22620_LE_05	0.08	0.31	180	0-180	-718	1160
22620_RE_06	0.76	0.27	0	45-225	-1253	-833
22620_RE_09	0.19	0.28	90	90-270	474	-115
22621_LE_01	0.18	0.26	0	0-180	670	-762
22621_LE_02	0.69	0.41	45	45-225	788	-329
22621_LE_07	0.29	0.74	270	90-270	-699	605
22621_LE_08	0.34	0.34	0	0-180	-750	627
22621_LE_09	0.07	0.52	0	135-315	-735	587
22621_LE_10	0.48	0.21	270	135-315	-783	618
22621_LE_13	0.01	0.05	135	135-315	-954	824
22621_LE_14	0.41	0.44	270	90-270	-1319	1258
22621_LE_17	0.46	0.26	45	90-270	-361	890
22621_LE_18	0.43	0.46	135	0-180	1080	480
22621_LE_20	0.18	0.31	225	45-225	-1018	-401
22621_LE_21	0.4	0.72	90	90-270	-955	-484
22621_LE_25	0.22	0.27	135	0-180	-644	289
22621_LE_26	0.52	0.32	0	45-225	-674	256
22621_LE_27	0.18	0.17	0	0-180	-737	208
22621_LE_29	0.84	0.13	270	90-270	-1060	-616
22621_RE_01	0.5	0.27	45	0-180	-371	900
22622_LE_02	0.48	0.22	135	135-315	-765	669
22622_LE_04	0.43	0.14	315	135-315	1096	-370
22622_LE_07	0.16	0.25	225	0-180	-702	1532
22622_LE_08	0.22	0.57	0	0-180	-863	1621
22622_LE_09	0.81	0.28	90	135-315	-1055	1196
22622_LE_10	0.49	0.11	0	45-225	-765	674
22622_LE_11	0.11	0.63	0	0-180	-807	748
22622_LE_12	0.57	0.24	90	90-270	-1054	1196
22622_RE_02	0.28	0.1	180	45-225	516	-802
22622_RE_04	0.12	0.09	270	45-225	-543	1392
22622_RE_05	0.11	0.31	135	135-315	794	-1525
22622_RE_07	0.13	0.42	135	135-315	-857	-909
22914_LE_01	0.17	0.32	225	90-270	1099	-417
22914_LE_02	0.03	0.37	270	90-270	1382	-218
22914_LE_03	0.07	0.37	180	0-180	1293	-434
22914_LE_04	0.38	0.43	0	135-315	584	665
22914_LE_08	0.27	0.39	270	135-315	583	-1231
22914_LE_09	0.28	0.21	0	0-180	0.497	-1277
22914_LE_10	0.27	0.18	0	0-180	901	-1535
22914_LE_12	0.28	0.63	135	135-315	900	-1531
22914_LE_13	0.25	0.4	180	135-315	478	-1470
22914_LE_15	0.21	0.21	0	135-315	496	-1274
22914_LE_16	0.43	0.15	0	0-180	1381	-218
22914_LE_17	0.58	0.23	0	45-225	-136	-1324
22915_RE_14	0.11	0.31	0	0-180	-302	411
22915_RE_15	0.15	0.4	0	45-225	-349	493
22915_RE_23	0.57	0.6	0	135-315	-636	553
22915_RE_30	0.63	0.51	0	0-180	522	1033
22915_RE_38	0.2	0.45	135	135-315	-545	271
22915_RE_40	0.38	0.31	0	135-315	-629	455

CURRICULUM VITAE

Megan Zipperer

2551 Glenmary Ave, Apt #3
Louisville, KY, 40204
(910) 322-4694
meganzipperer@gmail.com

EDUCATION

Expected 3/2023	PhD, Anatomical Sciences and Neurobiology <i>University of Louisville School of Medicine, Louisville, KY</i> <i>Dissertation title: "Towards a Comprehensive Account of Orientation Selectivity in the Retina"</i> <i>Advisor: Bart Borghuis, PhD</i>
2018-2020	Master of Science, Anatomical Sciences and Neurobiology <i>University of Louisville School of Medicine, Louisville, KY</i>
2012-2016	Bachelor of Science, Biology Minor in Neuroscience <i>University of North Carolina Wilmington, Wilmington, NC</i>

RESEARCH EXPERIENCE

2018-present	Graduate student in the Borghuis Laboratory for Neural Circuit Research <i>University of Louisville School of Medicine, Department of Anatomical Sciences</i> <i>and</i> <i>Neurobiology</i> <ul style="list-style-type: none">● Investigating retinal circuitry using a combination of two-photon imaging, electrophysiology, confocal imaging, immunohistochemistry, and viral tracing● Data analysis and figure making using: MATLAB programming, Adobe Illustrator, Adobe Photoshop, Microsoft Suite● Literature review, training in proposal writing, abstract writing
Spring 2016	Undergraduate research in the Satterlie Laboratory for Marine Invertebrate Locomotion Neurobiology

University of North Carolina Wilmington

- Investigated neural control of locomotion in marine invertebrates using immunohistochemistry and fluorescence microscopy

TEACHING EXPERIENCE

- Spring 2021 Synaptic Organization of the CNS Graduate Teaching Assistant
University of Louisville School of Medicine
- Prepared and delivered lectures for graduate and undergraduate neuroscience students
 - Developed and graded test questions for undergraduate neuroscience students
 - Facilitated article discussion groups on computational neuroscience
- Spring 2020 Advanced Head and Neck Anatomy Graduate Teaching Assistant
University of Louisville School of Medicine
- Prepared cadaveric prosections
 - Lectured dental residents on head and neck gross anatomy
 - Administered quizzes
- Fall 2019 Fundamentals of Neuroscience Graduate Teaching Assistant
University of Louisville School of Medicine
- Prepared and lectured on labs with a focus on human neuroanatomy
- Spring 2016 Undergraduate Teaching Assistant for Anatomy & Physiology lab
University of North Carolina Wilmington
- Prepared labs, taught specimen dissection, instructed on anatomy and physiology topics

ORGANIZATIONAL SERVICE AND LEADERSHIP

- 05/2020-5/2022 Science Policy and Outreach Group (SPOG) Director
University of Louisville
- Conceptualized and implemented initiatives and events to disseminate complex scientific topics with a focus on underserved communities and underrepresented minorities in STEM
 - Led and managed a team of SPOG officers in order to drive the organization forward
 - Established and fostered partnerships with other scientific organizations such as the Kentucky Science Center and the Louisville Regional Science and Engineering Fair
- 01/2020-5/2022 Society for Neuroscience Outreach Liaison

University of Louisville

- Facilitated and marketed for neuroscience events
- Created several speaker series to share neuroscience topics with students in the community
- The primary organizer for “Brain Days” — a 2 day neuroscience event for the community totaling 2000+ participants over the course of two days, 40+ volunteers, and 12+ vendors

2022 Diversity, Inclusion, and Well-Being Committee Member

University of Louisville | Department of Anatomical Sciences and Neurobiology

- Organized training workshops for faculty and students
- Developed initiatives to improve diversity in the department (to include: improving recruitment strategies and student/faculty retention)
- Facilitated “Diversity Book Club” for a semester

05/2020-present Louisville Regional Science and Engineering Fair (LRSEF) Board Member

05/2020-2021 LRSEF Educational Outreach Committee Co-Chair

- Conceptualized and carried out educational outreach initiatives in the community

2019-2020 Science Policy and Outreach Group (SPOG) Outreach Coordinator

University of Louisville

- Facilitated mentorship opportunities for graduate students
- Maintained contacts in the community — particularly from underserved schools — to provide STEM mentorship and resources
- Mentored students one-on-one on STEM topics

CONFERENCE PARTICIPATION

05/2022	The Association for Research in Vision and Ophthalmology (ARVO) 2022 Poster Presentation titled “Toward a Comprehensive Account of Orientation Selectivity in the Retina”
10/2021	Invited Speaker at the Vision Science Retreat at the University of Louisville
7/2021	Retinal Circuit Symposium talk: “Toward a Comprehensive Account of Orientation Selectivity in the Retina”
03/2021	Proposal titled “Bridging Inequities with STEM Outreach” presented at Engaged-Scholarship Symposium
04/30/2019	Paper presentation at ARVO conference in Vancouver, Canada titled “A Multimodal Classification of Retinal Ganglion Cell Types”
04/2019	ARVO foundation travel grant
04/2019	ARVO 2019 Annual Meeting abstract published in <i>Investigative Ophthalmology &</i>

	<i>Visual Science</i> (IOVS) volume 60, issue 9
04/2019	SfN Louisville Chapter Poster Presentation: “A Multimodal Classification of Retinal Ganglion Cell Types”
04/2019	SfN Louisville Chapter Datablitz Presentation: “A Multimodal Classification of Retinal Ganglion Cell Types”

OUTREACH AND COMMUNITY INVOLVEMENT

07/2022	“Exploring Human Anatomy” event with West Louisville Science and Math Projects: conceptualized and planned event with the organization, and facilitated/taught the nervous system portion of the event
03/2022	Brain Days organizer on behalf of the Louisville Chapter of the Society for Neuroscience
2018-2022	Annual participation in Louisville Regional Science and Engineering Fair (LRSEF) as: ambassador, category judge, special awards judge, and event organizer on behalf of the LRSEF board
Spring 2022	Waggener High School Speaker Series Coordinator
Fall 2018-2021	Central High School Science Fair Mentoring
Spring 2021	Olmstead Middle School Speaker Series Coordinator
Fall 2020	Youth Science Summit partner for Kentucky Science Center
04/06/2018	Girls STEM summit session leader at University of Louisville
03/09/2018	Kentucky Science Center Volunteer for Brain Days